PLANNING EXPERIMENTS WITH CAUSAL GRAPHS

DISSERTATION DEFENSE

NICHOLAS J. MATIASZ

4 MAY 2018

Perform experiment

Analyze data

Publish finding

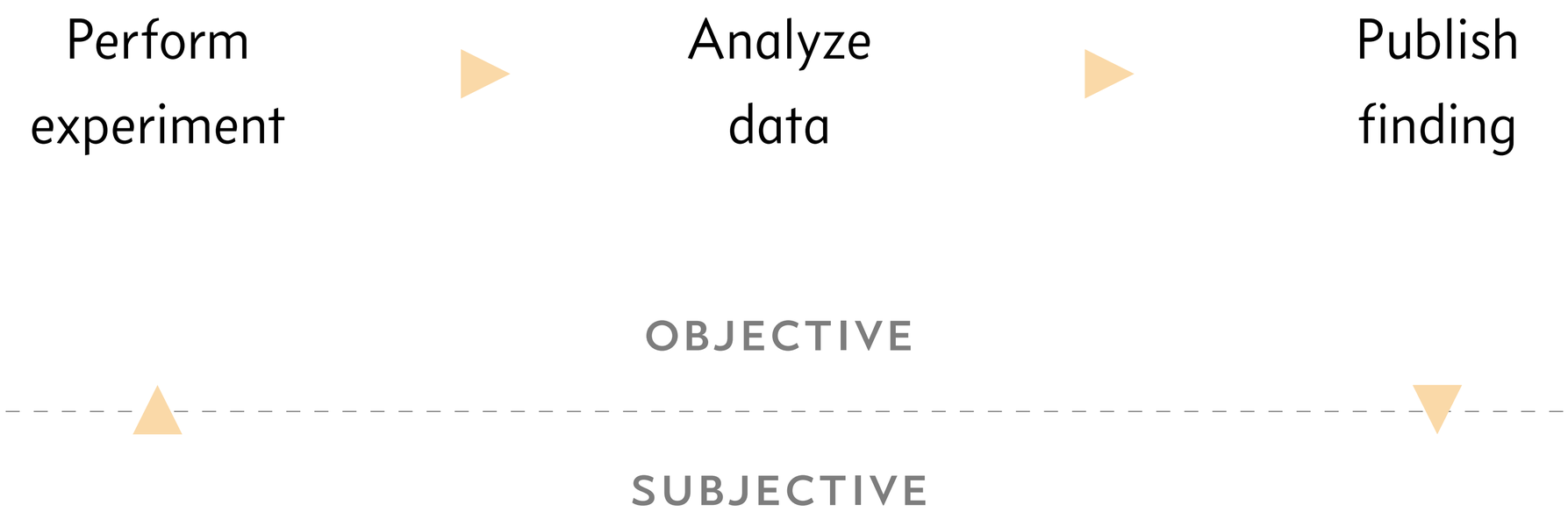
Perform experiment
Analyze data
Publish finding
OBJECTIVE
SUBJECTIVE
Design experiment
Synthesize evidence
Find literature

CONTRIBUTIONS

1. Cumulative evidence index (CEI)
2. Meta-analytic causal discovery
3. Heuristics for experiment planning

CONTRIBUTIONS

1. Cumulative evidence index (CEI)
2. Meta-analytic causal discovery
3. Heuristics for experiment planning

COMMENT · 23 JANUARY 2018

Robust research needs many lines of evidence

Replication is not enough. Marcus R. Munafò and George Davey Smith state the case for triangulation.

Marcus R. Munafò ✉ & George Davey Smith

PDF version

RELATED ARTICLES

Peer review would change too. Instead of a few reviewers looking at the entire manuscript, several would do so, each focusing closely on a particular substudy. In this way, submissions that use multiple, diverse techniques will get appropriate scrutiny, helping to avoid the publication of papers that are like "grand mansions of straw".

Finally, funders, research institutions and journals would need to explicitly support publication of weightier articles. Or perhaps we need to develop formal ways — beyond simple citations — to explicitly link and recognize substudies that triangulate a single question.

A proposal published early last year advocated for a new category of paper that combines hypothesis-generating work with robust, pre-registered confirmatory studies conducted by qualified independent labs[9]. Papers involving triangulation in a way we propose will clearly often involve considerable work coordinating groups of researchers from different disciplines. Reviewers and tenure committees should find ways to value them appropriately.

Nature **553**, 399-401 (2018)

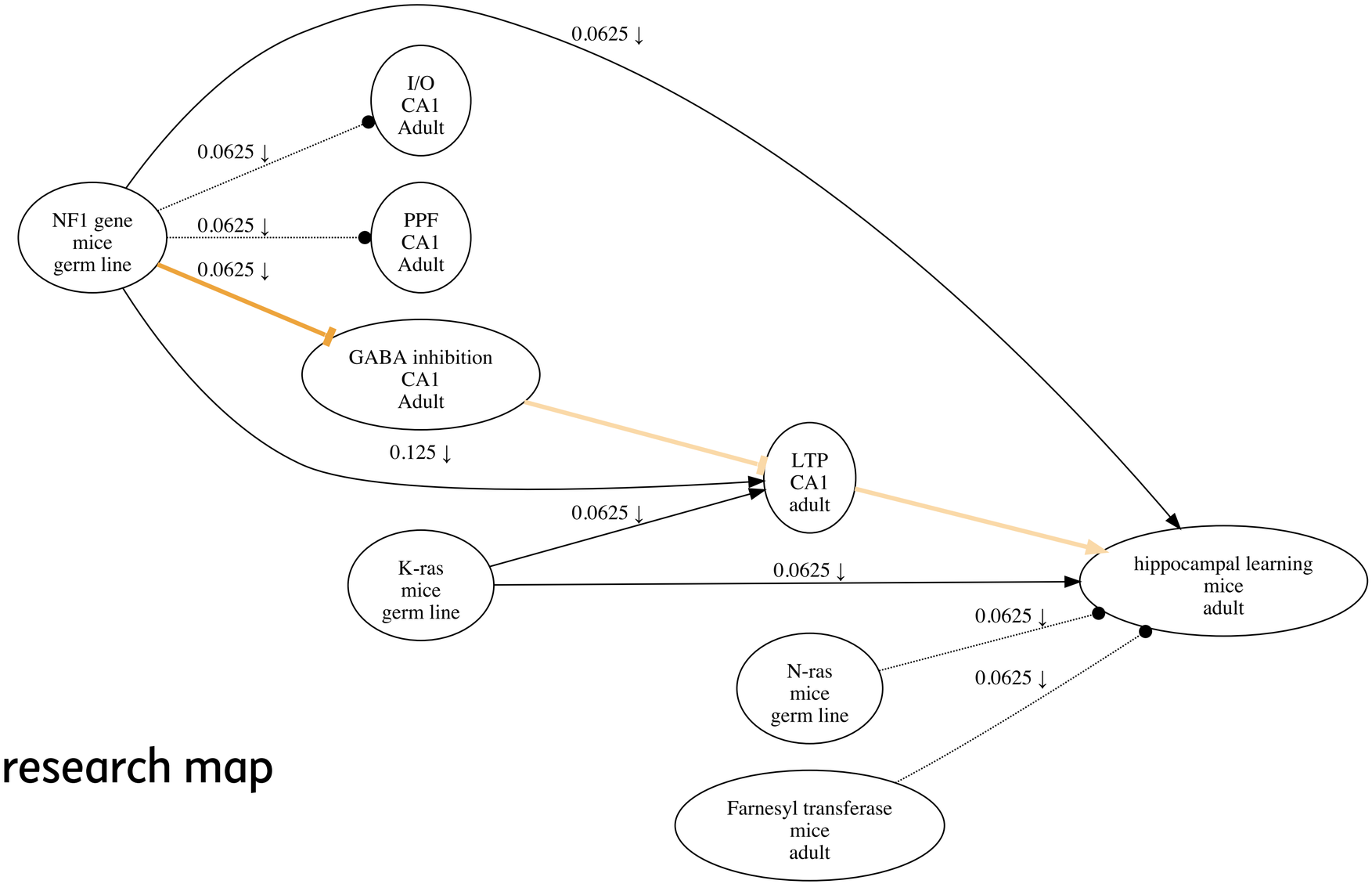

A research map

NODE

What

Where

When

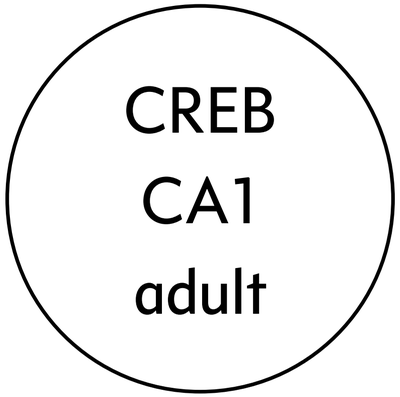

Agent

NODE

What

Where

When

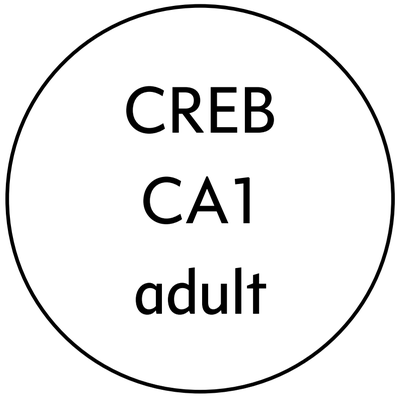

STUDY DESIGN

Intervention

Positive ↑

Negative ↓

Observation

Positive $\varnothing^{\uparrow}$

Negative $\varnothing^{\downarrow}$

Agent

NODE

What
Where
When

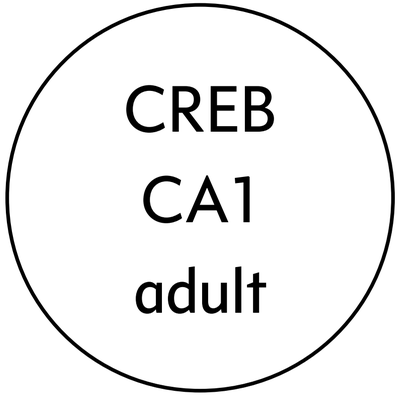

Target

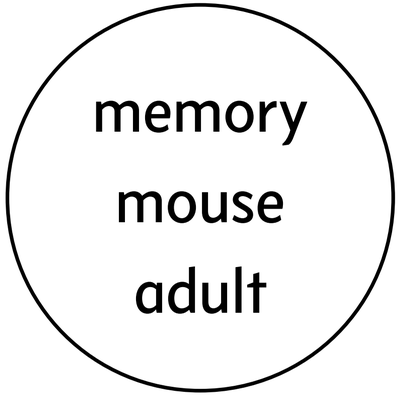

STUDY DESIGN

Intervention

Positive ↑

Negative ↓

Observation

Positive $\varnothing^{\uparrow}$

Negative $\varnothing^{\downarrow}$

RESULT

Increase +

No change 0

Decrease −

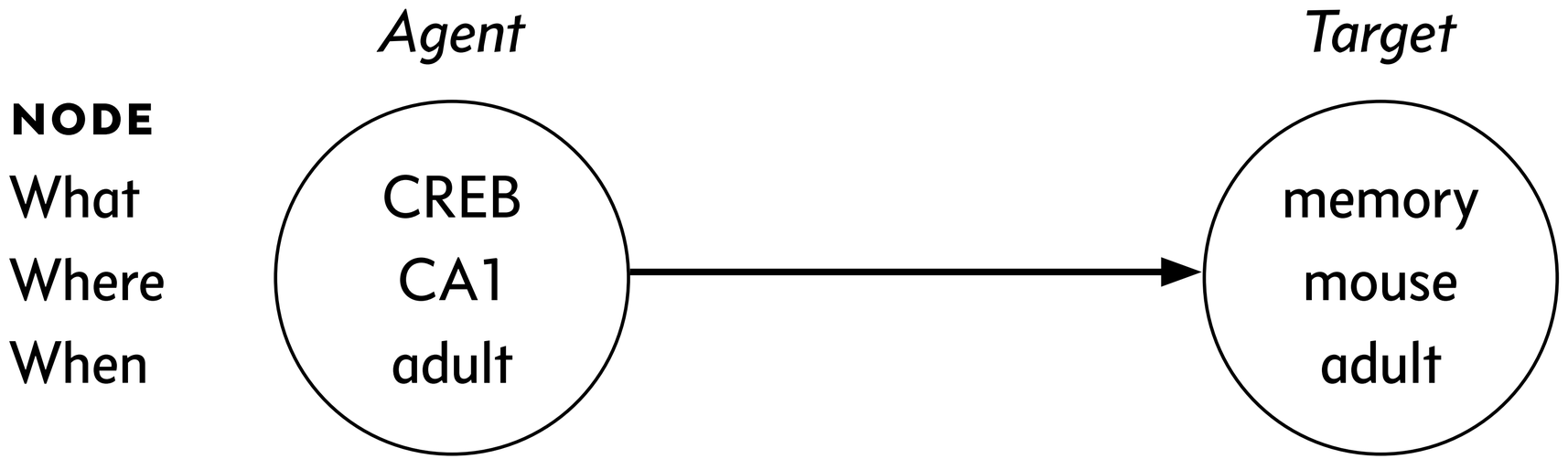

STUDY DESIGN

Intervention

- Positive ↑
- Negative ↓

Observation

- Positive $\varnothing^{\uparrow}$
- Negative $\varnothing^{\downarrow}$

RELATION

Excitatory

RESULT

Increase +

No change 0

Decrease −

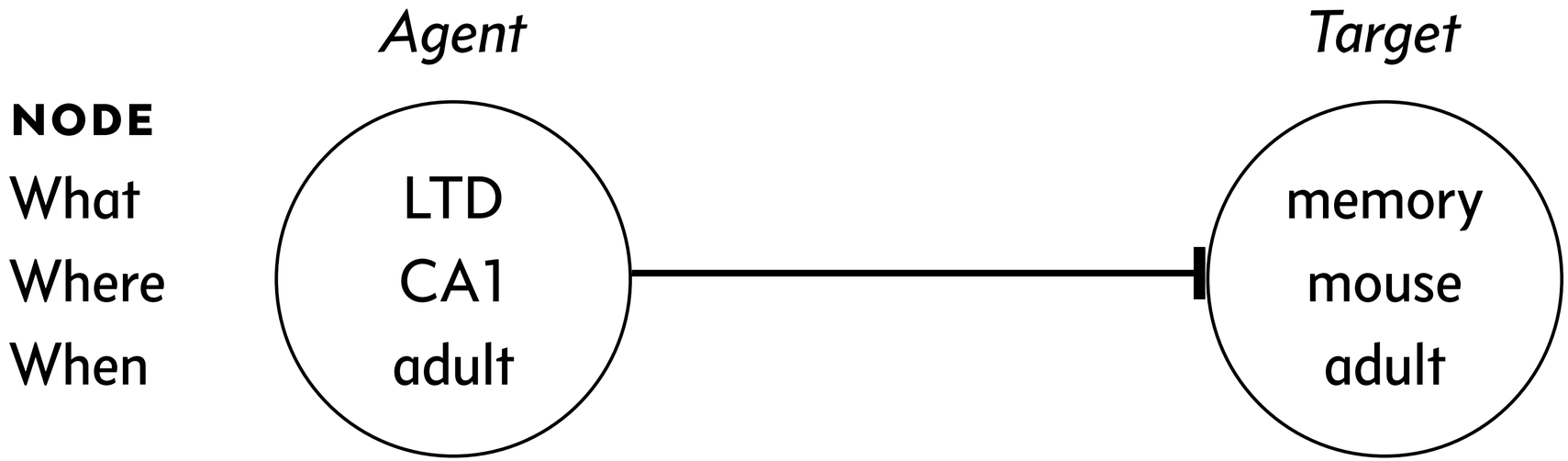

STUDY DESIGN

Intervention

- Positive ↑
- Negative ↓

Observation

- Positive $\varnothing^{\uparrow}$
- Negative $\varnothing^{\downarrow}$

RELATION

Excitatory

Inhibitory

RESULT

Increase +

No change 0

Decrease −

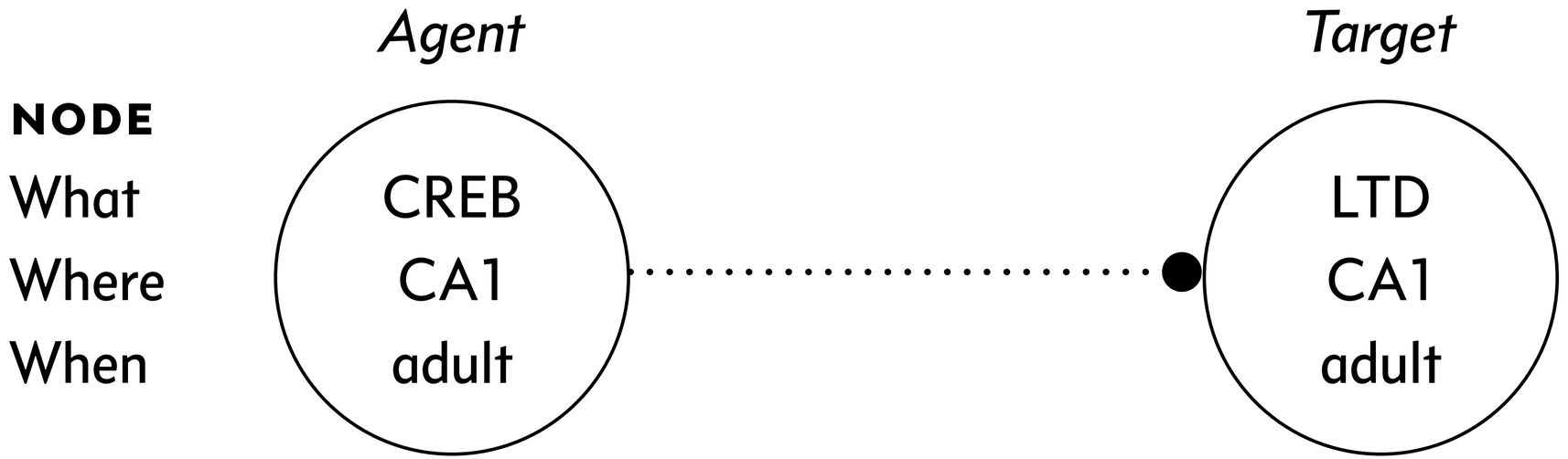

STUDY DESIGN

Intervention

- Positive ↑
- Negative ↓

Observation

- Positive $\varnothing^{\uparrow}$
- Negative $\varnothing^{\downarrow}$

RELATION

Excitatory

Inhibitory

None

RESULT

Increase +

No change 0

Decrease −

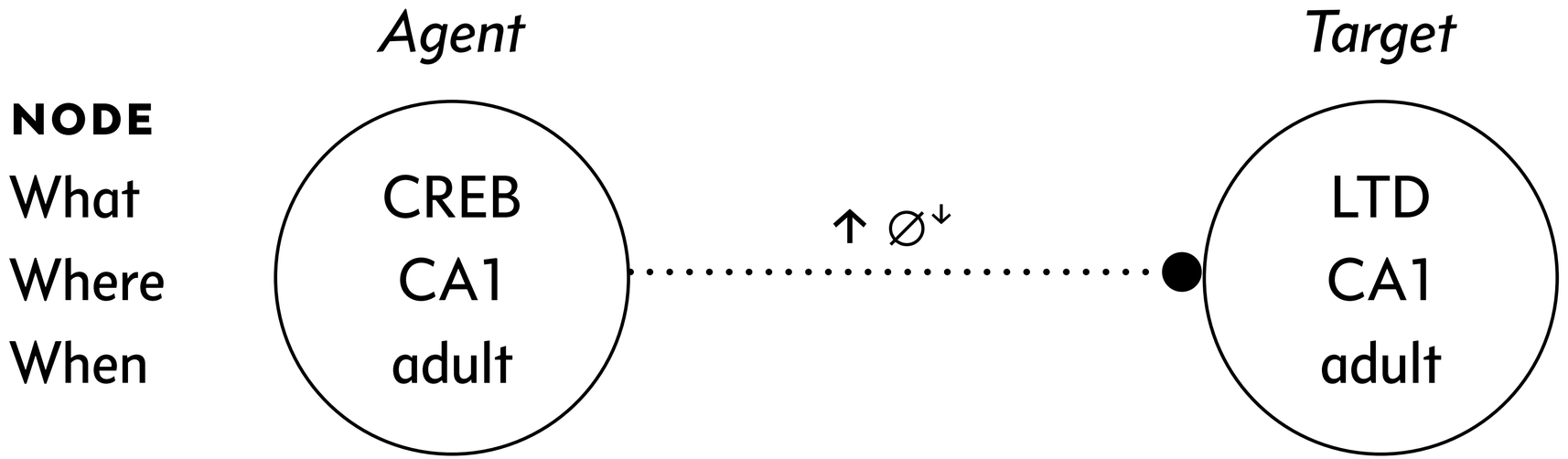

STUDY DESIGN

Intervention

- Positive ↑
- Negative ↓

Observation

- Positive ∅↑
- Negative ∅↓

RELATION

Excitatory

Inhibitory

None

RESULT

Increase +

No change 0

Decrease −

Consistency

Repeat the same experiment; get the same evidence.

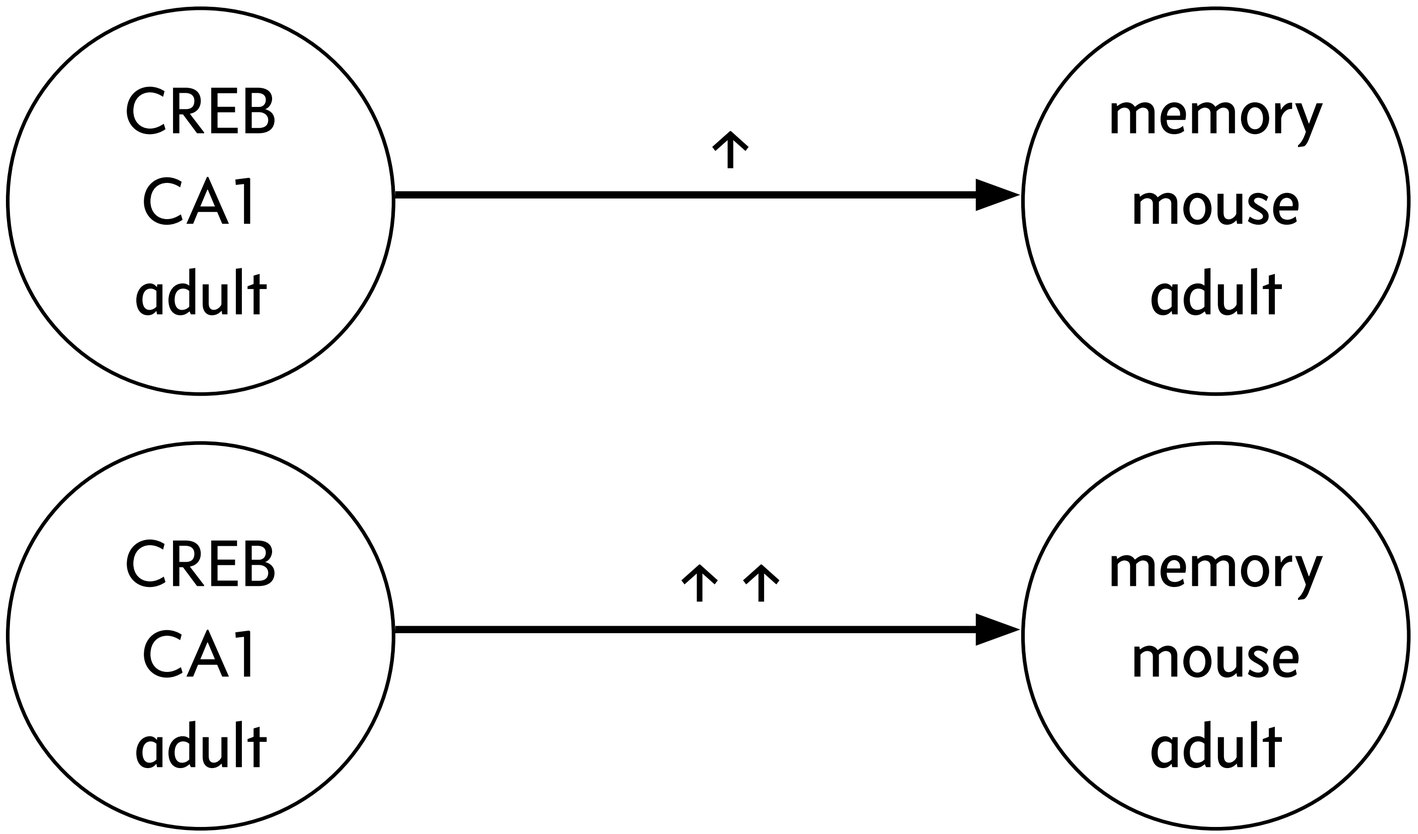

higher score

Convergence

Do different experiments; get the same evidence.

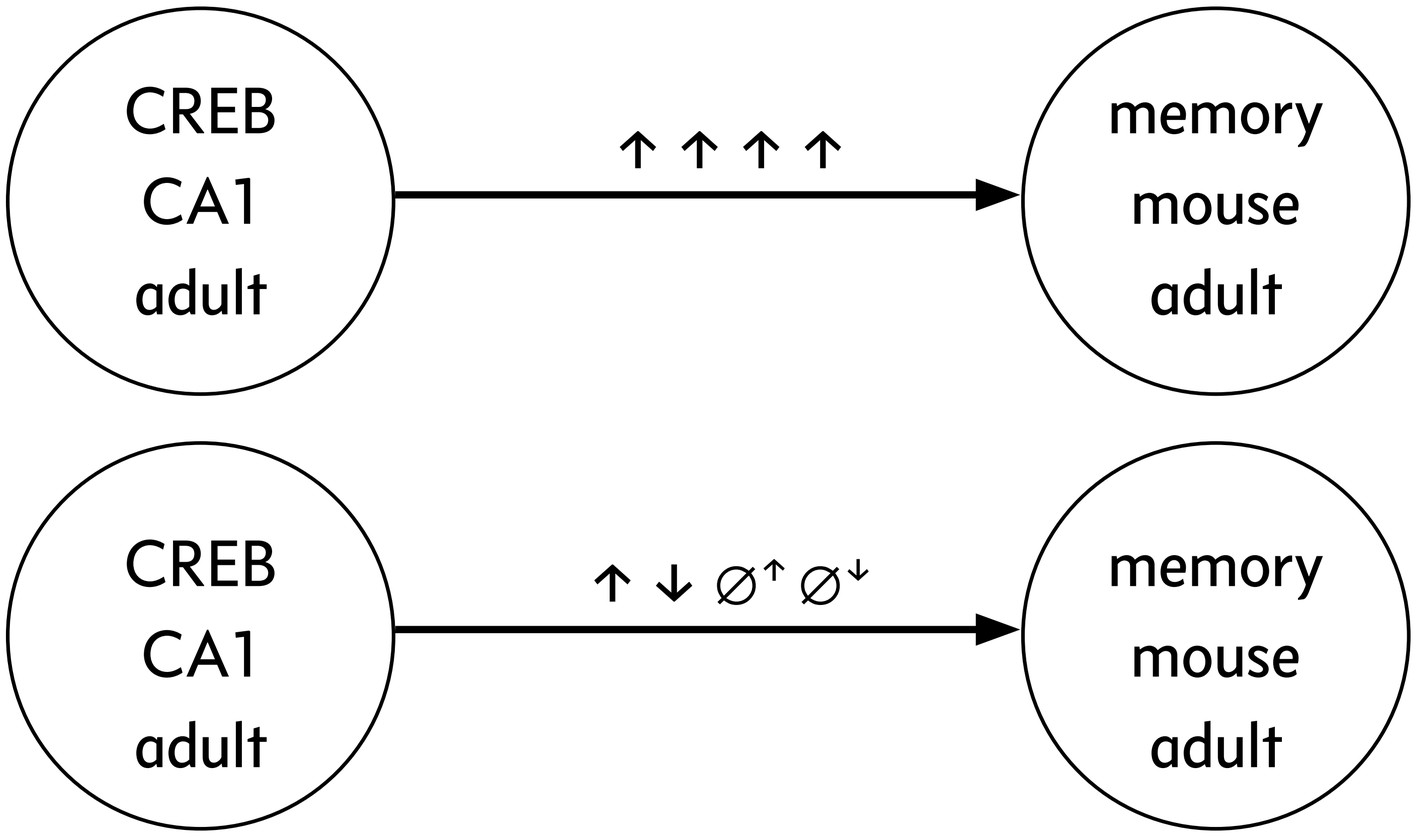

higher score

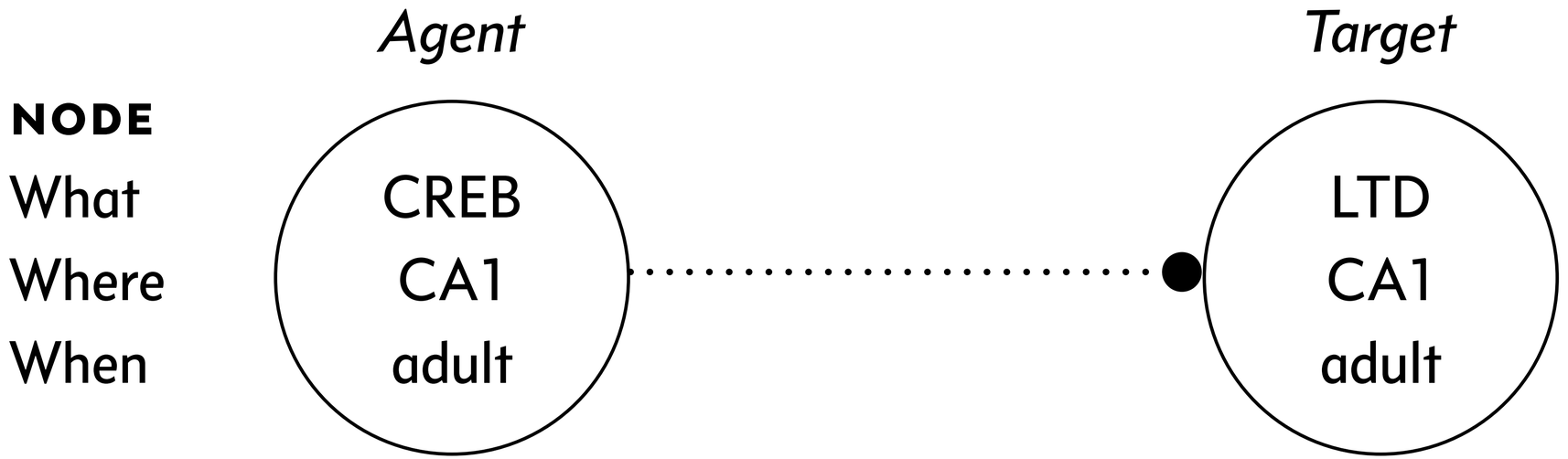

STUDY DESIGN

Intervention

- Positive ↑
- Negative ↓

Observation

- Positive ∅↑
- Negative ∅↓

RELATION

Excitatory

Inhibitory

None

RESULT

Increase +

No change 0

Decrease −

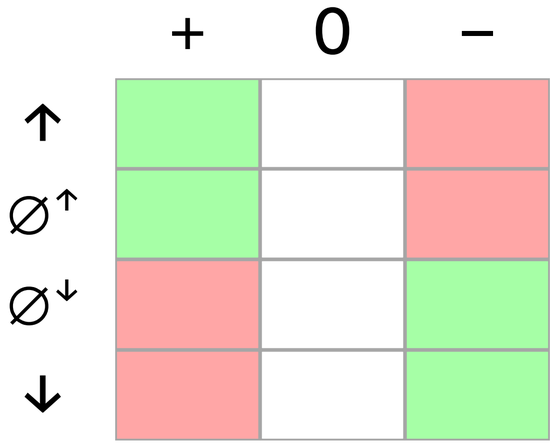

RELATION

Excitatory

Inhibitory

None

Original heuristic CEI

	+	0	–
↑	E↑	N↑	I↑
∅↑	E∅↑	N∅↑	I∅↑
∅↓	I∅↓	N∅↓	E∅↓
↓	I↓	N↓	E↓

$$CEI = \frac{(Max(E,N,I))^2}{E+N+I}$$

$$E = \tfrac{1}{4}(3 - 0.5^{E\uparrow} - 0.5^{E\varnothing\uparrow + E\varnothing\downarrow} - 0.5^{E\downarrow})$$

$$N = \tfrac{1}{4}(3 - 0.5^{N\uparrow} - 0.5^{N\varnothing\uparrow + N\varnothing\downarrow} - 0.5^{N\downarrow})$$

$$I = \tfrac{1}{4}(3 - 0.5^{I\uparrow} - 0.5^{I\varnothing\uparrow + I\varnothing\downarrow} - 0.5^{I\downarrow})$$

Original heuristic CEI

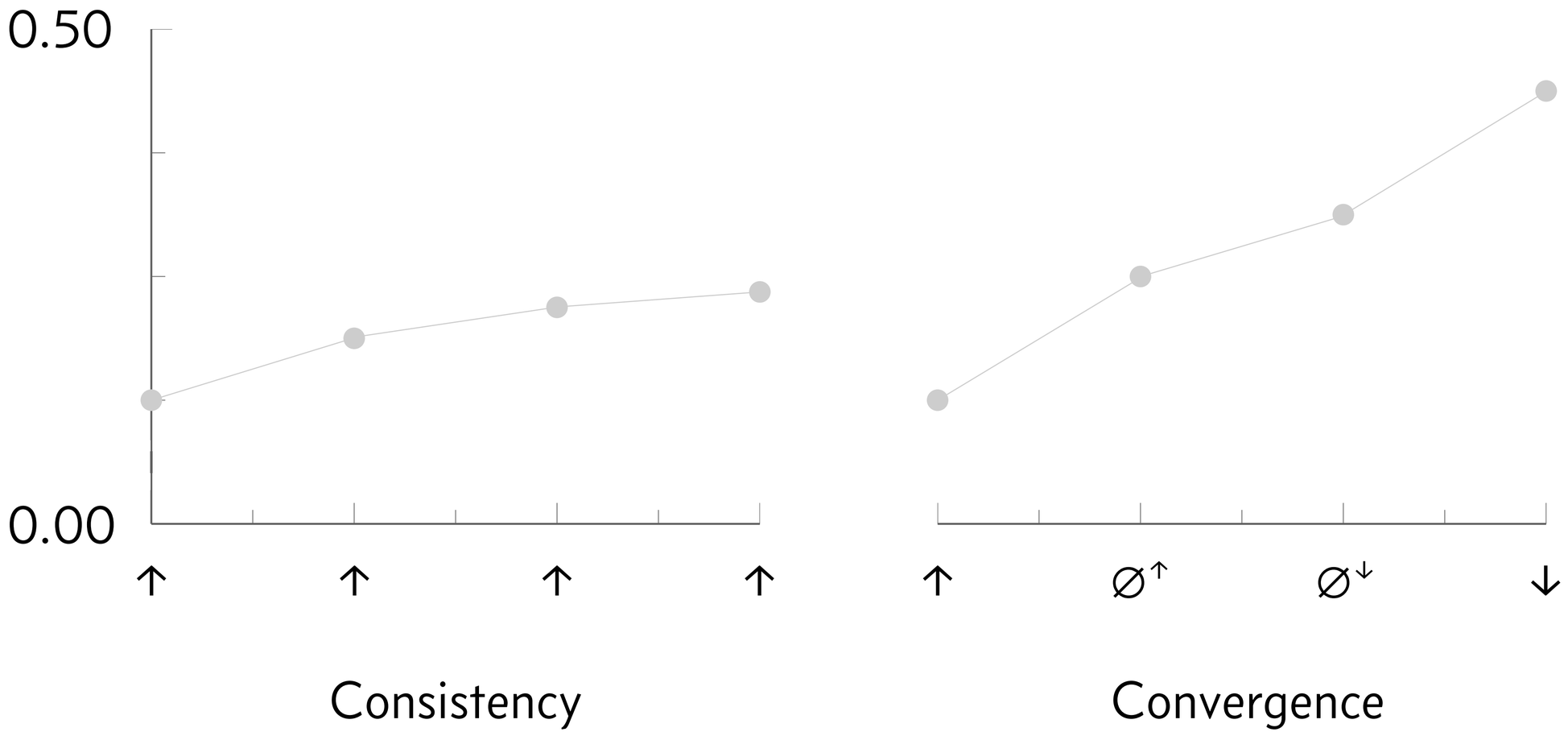

New Bayesian CEI

	+	0	−
↑	1	1	1
∅↑	1	1	1
∅↓	1	1	1
↓	1	1	1

$$P(\text{Excitatory}) = \tfrac{1}{4}(\tfrac{1}{3} + \tfrac{1}{3} + \tfrac{1}{3} + \tfrac{1}{3}) = 0.333$$

$$P(\text{None}) = \tfrac{1}{4}(\tfrac{1}{3} + \tfrac{1}{3} + \tfrac{1}{3} + \tfrac{1}{3}) = 0.333$$

$$P(\text{Inhibitory}) = \tfrac{1}{4}(\tfrac{1}{3} + \tfrac{1}{3} + \tfrac{1}{3} + \tfrac{1}{3}) = 0.333$$

New Bayesian CEI

	+	0	−
↑	2	1	1
∅↑	1	1	1
∅↓	1	1	1
↓	1	1	1

$$P(\text{Excitatory}) = \tfrac{1}{4}(\tfrac{2}{4} + \tfrac{1}{3} + \tfrac{1}{3} + \tfrac{1}{3}) = 0.375$$

$$P(\text{None}) = \tfrac{1}{4}(\tfrac{1}{4} + \tfrac{1}{3} + \tfrac{1}{3} + \tfrac{1}{3}) = 0.3125$$

$$P(\text{Inhibitory}) = \tfrac{1}{4}(\tfrac{1}{4} + \tfrac{1}{3} + \tfrac{1}{3} + \tfrac{1}{3}) = 0.3125$$

New Bayesian CEI

	+	0	−
↑	2	1	1
∅↑	1	1	1
∅↓	1	1	1
↓	1	1	1

$$\frac{0.375 - \frac{1}{3}}{1 - \frac{1}{3}} = 0.0625$$

$$P(\text{Excitatory}) = \frac{1}{4}\left(\frac{2}{4} + \frac{1}{3} + \frac{1}{3} + \frac{1}{3}\right) = 0.375$$

$$P(\text{None}) = \frac{1}{4}\left(\frac{1}{4} + \frac{1}{3} + \frac{1}{3} + \frac{1}{3}\right) = 0.3125$$

$$P(\text{Inhibitory}) = \frac{1}{4}\left(\frac{1}{4} + \frac{1}{3} + \frac{1}{3} + \frac{1}{3}\right) = 0.3125$$

New Bayesian CEI: **consistency**

	+	0	−
↑	5	1	1
∅↑	1	1	1
∅↓	1	1	1
↓	1	1	1

$$\frac{0.429 - \frac{1}{3}}{1 - \frac{1}{3}} = 0.1435$$

$$P(\text{Excitatory}) = \frac{1}{4}\left(\frac{5}{7} + \frac{1}{3} + \frac{1}{3} + \frac{1}{3}\right) = 0.429$$

$$P(\text{None}) = \frac{1}{4}\left(\frac{1}{7} + \frac{1}{3} + \frac{1}{3} + \frac{1}{3}\right) = 0.286$$

$$P(\text{Inhibitory}) = \frac{1}{4}\left(\frac{1}{7} + \frac{1}{3} + \frac{1}{3} + \frac{1}{3}\right) = 0.286$$

New Bayesian CEI: **convergence**

	+	0	−
↑	(2)	1	1
∅↑	(2)	1	1
∅↓	1	1	(2)
↓	1	1	(2)

$$\frac{0.500 - \frac{1}{3}}{1 - \frac{1}{3}} = 0.2500$$

$$P(\text{Excitatory}) = \frac{1}{4}\left(\frac{2}{4} + \frac{2}{4} + \frac{2}{4} + \frac{2}{4}\right) = 0.500$$

$$P(\text{None}) = \frac{1}{4}\left(\frac{1}{4} + \frac{1}{4} + \frac{1}{4} + \frac{1}{4}\right) = 0.250$$

$$P(\text{Inhibitory}) = \frac{1}{4}\left(\frac{1}{4} + \frac{1}{4} + \frac{1}{4} + \frac{1}{4}\right) = 0.250$$

Comparison of old & new CEIs

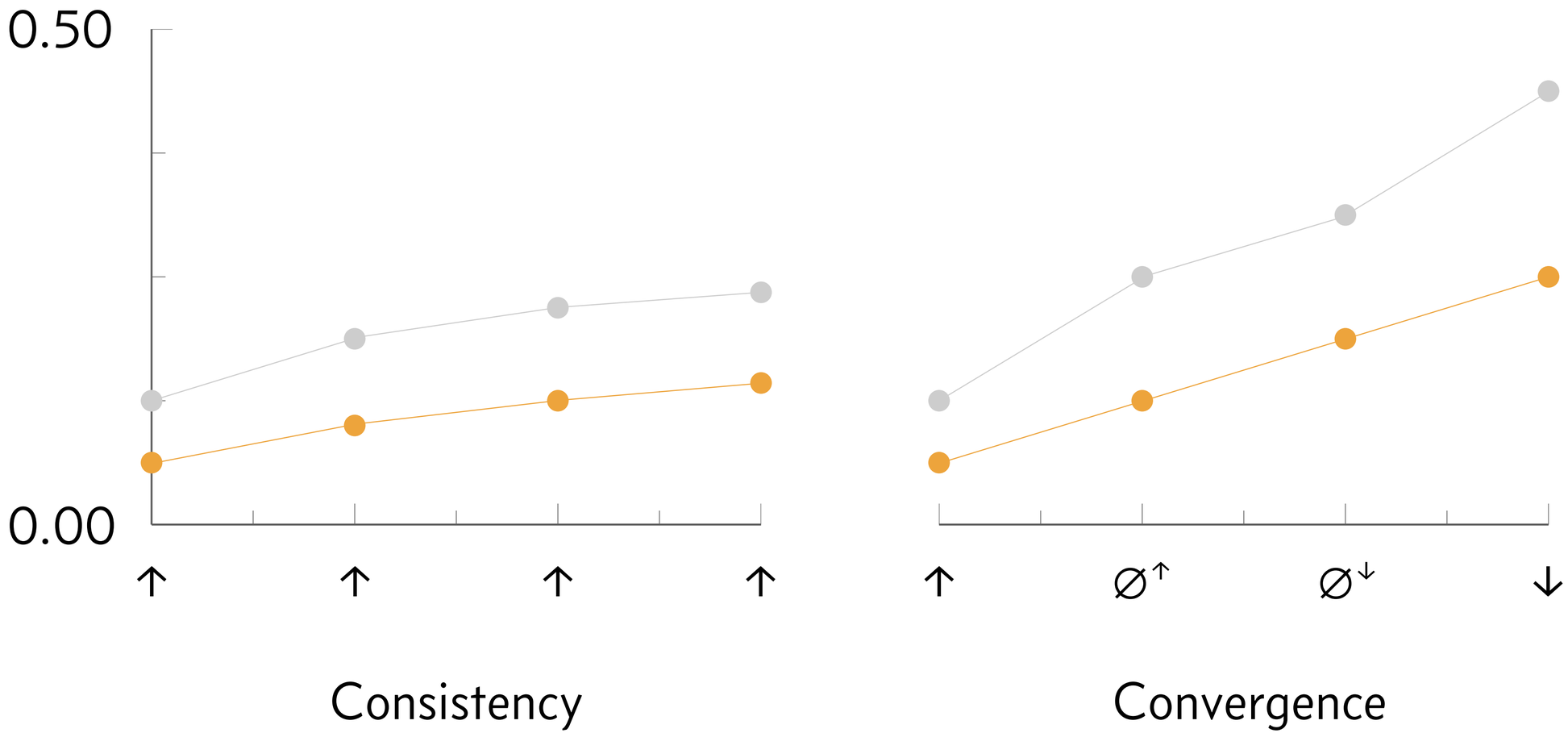

New Bayesian CEI: **divergence**

Scientists tend to trust evidence from a particular study class to the extent that studies within this class yield consistent results.

Conflicting information within a study class limits the amount that the study class can add to the score.

ResearchMaps

LOG IN

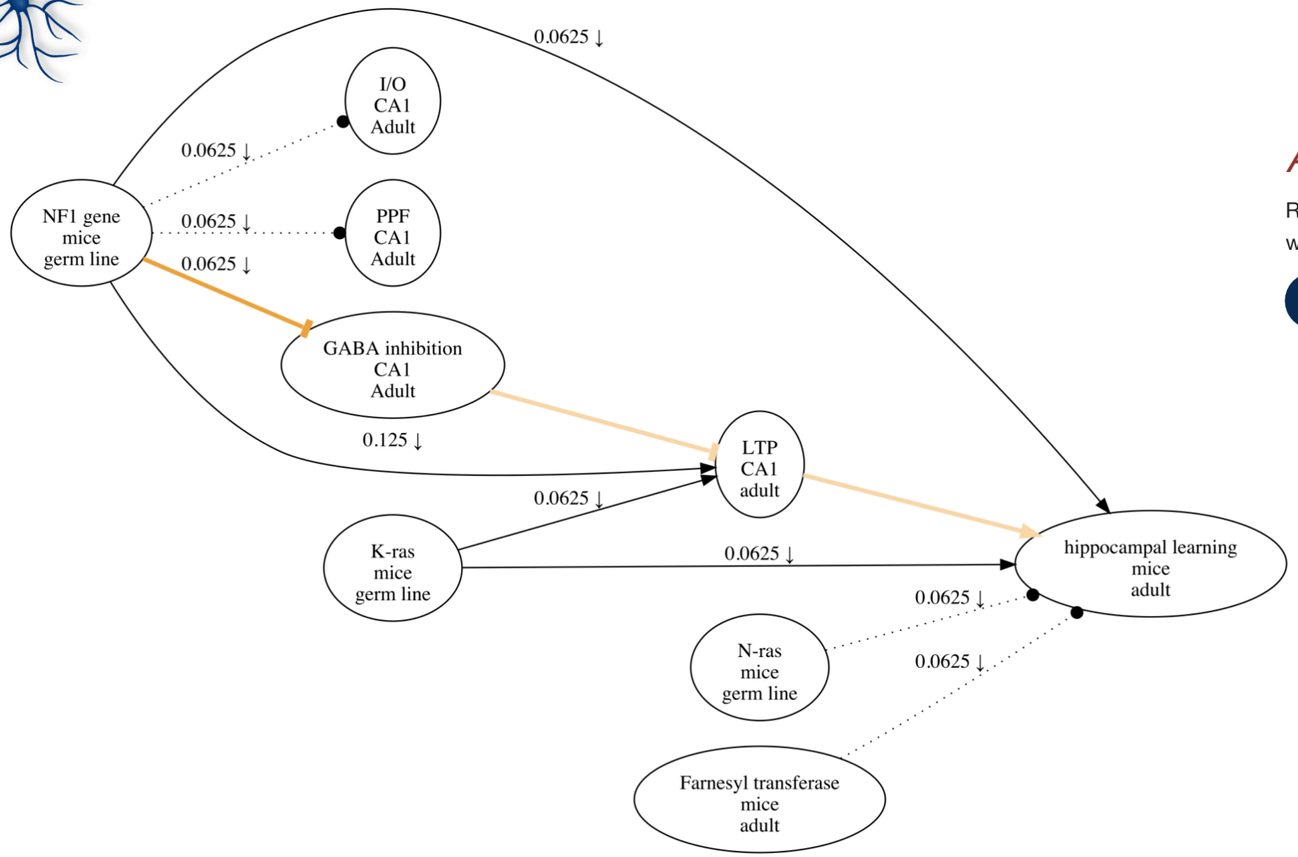

A tool for research planning

ResearchMaps integrates and summarizes large amounts of causal information with a searchable, graphical format.

SIGN UP FOR FREE!

Mechanism for the learning deficits in a mouse model of neurofibromatosis type 1.

Costa RM, Federov NB, Kogan JH, Murphy GG, Stern J, Ohno M, Kucherlapati R, Jacks T, Silva AJDepartments of Neurobiology, Psychiatry and Psychology, BRI, University of California at Los Angeles, Los Angeles, California 90095-1761, USA.

Nature 2002 Jan 31;415(6871):526-30

Search PubMed for this article

Add Experiment

Empirical | Hypothetical

Agent

What

Required

Where

Required

When

Required

Experiment

↑ ↓ ⌀↑ ⌀↓

Agent Approach

Required

Target

What

Required

Where

Required

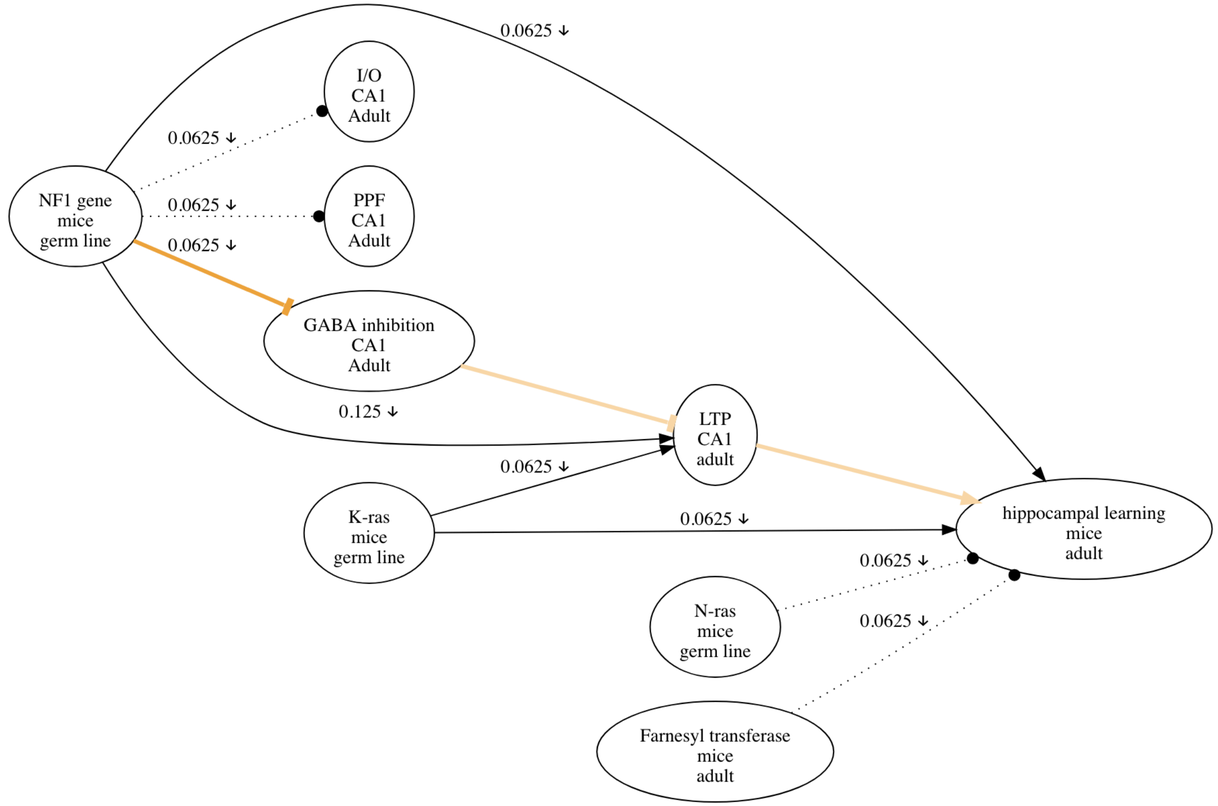

EMPIRICAL

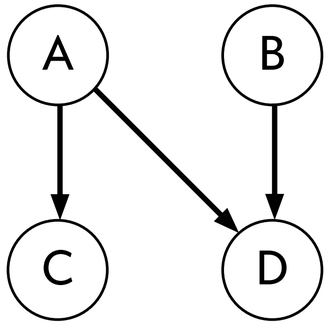

HYPOTHETICAL

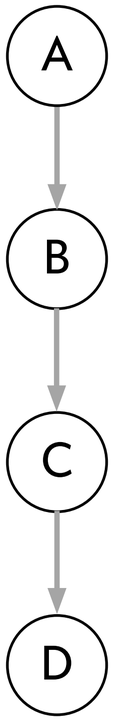

PATHWAY

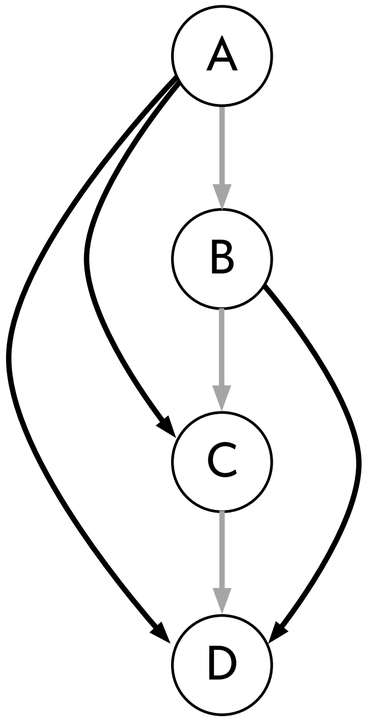

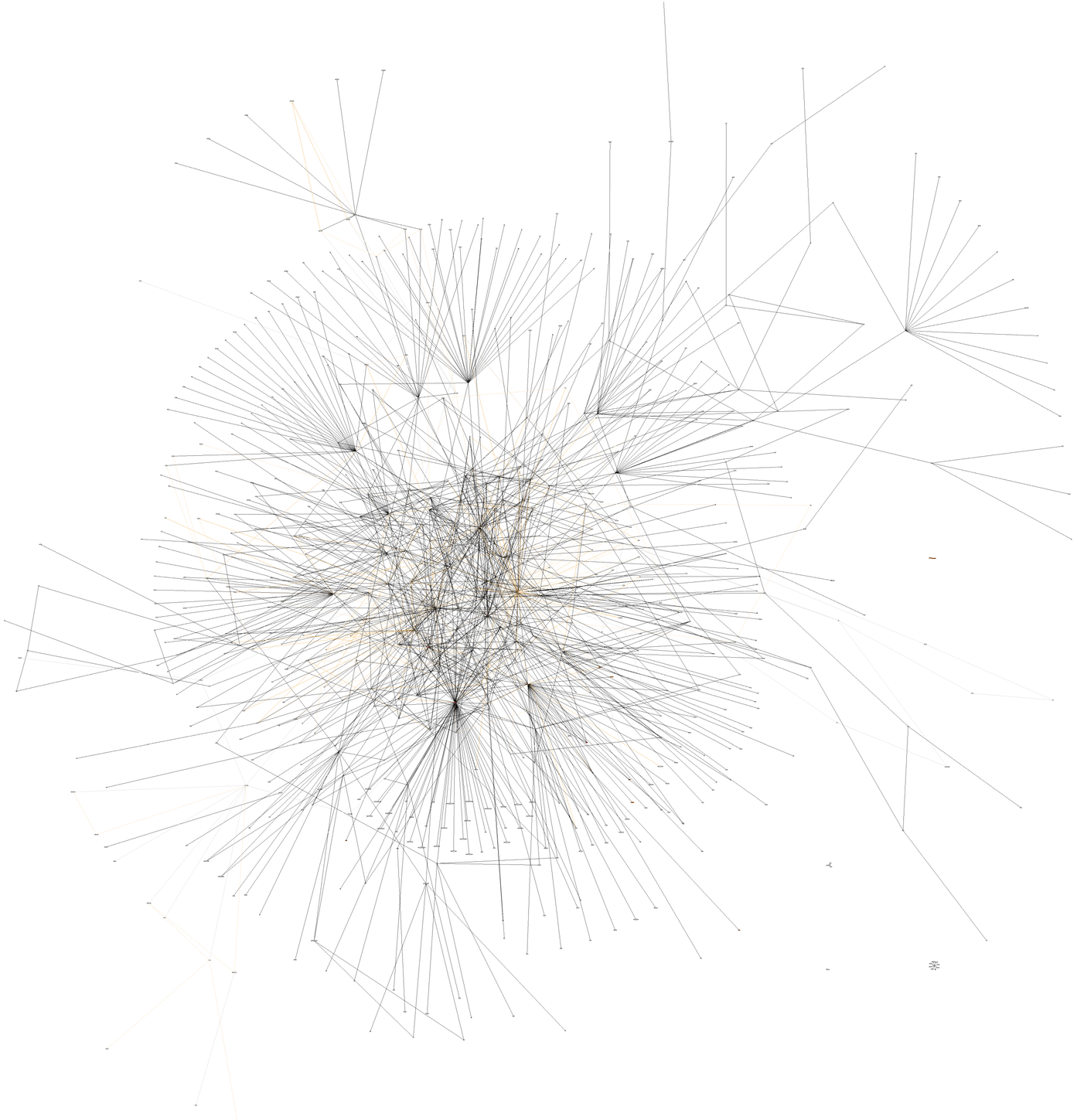

PUBLICATION

PLOS One 2018

PLOS ONE

RESEARCH ARTICLE

ResearchMaps.org for integrating and planning research

Nicholas J. Matiasz[1,2,3☯], Justin Wood[1,2,4☯], Pranay Doshi[1,4☯], William Speier[2,5], Barry Beckemeyer[1,4], Wei Wang[4], William Hsu[2,3], Alcino J. Silva[1,6,7,8,9*]

1 Department of Neurobiology, University of California Los Angeles, Los Angeles, California, United States of America, **2** Medical Imaging Informatics, Department of Radiological Sciences, University of California Los Angeles, Los Angeles, California, United States of America, **3** Department of Bioengineering, University of California Los Angeles, Los Angeles, CA, United States of America, **4** Department of Computer Science, University of California Los Angeles, Los Angeles, CA, United States of America, **5** Department of Neurosurgery, University of California Los Angeles, Los Angeles, CA, United States of America, **6** Department of Psychiatry & Biobehavioral Sciences, University of California Los Angeles, Los Angeles, California, United States of America, **7** Department of Psychology, University of California Los Angeles, Los Angeles, California, United States of America, **8** Integrative Center for Learning and Memory, University of California Los Angeles, Los Angeles, California, United States of America, **9** Brain Research Institute, University of California Los Angeles, Los Angeles, California, United States of America

☯ These authors contributed equally to this work.
* silvaa@mednet.ucla.edu

OPEN ACCESS

Citation: Matiasz NJ, Wood J, Doshi P, Speier W, Beckemeyer B, Wang W, et al. (2018) ResearchMaps.org for integrating and planning research. PLoS ONE 13(5): e0195271. https://doi.org/10.1371/journal.pone.0195271

Editor: Roeland M.H. Merks, Centrum Wiskunde & Informatica (CWI) & Netherlands Institute for Systems Biology, NETHERLANDS

Received: August 24, 2017

Accepted: March 19, 2018

Published: May 3, 2018

Data Availability Statement: All relevant data are within the paper, its Supporting Information files, and available at ResearchMaps.org and www.github.com/ResearchMaps.

Funding: This work was supported by the Leslie Chair in Pioneering Brain Research to AJS, an NIH T32 (T32EB016640-02) to NJM, an NIH-NCI T32 (T32CA201160) to JW, and NIH/NCATS UCLA Clinical and Translational Science Institute (CTSI) UL1TR000124 to both NJM and WH. The funders had no role in study design, data collection and

Abstract

To plan experiments, a biologist needs to evaluate a growing set of empirical findings and hypothetical assertions from diverse fields that use increasingly complex techniques. To address this problem, we operationalized principles (e.g., convergence and consistency) that biologists use to test causal relations and evaluate experimental evidence. With the framework we derived, we then created a free, open-source web application that allows biologists to create *research maps*, graph-based representations of empirical evidence and hypothetical assertions found in research articles, reviews, and other sources. With our *ResearchMaps* web application, biologists can systematically reason through the research that is most important to them, as well as evaluate and plan experiments with a breadth and precision that are unlikely without such a tool.

Introduction

Information in biology falls into at least two categories: (1) the information that individual biologists curate from articles they read, and (2) the vast body of other information that biologists can access, at least in principle, through resources like PubMed. Most informatics tools target the second category: the literature's accelerating growth makes it exceedingly impractical for biologists to find all the information that is relevant to their work. But even within the first category, it is ever more difficult for biologists to synthesize the information that they personally curate. Part of this challenge is caused by the increasing complexity of biological research.

Individual biologists must now keep track of empirical findings and hypothetical assertions from diverse fields that use a growing number of sophisticated techniques. Perhaps an even

MANUSCRIPT IN PREPARATION

Nature Comment

COMMENT · DD MM 2018

Quantifying the convergence of evidence

The replication crisis may be misdiagnosed. Science needs a more holistic view of evidence.

Nicholas J. Matiasz and Alcino J. Silva

For 40 years, meta-analysis has comprised increasingly sophisticated methods for quantifying an important aspect of evidence: its *consistency*, or replicability[1]. But meta-analysis does not explicitly quantify another crucial aspect of evidence: its *convergence*, the extent to which a hypothesis is supported by very different types of studies. This second aspect of evidence — often called *triangulation* — has long been acknowledged for its importance and has been highlighted recently as a strategy to address the replication crisis[2]. We prefer the term *convergence* because scientists can evaluate more than three different lines of evidence.

To address this gap in meta-analysis, we developed a Bayesian model of scientific consensus that expresses both consistency and convergence[3]. On the basis of this Bayesian model, we defined a numerical score called

Rules of integration in research maps:

consistency

convergence

divergence

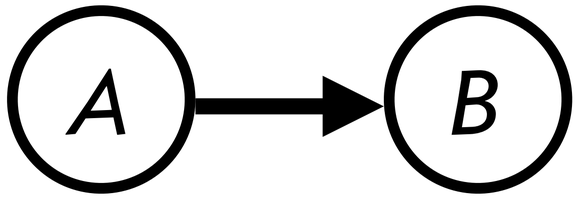

Rules of integration in research maps:

consistency

convergence

divergence

pioneering

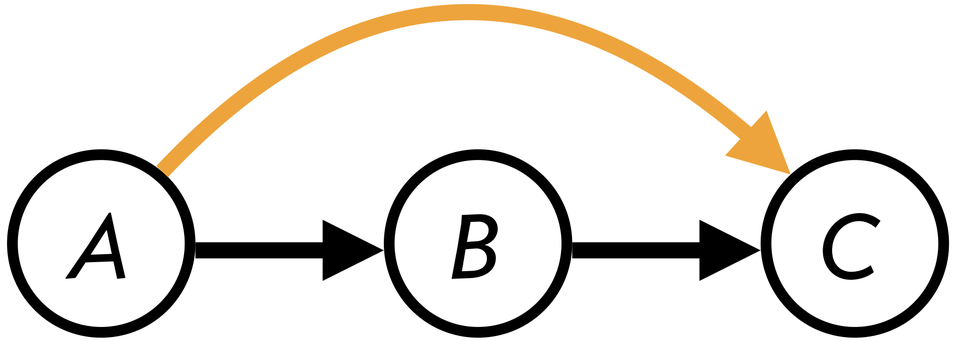

Rules of integration in research maps:

consistency

convergence

divergence

pioneering

weakest-link

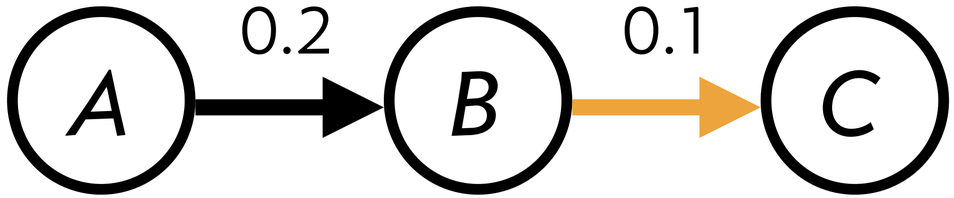

Rules of integration in research maps:

consistency

convergence

divergence

pioneering

weakest-link

multi-edge convergence

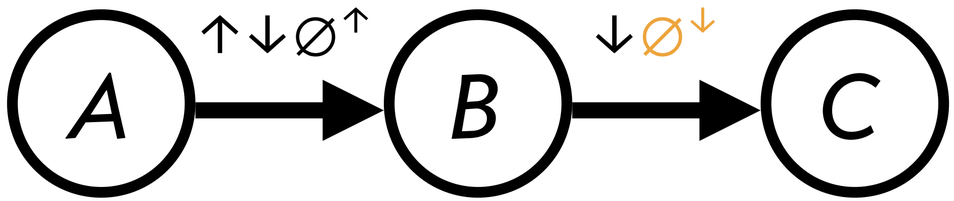

PUBLICATION

Frontiers in Neuroinformatics 2017

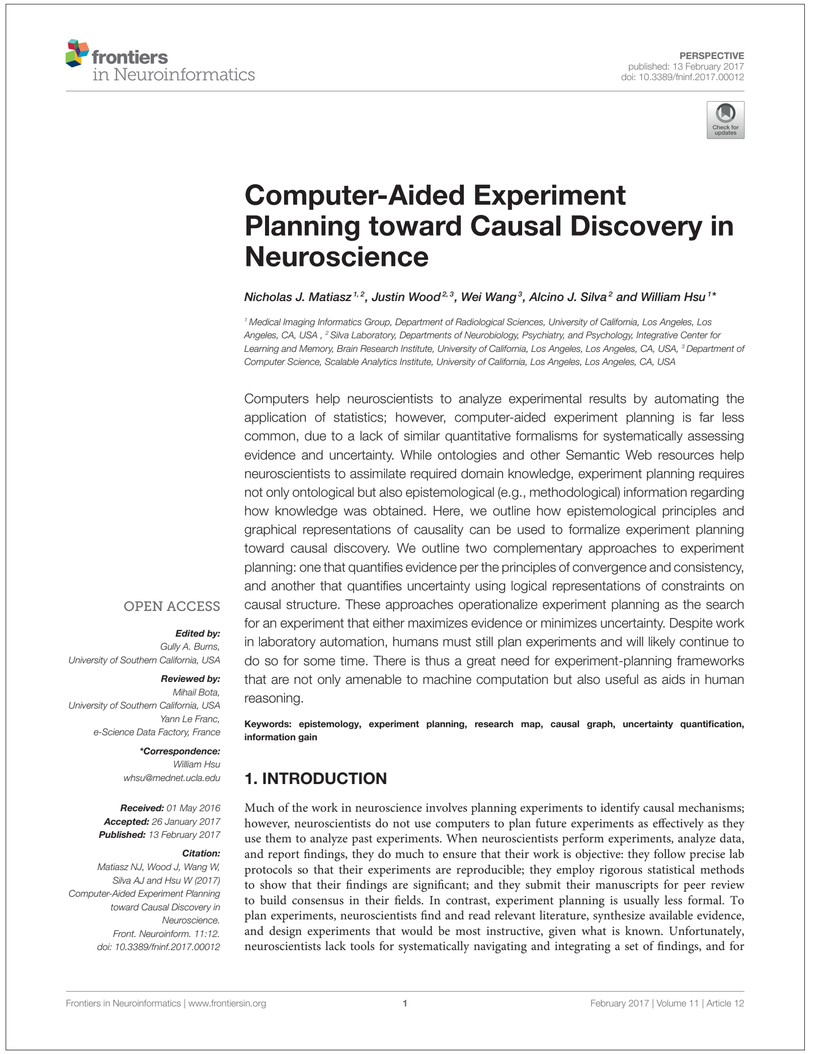

frontiers in Neuroinformatics

PERSPECTIVE
published: 13 February 2017
doi: 10.3389/fninf.2017.00012

Computer-Aided Experiment Planning toward Causal Discovery in Neuroscience

*Nicholas J. Matiasz[1,2], Justin Wood[2,3], Wei Wang[3], Alcino J. Silva[2] and William Hsu[1]**

[1] Medical Imaging Informatics Group, Department of Radiological Sciences, University of California, Los Angeles, Los Angeles, CA, USA , [2] Silva Laboratory, Departments of Neurobiology, Psychiatry, and Psychology, Integrative Center for Learning and Memory, Brain Research Institute, University of California, Los Angeles, Los Angeles, CA, USA, [3] Department of Computer Science, Scalable Analytics Institute, University of California, Los Angeles, Los Angeles, CA, USA

Computers help neuroscientists to analyze experimental results by automating the application of statistics; however, computer-aided experiment planning is far less common, due to a lack of similar quantitative formalisms for systematically assessing evidence and uncertainty. While ontologies and other Semantic Web resources help neuroscientists to assimilate required domain knowledge, experiment planning requires not only ontological but also epistemological (e.g., methodological) information regarding how knowledge was obtained. Here, we outline how epistemological principles and graphical representations of causality can be used to formalize experiment planning toward causal discovery. We outline two complementary approaches to experiment planning: one that quantifies evidence per the principles of convergence and consistency, and another that quantifies uncertainty using logical representations of constraints on causal structure. These approaches operationalize experiment planning as the search for an experiment that either maximizes evidence or minimizes uncertainty. Despite work in laboratory automation, humans must still plan experiments and will likely continue to do so for some time. There is thus a great need for experiment-planning frameworks that are not only amenable to machine computation but also useful as aids in human reasoning.

Keywords: epistemology, experiment planning, research map, causal graph, uncertainty quantification, information gain

OPEN ACCESS

Edited by:
Gully A. Burns,
University of Southern California, USA

Reviewed by:
Mihail Bota,
University of Southern California, USA
Yann Le Franc,
e-Science Data Factory, France

****Correspondence:***
William Hsu
whsu@mednet.ucla.edu

Received: *01 May 2016*
Accepted: *26 January 2017*
Published: *13 February 2017*

Citation:
Matiasz NJ, Wood J, Wang W, Silva AJ and Hsu W (2017) Computer-Aided Experiment Planning toward Causal Discovery in Neuroscience. Front. Neuroinform. 11:12. doi: 10.3389/fninf.2017.00012

1. INTRODUCTION

Much of the work in neuroscience involves planning experiments to identify causal mechanisms; however, neuroscientists do not use computers to plan future experiments as effectively as they use them to analyze past experiments. When neuroscientists perform experiments, analyze data, and report findings, they do much to ensure that their work is objective: they follow precise lab protocols so that their experiments are reproducible; they employ rigorous statistical methods to show that their findings are significant; and they submit their manuscripts for peer review to build consensus in their fields. In contrast, experiment planning is usually less formal. To plan experiments, neuroscientists find and read relevant literature, synthesize available evidence, and design experiments that would be most instructive, given what is known. Unfortunately, neuroscientists lack tools for systematically navigating and integrating a set of findings, and for

CONTRIBUTIONS

1. Cumulative evidence index (CEI)
2. Meta-analytic causal discovery
3. Heuristics for experiment planning

WHEN SCIENTISTS SEEK TO LEARN NEW, interesting truths, to find important patterns hiding in vast arrays of data, they are often trying to do something like searching for a needle in a really huge haystack of falsehoods, for a correct network among many possible networks…

—CLARK GLYMOUR

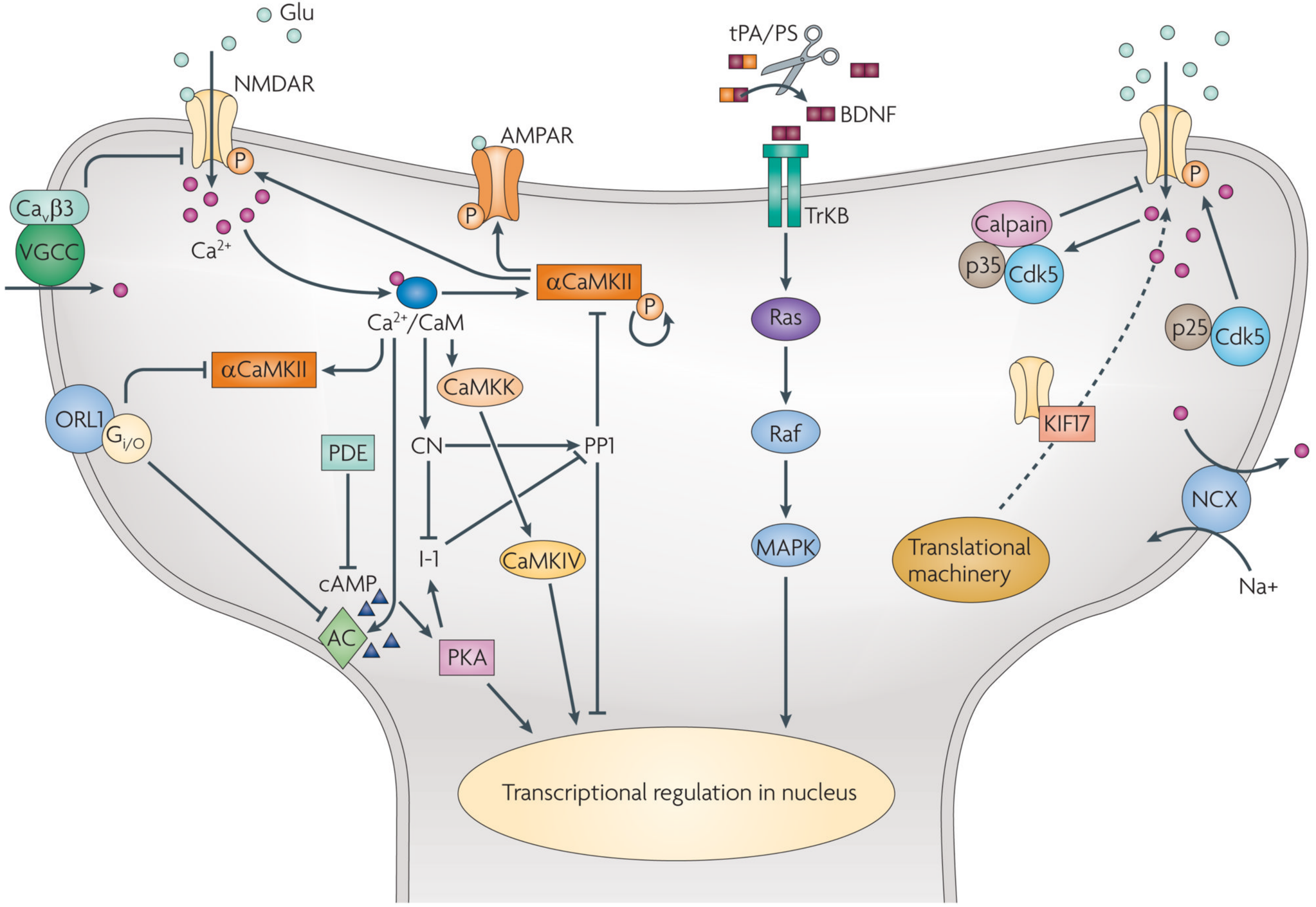
Glu
NMDAR
P
$Ca_v\beta3$
VGCC
Ca^{2+}
AMPAR
P
tPA/PS
BDNF
TrKB
Ras
Raf
MAPK
Calpain
p35
Cdk5
p25
Cdk5
P
αCaMKII
P
Ca^{2+}/CaM
αCaMKII
CaMKK
ORL1
$G_{i/O}$
PDE
CN
PP1
I-1
CaMKIV
cAMP
AC
PKA
KIF17
Translational machinery
NCX
Na+
Transcriptional regulation in nucleus

Biological pathway diagrams can’t be stitched together

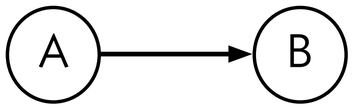

diagram 1

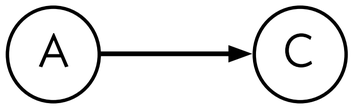

diagram 2

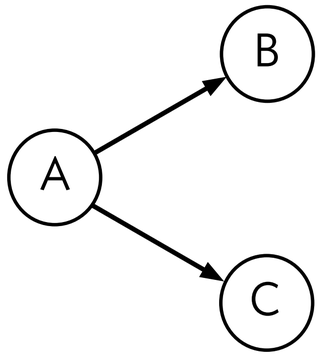

stitched diagram

Biological pathway diagrams can’t be stitched together

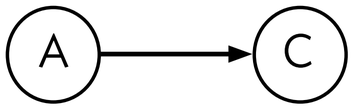

diagram 1

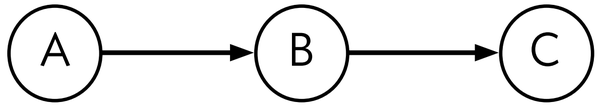

diagram 2

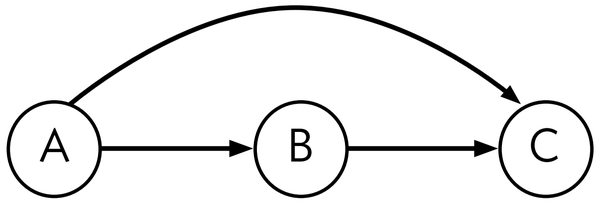

stitched diagram

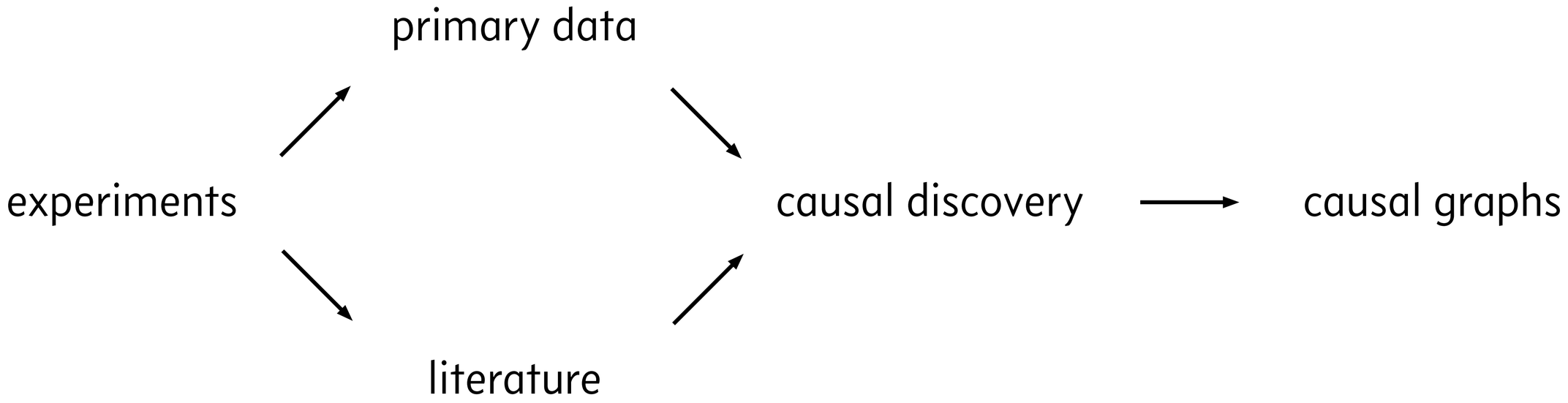
primary data
experiments
causal discovery
causal graphs
literature

Meta-analytic causal discovery & experiment selection

literature

research maps

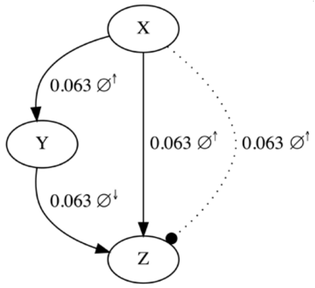

(in)dependencies

$$X \not\perp\!\!\!\perp Y \mid \varnothing \,||\, \varnothing$$

$$Y \not\perp\!\!\!\perp Z \mid \varnothing \,||\, \varnothing$$

$$X \not\perp\!\!\!\perp Z \mid \varnothing \,||\, \varnothing$$

$$X \perp\!\!\!\perp Z \mid Y \,||\, \varnothing$$

causal graphs

$$X \longrightarrow Y \longrightarrow Z$$

$$X \longleftarrow Y \longrightarrow Z$$

$$X \longleftarrow Y \longleftarrow Z$$

degrees of freedom

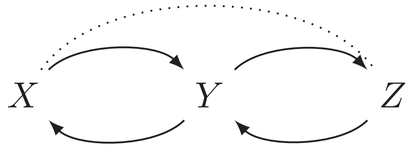

What information in the literature can provide constraints on the causal structure of the system?

literature → research maps → (in)dependencies → causal graphs → degrees of freedom

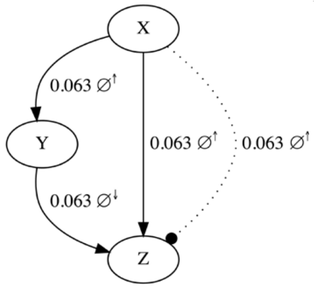

$$X \not\perp\!\!\!\perp Y \mid \varnothing \,||\, \varnothing$$
$$Y \not\perp\!\!\!\perp Z \mid \varnothing \,||\, \varnothing$$
$$X \not\perp\!\!\!\perp Z \mid \varnothing \,||\, \varnothing$$
$$X \perp\!\!\!\perp Z \mid Y \,||\, \varnothing$$

$X \longrightarrow Y \longrightarrow Z$

$X \longleftarrow Y \longrightarrow Z$

$X \longleftarrow Y \longleftarrow Z$

Findings in the literature can be expressed as statistical (in)dependence statements

33. The authors thank A. R. Pearson, B. J. Johnson, C. M. Wilmot, and D. H. Ohlendorf for their guidance and critical discussions during the course of this work, and J. C. Nix for technical assistance in data collection. This work was supported by National Institute of General Medical Sciences GM24689. We are grateful for beam time and assistance with x-ray data collection at the Lawrence Berkeley Laboratory Advanced Light Source (ALS), and for facilities and computer support from the Minnesota Supercomputing Institute. Coordinates have been deposited in the Protein Data Bank (PDB) [www.rcsb.org/pdb] as entries 2IG9 (full-length enzyme) and 2IGA (enzyme reacted with 4NC and O_2).

Supporting Online Material
www.sciencemag.org/cgi/content/full/316/5823/453/DC1
Materials and Methods
SOM Text
Figs. S1 to S5
Tables S1 to S3
References

5 September 2006; accepted 12 February 2007
10.1126/science.1134697

Neuronal Competition and Selection During Memory Formation

Jin-Hee Han,[1,2,3]* Steven A. Kushner,[4,5,6]* Adelaide P. Yiu,[1,3] Christy J. Cole,[1,2] Anna Matynia,[4] Robert A. Brown,[4] Rachael L. Neve,[7] John F. Guzowski,[8] Alcino J. Silva,[4] Sheena A. Josselyn[1,2,3]†

Competition between neurons is necessary for refining neural circuits during development and may be important for selecting the neurons that participate in encoding memories in the adult brain. To examine neuronal competition during memory formation, we conducted experiments with mice in which we manipulated the function of CREB (adenosine 3′,5′-monophosphate response element–binding protein) in subsets of neurons. Changes in CREB function influenced the probability that individual lateral amygdala neurons were recruited into a fear memory trace. Our results suggest a competitive model underlying memory formation, in which eligible neurons are selected to participate in a memory trace as a function of their relative CREB activity at the time of learning.

Competition is a fundamental property of many biological systems and creates selective pressure between individual elements. For example, competition between bilateral monocular neural inputs mediates ocular dominance plasticity (*1*, *2*). The transcription factor CREB (adenosine 3′,5′-monophosphate response element–binding protein) has been implicated in this competition in the developing brain (*3*, *4*). The finding that only a portion of eligible neurons participate in a given memory (*5*–*8*) suggests that competition between neurons may also underlie plasticity in adult brain.

Plasticity within the lateral amygdala (LA) is required for auditory conditioned-fear memories (*7*, *9*–*11*). Although ~70% of LA neurons receive the necessary sensory input, only one-quarter exhibit auditory fear conditioning–induced plasticity (*6*, *7*). We found that a similar proportion of LA cells show activated CREB (phosphorylation at Ser^{133}) after auditory fear conditioning (Fig. 1A), which suggests a role for CREB in determining which neurons are recruited into the fear memory trace. To examine this result, we manipulated CREB function in a similar portion of LA neurons by microinjecting replication-defective herpes simplex viral vectors expressing endogenous or dominant-negative CREB ($CREB^{WT}$ and $CREB^{S133A}$, respectively) fused with green fluorescent protein (GFP) (*12*).

To maximize the relative difference in CREB function between neurons, we first increased CREB levels in a subset of LA neurons in mutant mice that have reduced CREB function. Mice lacking the major isoforms of CREB (α and δ; CREB-deficient mice) show deficits in developmental and adult plasticity, including auditory fear memory (*13*, *14*) (Fig. 1B and fig. S1A). We microinjected $CREB^{WT}$ or control vector into the LA of CREB-deficient or wild-type littermate mice before fear conditioning and assessed memory (the percentage of time mice spent freezing during subsequent tone presentation) 24 hours later. Although $CREB^{WT}$ vector

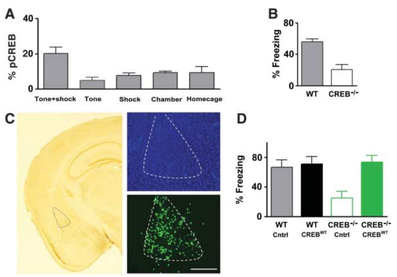

Fig. 1. Auditory fear conditioning activates CREB in ~20% of LA cells in wild-type (WT) mice; increasing CREB function in a similar portion of LA neurons rescues the fear memory deficit in CREB-deficient mice. (**A**) Percentages of LA cells expressing phosphorylated CREB after fear conditioning (tone + shock, $n = 6$) was higher than after control conditions [tone alone ($n = 4$), immediate shock ($n = 4$), exposure to chamber ($n = 4$), or homecage control ($n = 4$), $F(4,17) = 5.36$, $P < 0.05$]. Error bars in all figures represent SEM. (**B**) CREB-deficient ($CREB^{-/-}$) mice show impaired auditory fear memory [$F(1,20) = 24.23$, $P < 0.05$; WT $n = 12$, CREB-deficient $n = 10$]. (**C**) Left: Outline of the LA. Right: Roughly 20% of LA neurons expressed GFP after infusion of $CREB^{WT}$ vector [top, nuclei stained with 4′,6′-diamidino-2-phenylindole (DAPI); bottom, GFP]. Scale bar, 250 μm. (**D**) Microinjection of control vector (Cntrl; $n = 8$) or $CREB^{WT}$ vector ($n = 9$) did not change the high freezing in WT mice, whereas microinjection of $CREB^{WT}$ vector ($n = 9$), but not control vector ($n = 8$), into the LA of CREB-deficient mice rescued this memory deficit [Genotype × Vector $F(1,30) = 6.64$, $P < 0.05$].

[1]Program in Neurosciences and Mental Health, Hospital for Sick Children, 555 University Avenue, Toronto, Ontario M5G 1X8, Canada. [2]Department of Physiology, University of Toronto, Toronto, Ontario M5S 1A8, Canada. [3]Institute of Medical Sciences, University of Toronto, Toronto, Ontario M5S 1A8, Canada. [4]Departments of Neurobiology, Psychology, and Psychiatry, and Brain Research Institute, Gonda Building, 695 Young Drive South, University of California, Los Angeles, CA 90095, USA. [5]Department of Psychiatry, Columbia University, New York, NY 10032, USA. [6]New York State Psychiatric Institute, New York, NY 10032, USA. [7]Molecular Neurogenetics Laboratory, Department of Psychiatry, Harvard Medical School, McLean Hospital, Belmont, MA 02478, USA. [8]Neurobiology and Behavior, School of Biological Sciences, University of California, Irvine, CA 92697, USA.

*These authors contributed equally to this work.
†To whom correspondence should be addressed. E-mail: sheena.josselyn@sickkids.ca

the effects of increasing CREB function in wild-type mice. Increasing CREB function enhanced memory (Fig. 3A), consistent with results in flies (*16*), *Aplysia* (*17*), rats (*18*, *19*), and hamsters (*20*). Furthermore, the probability of detecting Arc^+ nuclei was higher by a factor of ~3 in neurons with $CREB^{WT}$ vector (65.8 ± 5.0%) than in neighboring neurons (21.9 ± 4.2%) (Fig. 3A and fig. S3), similar to the distribution of Arc observed in wild-type mice trained with a more intense protocol.

These imaging data could be simply explained if increasing CREB function directly induces *Arc* transcription. Previous findings do not support this idea (*21*), likely because the *Arc* promoter lacks a consensus CRE site (*22*). Nonetheless, to examine whether neurons with increased CREB function were more likely than their neighbors to be Arc^+ independent of fear conditioning, we microinjected $CREB^{WT}$ vector into the LA of wild-type mice that were not fear-conditioned. If increasing CREB function is sufficient to induce *Arc* expression, then neurons with $CREB^{WT}$ vector should be more likely than neighboring neurons to be Arc^+. However, the distribution of Arc^+ nuclei was similar in neurons with and without $CREB^{WT}$ vector in these homecage mice (Fig. 3B). Because CREB may not be transcriptionally active under these conditions, we infused a vector encoding a constitutively active form of CREB [$CREB^{Y134F}$ (*23*)]. Again, neurons with increased CREB function (with $CREB^{Y134F}$ vector) were no more likely to be Arc^+ than their neighbors (Fig. 3C). Therefore, increasing CREB function in a subset of LA neurons in untrained mice does not affect the distribution of Arc, which highlights the importance of training and learning (fig. S4) in the preferential localization of Arc in neurons with increased CREB function.

Alternatively, neurons with increased CREB function may have a lower threshold for inducing *Arc* transcription that only becomes apparent in the fear memory test. We therefore microinjected wild-type mice with $CREB^{WT}$ vector 24 hours after training. Mice were tested 4 days after infusion and the distribution of Arc^+ was quantified. If the fear memory trace is consolidated in the LA within 24 hours after training (*24*, *25*), a preferential distribution of Arc in neurons with increased CREB function would not be expected. Although Arc^+ levels were comparable to those found in previous experiments in which wild-type mice were fear-conditioned (25.4 ± 4.0%), Arc was not preferentially localized in neurons with increased CREB function [$CREB^{WT}$ vector = 9.7 ± 1.6%, endogenous = 28.4 ± 3.7%, $F(1,4) = 27.58$, $P < 0.05$]. Together, these data suggest that increased CREB function enhances neuronal selection only during sufficiently salient learning.

We next investigated the effects of decreasing CREB function in a similar portion of LA neurons. We hypothesized that memory would be normal because the remaining neurons with intact CREB function would outcompete this subset for inclusion in the memory trace. Wild-type mice were microinjected with a vector expressing a dominant-negative form of CREB ($CREB^{S133A}$) before auditory fear training. Indeed, these mice showed normal memory (Fig. 3D). Consistent with this, the probability of detecting Arc^+ nuclei was lower by a factor of ~12 in neurons with $CREB^{S133A}$ vector (2.7 ± 0.6%) than in neurons without it (33.7 ± 0.9%) (Fig. 3D).

Together, these data provide evidence for neuronal selection during memory formation. The overall size of the Arc^+ fear memory trace was both consistent with electrophysiological estimates of the fear memory trace (*6*, *7*) and stable across experiments in fear-conditioned wild-type mice (Fig. 4A). That a constant proportion of LA neurons is recruited to the memory trace, regardless of CREB manipulation, suggests that the rules governing neuronal selection during memory formation are competitive rather than cell-autonomous. If neuronal selection were cell-autonomous, the size of the Arc^+ memory trace

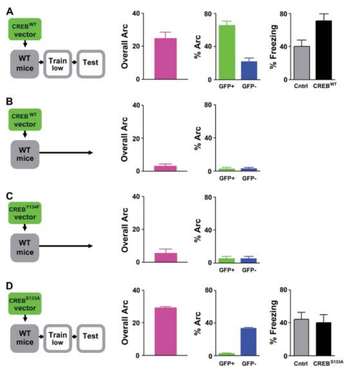

Fig. 3. Relative CREB function influences the recruitment of neurons into the memory trace. (**A**) Left: Proportion of Arc^+ LA neurons in WT mice with $CREB^{WT}$ vector. Middle: Arc^+ nuclei were more likely to be in neurons with $CREB^{WT}$ vector (GFP^+) than in noninfected (GFP^-) neurons [$F(1,3) = 23.62$, $P < 0.05$]. Right: $CREB^{WT}$ vector enhanced memory in WT mice trained with low-intensity shock [$F(1,11) = 7.31$, $P < 0.05$, control $n = 7$, $CREB^{WT}$ vector $n = 6$]. (**B** and **C**) Middle: Proportion of Arc^+ LA neurons in untrained WT mice with $CREB^{WT}$ (B) or constitutively active $CREB^{Y134F}$ (C) vector. Left: Neurons containing $CREB^{WT}$ (B) or constitutively active $CREB^{Y134F}$ (C) vector (GFP^+) were no more likely than noninfected neurons (GFP^-) to be Arc^+ in untrained mice ($P > 0.05$). (**D**) Neurons with decreased CREB function were less likely to be recruited to the memory trace. Left: Proportion of Arc^+ LA neurons. Middle: Arc^+ nuclei were less likely to be in neurons with $CREB^{S133A}$ vector (GFP^+) than in noninfected neurons (GFP^-) [$F(1,2) = 405.28$, $P < 0.05$]. Right: WT mice infused with $CREB^{S133A}$ vector show normal memory, even when trained with a lower-intensity shock [$F(1,13) = 2.08$, $P > 0.05$; control $n = 7$, $CREB^{S133A}$ $n = 8$].

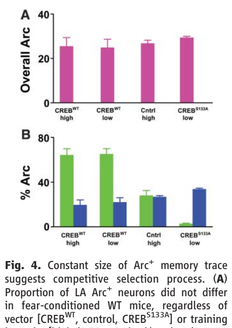

Fig. 4. Constant size of Arc^+ memory trace suggests competitive selection process. (**A**) Proportion of LA Arc^+ neurons did not differ in fear-conditioned WT mice, regardless of vector [$CREB^{WT}$, control, $CREB^{S133A}$] or training intensity [high (0.75-mA shock) or low (0.4-mA shock)] [$F(3,12) = 0.31$, $P < 0.05$]. (**B**) Distribution of Arc^+ varied according to CREB manipulation. First and second pairs of bars: Arc^+ nuclei were more likely to be in neurons with high CREB function (with $CREB^{WT}$ vector; GFP^+, green) than in noninfected neighbors (GFP^-, blue) in WT mice trained with high (first pair) or low (third pair) intensities. Third pair of bars: Arc^+ nuclei were equally distributed in neurons with (GFP^+, green) and without (GFP^-, blue) control vector. Fourth pair of bars: Arc^+ nuclei were less likely to be in neurons with decreased CREB function (with $CREB^{S133A}$ vector; GFP^+, green) relative to neighbors with intact CREB function (GFP^-, blue).

Findings in the literature can be expressed as statistical (in)dependence statements

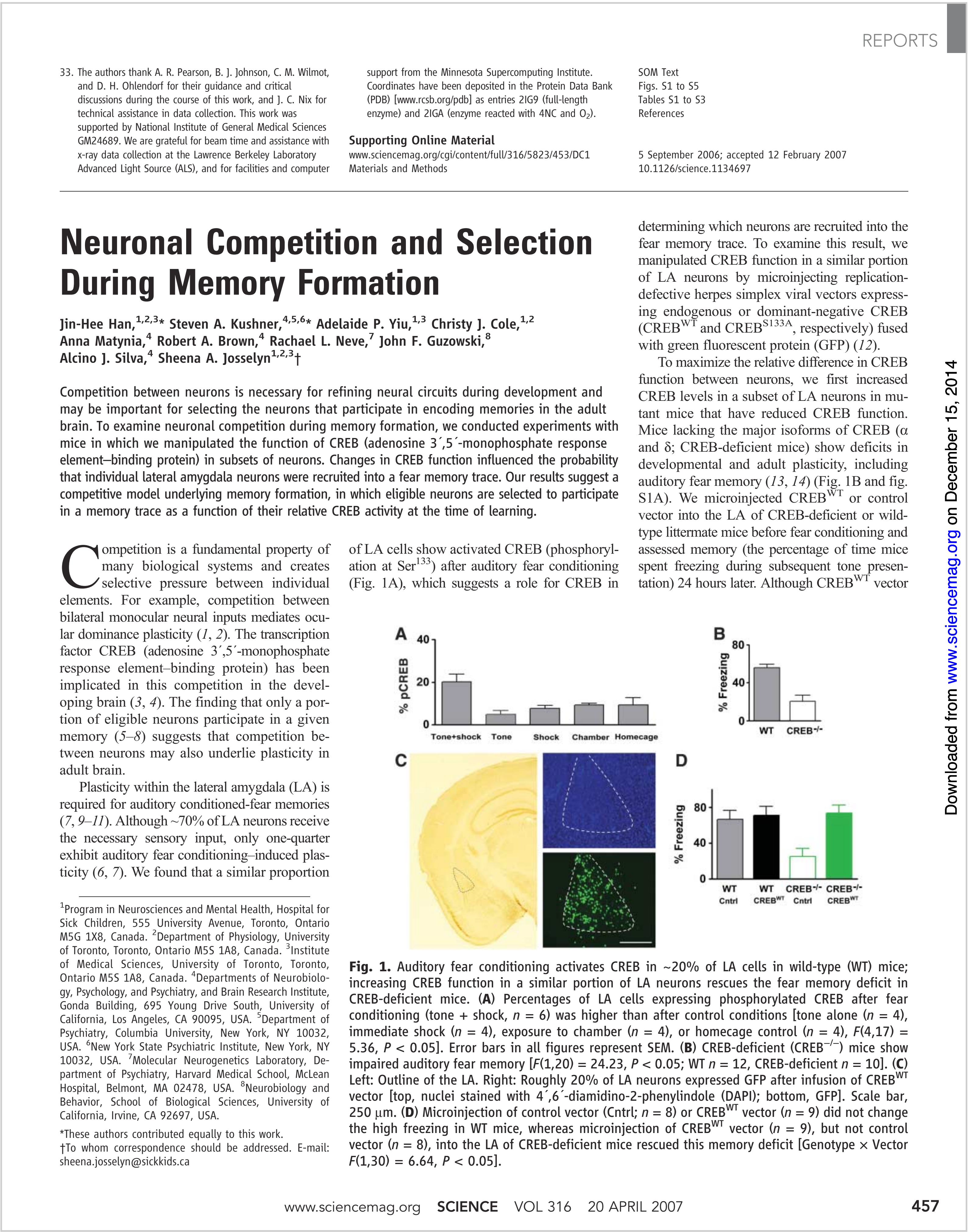

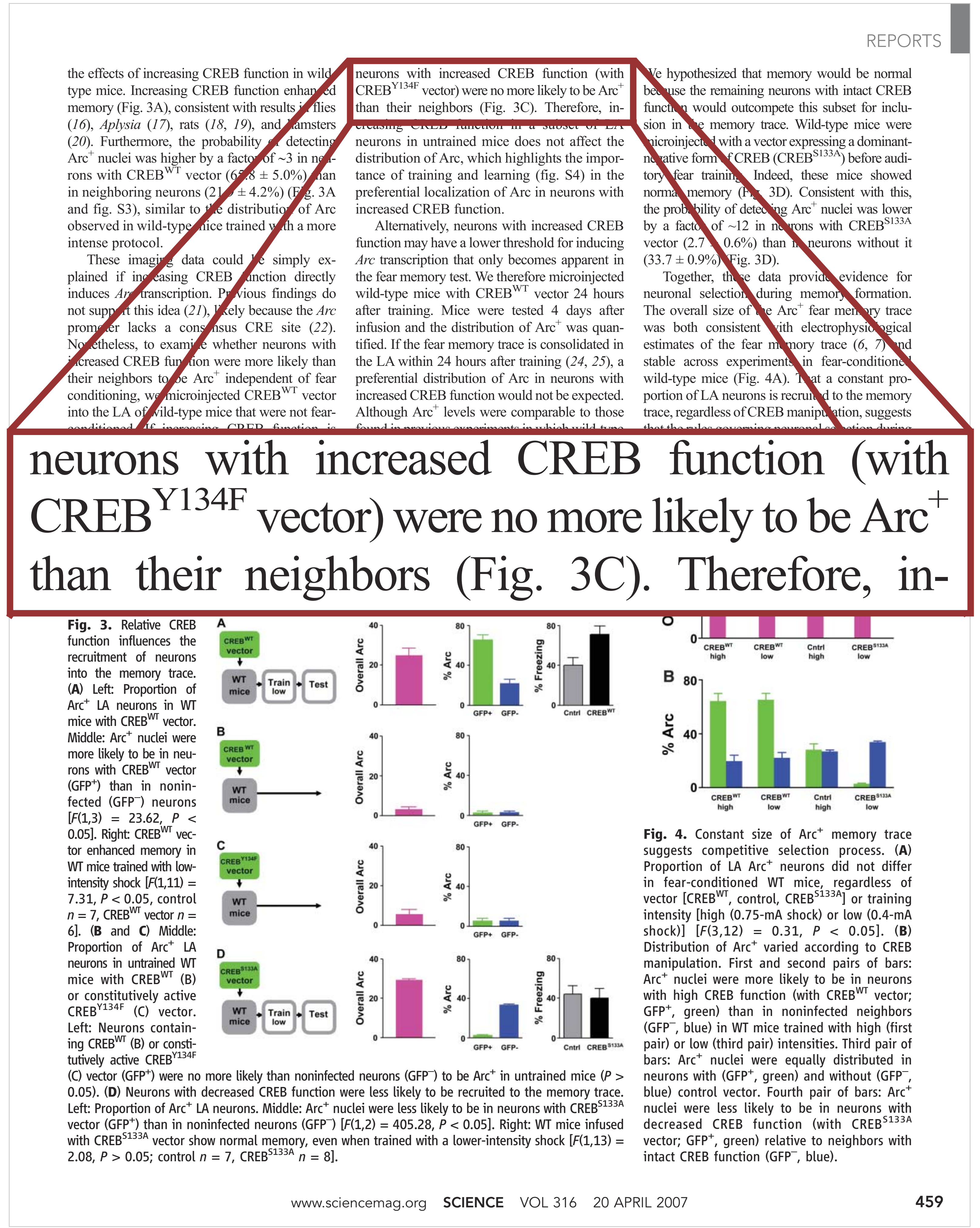

neurons with increased CREB function (with CREB^{Y134F} vector) were no more likely to be Arc^{+} than their neighbors (Fig. 3C). Therefore, in-

Findings in the literature can be expressed as statistical (in)dependence statements

33. The authors thank A. R. Pearson, B. J. Johnson, C. M. Wilmot, and D. H. Ohlendorf for their guidance and critical discussions during the course of this work, and J. C. Nix for technical assistance in data collection. This work was supported by National Institute of General Medical Sciences GM24689. We are grateful for beam time and assistance with x-ray data collection at the Lawrence Berkeley Laboratory Advanced Light Source (ALS), and for facilities and computer support from the Minnesota Supercomputing Institute. Coordinates have been deposited in the Protein Data Bank (PDB) [www.rcsb.org/pdb] as entries 2IG9 (full-length enzyme) and 2IGA (enzyme reacted with 4NC and O_2).

Supporting Online Material
www.sciencemag.org/cgi/content/full/316/5823/453/DC1
Materials and Methods
SOM Text
Figs. S1 to S5
Tables S1 to S3
References

5 September 2006; accepted 12 February 2007
10.1126/science.1134697

Neuronal Competition and Selection During Memory Formation

Jin-Hee Han,[1,2,3]* Steven A. Kushner,[4,5,6]* Adelaide P. Yiu,[1,3] Christy J. Cole,[1,2] Anna Matynia,[4] Robert A. Brown,[4] Rachael L. Neve,[7] John F. Guzowski,[8] Alcino J. Silva,[4] Sheena A. Josselyn[1,2,3]†

Competition between neurons is necessary for refining neural circuits during development and may be important for selecting the neurons that participate in encoding memories in the adult brain. To examine neuronal competition during memory formation, we conducted experiments with mice in which we manipulated the function of CREB (adenosine 3′,5′-monophosphate response element–binding protein) in subsets of neurons. Changes in CREB function influenced the probability that individual lateral amygdala neurons were recruited into a fear memory trace. Our results suggest a competitive model underlying memory formation, in which eligible neurons are selected to participate in a memory trace as a function of their relative CREB activity at the time of learning.

Competition is a fundamental property of many biological systems and creates selective pressure between individual elements. For example, competition between bilateral monocular neural inputs mediates ocular dominance plasticity (*1*, *2*). The transcription factor CREB (adenosine 3′,5′-monophosphate response element–binding protein) has been implicated in this competition in the developing brain (*3*, *4*). The finding that only a portion of eligible neurons participate in a given memory (*5*–*8*) suggests that competition between neurons may also underlie plasticity in adult brain.

Plasticity within the lateral amygdala (LA) is required for auditory conditioned-fear memories (*7*, *9*–*11*). Although ~70% of LA neurons receive the necessary sensory input, only one-quarter exhibit auditory fear conditioning–induced plasticity (*6*, *7*). We found that a similar proportion of LA cells show activated CREB (phosphorylation at Ser^{133}) after auditory fear conditioning (Fig. 1A), which suggests a role for CREB in determining which neurons are recruited into the fear memory trace. To examine this result, we manipulated CREB function in a similar portion of LA neurons by microinjecting replication-defective herpes simplex viral vectors expressing endogenous or dominant-negative CREB ($CREB^{WT}$ and $CREB^{S133A}$, respectively) fused with green fluorescent protein (GFP) (*12*).

To maximize the relative difference in CREB function between neurons, we first increased CREB levels in a subset of LA neurons in mutant mice that have reduced CREB function. Mice lacking the major isoforms of CREB (α and δ; CREB-deficient mice) show deficits in developmental and adult plasticity, including auditory fear memory (*13*, *14*) (Fig. 1B and fig. S1A). We microinjected $CREB^{WT}$ or control vector into the LA of CREB-deficient or wild-type littermate mice before fear conditioning and assessed memory (the percentage of time mice spent freezing during subsequent tone presentation) 24 hours later. Although $CREB^{WT}$ vector

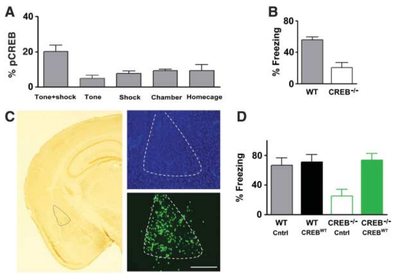

Fig. 1. Auditory fear conditioning activates CREB in ~20% of LA cells in wild-type (WT) mice; increasing CREB function in a similar portion of LA neurons rescues the fear memory deficit in CREB-deficient mice. (**A**) Percentages of LA cells expressing phosphorylated CREB after fear conditioning (tone + shock, $n = 6$) was higher than after control conditions [tone alone ($n = 4$), immediate shock ($n = 4$), exposure to chamber ($n = 4$), or homecage control ($n = 4$), $F(4,17) = 5.36$, $P < 0.05$]. Error bars in all figures represent SEM. (**B**) CREB-deficient ($CREB^{-/-}$) mice show impaired auditory fear memory [$F(1,20) = 24.23$, $P < 0.05$; WT $n = 12$, CREB-deficient $n = 10$]. (**C**) Left: Outline of the LA. Right: Roughly 20% of LA neurons expressed GFP after infusion of $CREB^{WT}$ vector [top, nuclei stained with 4′,6′-diamidino-2-phenylindole (DAPI); bottom, GFP]. Scale bar, 250 μm. (**D**) Microinjection of control vector (Cntrl; $n = 8$) or $CREB^{WT}$ vector ($n = 9$) did not change the high freezing in WT mice, whereas microinjection of $CREB^{WT}$ vector ($n = 9$), but not control vector ($n = 8$), into the LA of CREB-deficient mice rescued this memory deficit [Genotype × Vector $F(1,30) = 6.64$, $P < 0.05$].

[1]Program in Neurosciences and Mental Health, Hospital for Sick Children, 555 University Avenue, Toronto, Ontario M5G 1X8, Canada. [2]Department of Physiology, University of Toronto, Toronto, Ontario M5S 1A8, Canada. [3]Institute of Medical Sciences, University of Toronto, Toronto, Ontario M5S 1A8, Canada. [4]Departments of Neurobiology, Psychology, and Psychiatry, and Brain Research Institute, Gonda Building, 695 Young Drive South, University of California, Los Angeles, CA 90095, USA. [5]Department of Psychiatry, Columbia University, New York, NY 10032, USA. [6]New York State Psychiatric Institute, New York, NY 10032, USA. [7]Molecular Neurogenetics Laboratory, Department of Psychiatry, Harvard Medical School, McLean Hospital, Belmont, MA 02478, USA. [8]Neurobiology and Behavior, School of Biological Sciences, University of California, Irvine, CA 92697, USA.

*These authors contributed equally to this work.
†To whom correspondence should be addressed. E-mail: sheena.josselyn@sickkids.ca

the effects of increasing CREB function in wild-type mice. Increasing CREB function enhanced memory (Fig. 3A), consistent with results in flies (*16*), *Aplysia* (*17*), rats (*18*, *19*), and hamsters (*20*). Furthermore, the probability of detecting Arc^+ nuclei was higher by a factor of ~3 in neurons with $CREB^{WT}$ vector (65.8 ± 5.0%) than in neighboring neurons (21.9 ± 4.2%) (Fig. 3A and fig. S3), similar to the distribution of Arc observed in wild-type mice trained with a more intense protocol.

These imaging data could be simply explained if increasing CREB function directly induces *Arc* transcription. Previous findings do not support this idea (*21*), likely because the *Arc* promoter lacks a consensus CRE site (*22*). Nonetheless, to examine whether neurons with increased CREB function were more likely than their neighbors to be Arc^+ independent of fear conditioning, we microinjected $CREB^{WT}$ vector into the LA of wild-type mice that were not fear-

neurons with increased CREB function (with $CREB^{Y134F}$ vector) were no more likely to be Arc^+ than their neighbors (Fig. 3C). Therefore, increasing CREB function in a subset of LA neurons in untrained mice does not affect the distribution of Arc, which highlights the importance of training and learning (fig. S4) in the preferential localization of Arc in neurons with increased CREB function.

Alternatively, neurons with increased CREB function may have a lower threshold for inducing *Arc* transcription that only becomes apparent in the fear memory test. We therefore microinjected wild-type mice with $CREB^{WT}$ vector 24 hours after training. Mice were tested 4 days after infusion and the distribution of Arc^+ was quantified. If the fear memory trace is consolidated in the LA within 24 hours after training (*24*, *25*), a preferential distribution of Arc in neurons with increased CREB function would not be expected. Although Arc^+ levels were comparable to those

We hypothesized that memory would be normal because the remaining neurons with intact CREB function would outcompete this subset for inclusion in the memory trace. Wild-type mice were microinjected with a vector expressing a dominant-negative form of CREB ($CREB^{S133A}$) before auditory fear training. Indeed, these mice showed normal memory (Fig. 3D). Consistent with this, the probability of detecting Arc^+ nuclei was lower by a factor of ~12 in neurons with $CREB^{S133A}$ vector (2.7 ± 0.6%) than in neurons without it (33.7 ± 0.9%) (Fig. 3D).

Together, these data provide evidence for neuronal selection during memory formation. The overall size of the Arc^+ fear memory trace was both consistent with electrophysiological estimates of the fear memory trace (*6*, *7*) and stable across experiments in fear-conditioned wild-type mice (Fig. 4A). That a constant proportion of LA neurons is recruited to the memory trace, regardless of CREB manipulation, suggests

neurons with increased CREB function (with $CREB^{Y134F}$ vector) were no more likely to be Arc^+ than their neighbors (Fig. 3C). Therefore, in-

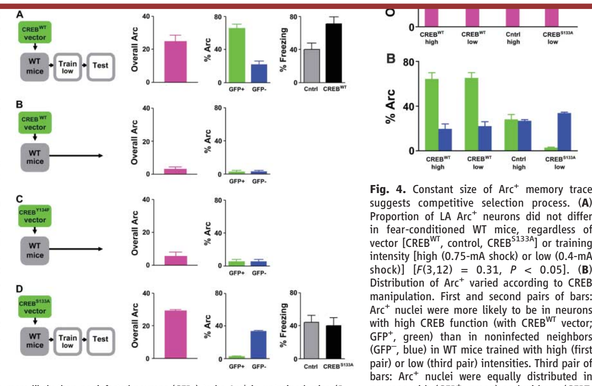

Fig. 3. Relative CREB function influences the recruitment of neurons into the memory trace. (**A**) Left: Proportion of Arc^+ LA neurons in WT mice with $CREB^{WT}$ vector. Middle: Arc^+ nuclei were more likely to be in neurons with $CREB^{WT}$ vector (GFP^+) than in noninfected (GFP^-) neurons [$F(1,3) = 23.62$, $P < 0.05$]. Right: $CREB^{WT}$ vector enhanced memory in WT mice trained with low-intensity shock [$F(1,11) = 7.31$, $P < 0.05$, control $n = 7$, $CREB^{WT}$ vector $n = 6$]. (**B** and **C**) Middle: Proportion of Arc^+ LA neurons in untrained WT mice with $CREB^{WT}$ (B) or constitutively active $CREB^{Y134F}$ (C) vector. Left: Neurons containing $CREB^{WT}$ (B) or constitutively active $CREB^{Y134F}$ (C) vector (GFP^+) were no more likely than noninfected neurons (GFP^-) to be Arc^+ in untrained mice ($P > 0.05$). (**D**) Neurons with decreased CREB function were less likely to be recruited to the memory trace. Left: Proportion of Arc^+ LA neurons. Middle: Arc^+ nuclei were less likely to be in neurons with $CREB^{S133A}$ vector (GFP^+) than in noninfected neurons (GFP^-) [$F(1,2) = 405.28$, $P < 0.05$]. Right: WT mice infused with $CREB^{S133A}$ vector show normal memory, even when trained with a lower-intensity shock [$F(1,13) = 2.08$, $P > 0.05$; control $n = 7$, $CREB^{S133A}$ $n = 8$].

Fig. 4. Constant size of Arc^+ memory trace suggests competitive selection process. (**A**) Proportion of LA Arc^+ neurons did not differ in fear-conditioned WT mice, regardless of vector [$CREB^{WT}$, control, $CREB^{S133A}$] or training intensity [high (0.75-mA shock) or low (0.4-mA shock)] [$F(3,12) = 0.31$, $P < 0.05$]. (**B**) Distribution of Arc^+ varied according to CREB manipulation. First and second pairs of bars: Arc^+ nuclei were more likely to be in neurons with high CREB function (with $CREB^{WT}$ vector; GFP^+, green) than in noninfected neighbors (GFP^-, blue) in WT mice trained with high (first pair) or low (third pair) intensities. Third pair of bars: Arc^+ nuclei were equally distributed in neurons with (GFP^+, green) and without (GFP^-, blue) control vector. Fourth pair of bars: Arc^+ nuclei were less likely to be in neurons with decreased CREB function (with $CREB^{S133A}$ vector; GFP^+, green) relative to neighbors with intact CREB function (GFP^-, blue).

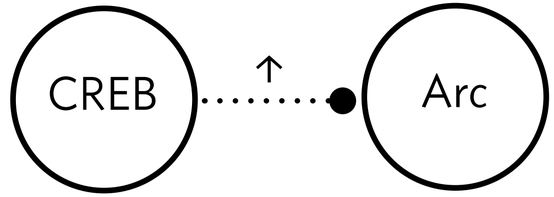

CREB and Arc were (unconditionally) independent when we intervened on CREB

$$\text{CREB} \perp\!\!\!\perp \text{Arc} \mid \varnothing \;||\; \text{CREB}$$

Method	Agent's change	Target's change	Relation	Constraint
intervention	increase	increase	excitatory	$A \not\perp\!\!\!\perp T \mid \varnothing \mid\mid A$
		no change	no-connection	$A \perp\!\!\!\perp T \mid \varnothing \mid\mid A$
		decrease	inhibitory	$A \not\perp\!\!\!\perp T \mid \varnothing \mid\mid A$
	decrease	increase	inhibitory	$A \not\perp\!\!\!\perp T \mid \varnothing \mid\mid A$
		no change	no-connection	$A \perp\!\!\!\perp T \mid \varnothing \mid\mid A$
		decrease	excitatory	$A \not\perp\!\!\!\perp T \mid \varnothing \mid\mid A$
observation	increase	increase	excitatory	$A \not\perp\!\!\!\perp T \mid \varnothing \mid\mid \varnothing$
		no change	no-connection	$A \perp\!\!\!\perp T \mid \varnothing \mid\mid \varnothing$
		decrease	inhibitory	$A \not\perp\!\!\!\perp T \mid \varnothing \mid\mid \varnothing$
	decrease	increase	inhibitory	$A \not\perp\!\!\!\perp T \mid \varnothing \mid\mid \varnothing$
		no change	no-connection	$A \perp\!\!\!\perp T \mid \varnothing \mid\mid \varnothing$
		decrease	excitatory	$A \not\perp\!\!\!\perp T \mid \varnothing \mid\mid \varnothing$

Which causal graphs are consistent with the (in)dependence relations that we've collected?

literature → research maps → (in)dependencies → causal graphs → degrees of freedom

$X \not\perp\!\!\!\perp Y \mid \varnothing \,||\, \varnothing$

$Y \not\perp\!\!\!\perp Z \mid \varnothing \,||\, \varnothing$

$X \not\perp\!\!\!\perp Z \mid \varnothing \,||\, \varnothing$

$X \perp\!\!\!\perp Z \mid Y \,||\, \varnothing$

$X \longrightarrow Y \longrightarrow Z$

$X \longleftarrow Y \longrightarrow Z$

$X \longleftarrow Y \longleftarrow Z$

Constraint-based Causal Discovery: Conflict Resolution with Answer Set Programming

Antti Hyttinen and **Frederick Eberhardt**
California Institute of Technology
Pasadena, CA, USA

Matti Järvisalo
HIIT & Department of Computer Science
University of Helsinki, Finland

Abstract

Recent approaches to causal discovery based on Boolean satisfiability solvers have opened new opportunities to consider search spaces for causal models with both feedback cycles and unmeasured confounders. However, the available methods have so far not been able to provide a principled account of how to handle conflicting constraints that arise from statistical variability. Here we present a new approach that preserves the versatility of Boolean constraint solving *and* attains a high accuracy despite the presence of statistical errors. We develop a new logical encoding of (in)dependence constraints that is both well

faithfulness (Spirtes et al., 1993). Unlike many other approaches, these constraint-based causal discovery methods can allow for the presence of latent confounders, feedback cycles and the utilisation of several (partially overlapping) observational or experimental data sets.

Even without experimentation (or additional assumptions, such as time order), and despite the generality of the model space, constraint-based methods can infer some causal orientations on the basis of *v-structures* (unshielded colliders). A v-structure in a graph is a triple of variables, such as $\langle x, z, y \rangle$ in Figure 1, where z is a common child of x and y, but x and y are non-adjacent in the graph. V-structures can be identified because of the specific (in)dependence relations they imply (here, $x \not\perp\!\!\!\perp z$, $z \not\perp\!\!\!\perp y$ and $x \perp\!\!\!\perp y$ are jointly sufficient to identify the v-structure). The edges that are

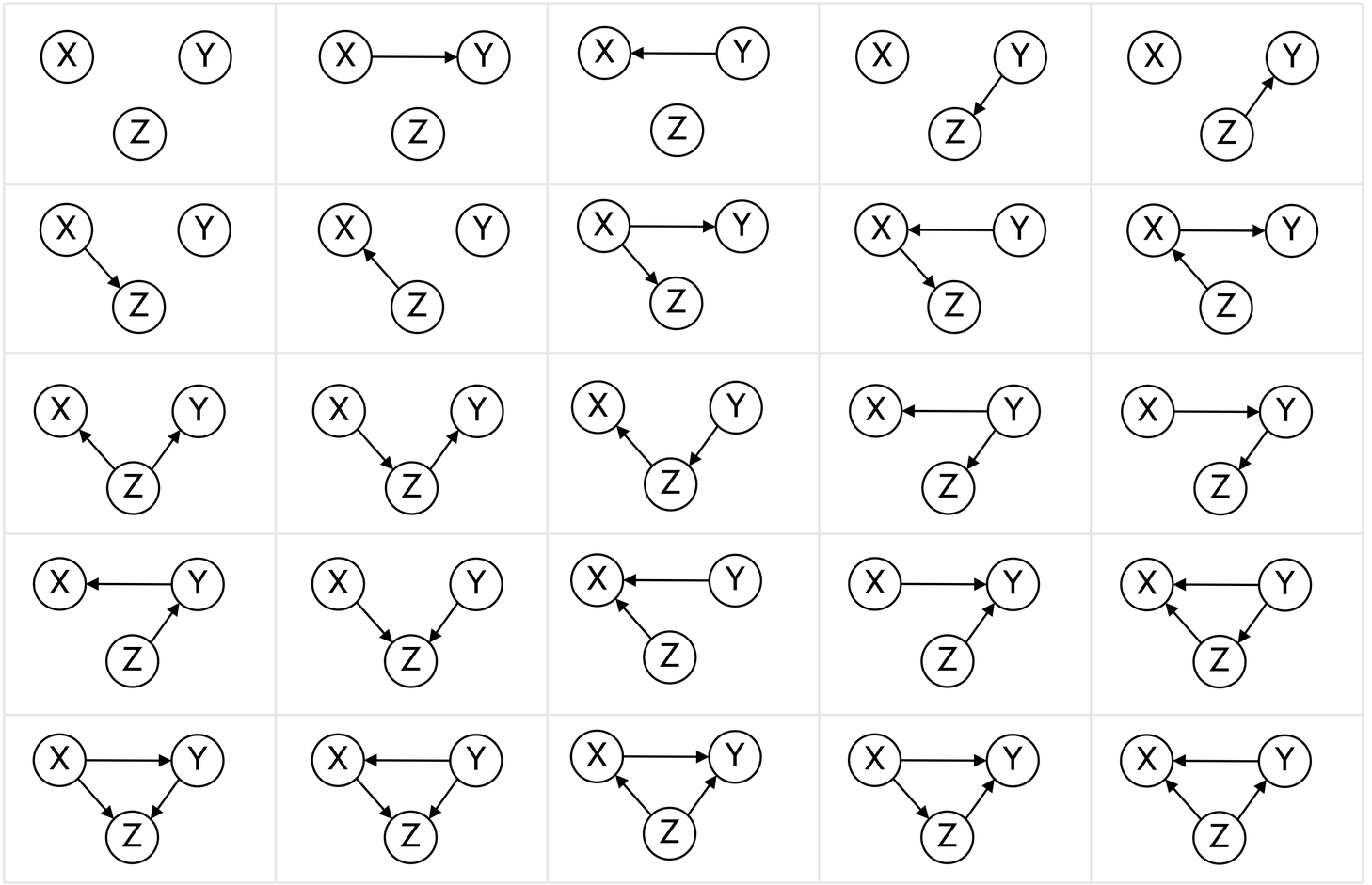
X
Y
Z

$X \not\perp\!\!\!\perp Y \mid \varnothing \;||\; \varnothing$

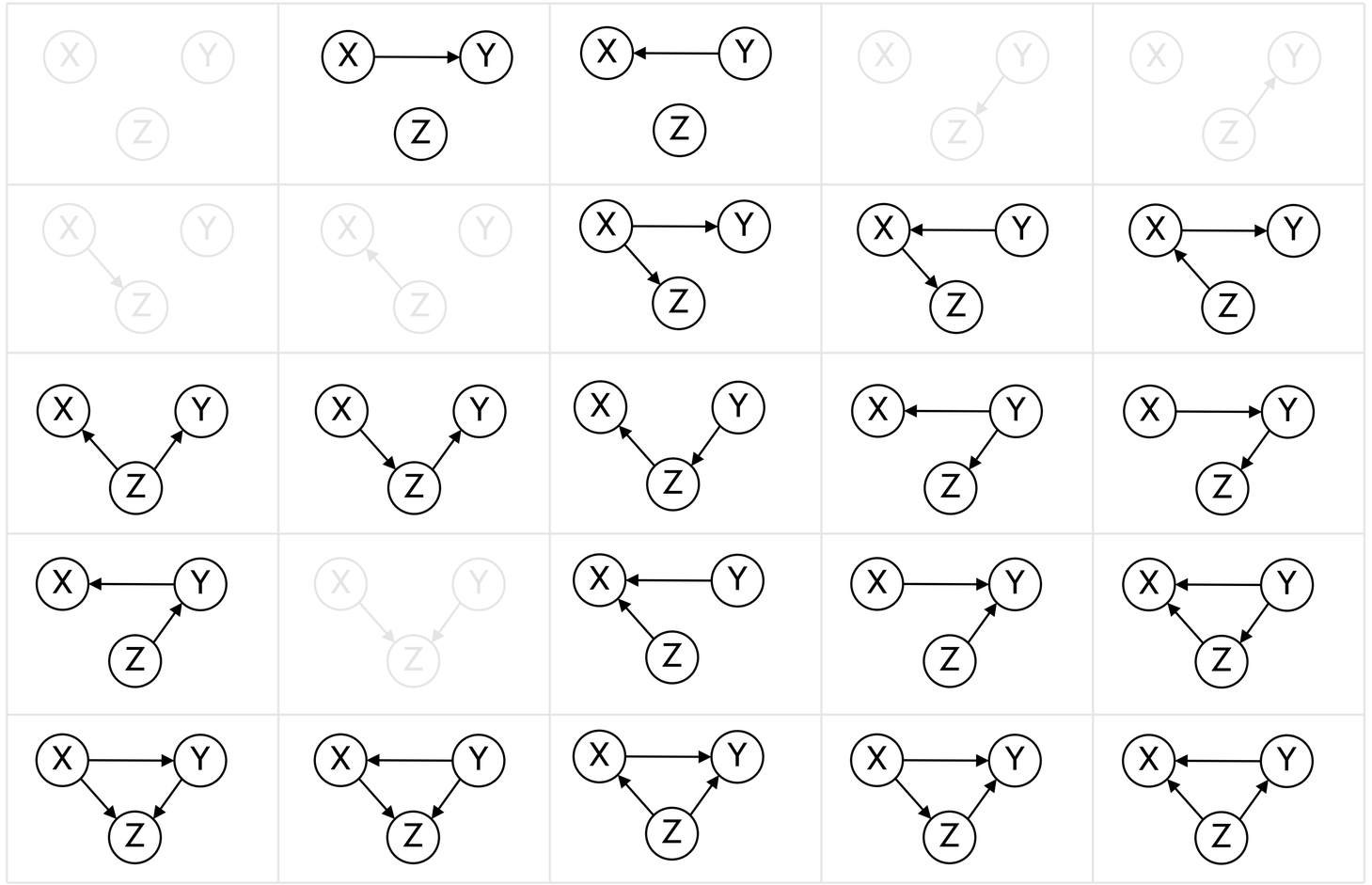

$X \not\perp\!\!\!\perp Y \mid \varnothing \;||\; \varnothing$

$X \perp\!\!\!\perp Y \mid \varnothing \;||\; Y$

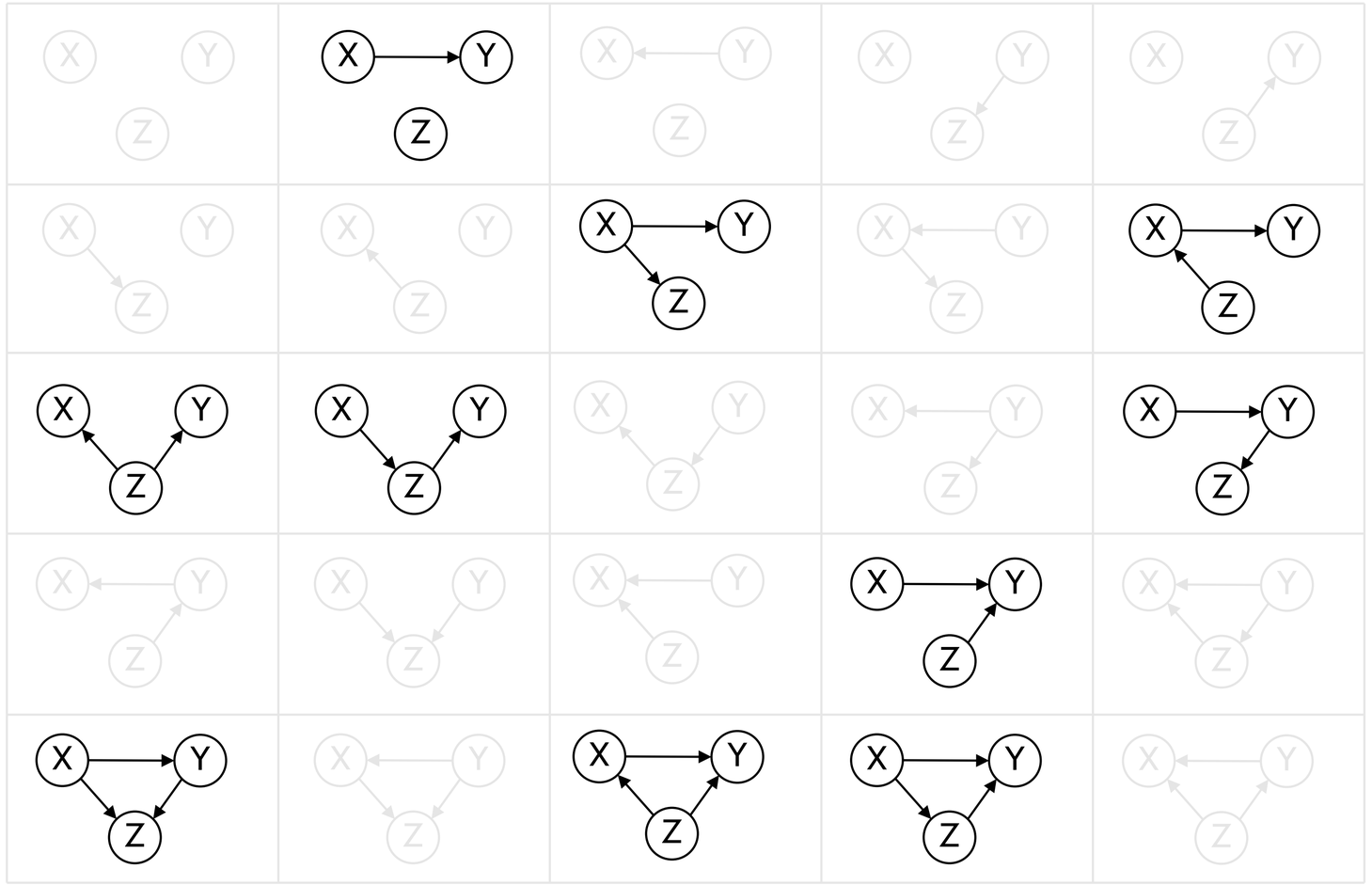

$X \not\perp\!\!\!\perp Y \mid \varnothing \;||\; \varnothing$

$X \perp\!\!\!\perp Y \mid \varnothing \;||\; Y$

…

…

…

…

…

$X \not\perp\!\!\!\perp Y \mid \varnothing \;||\; \varnothing$

$X \perp\!\!\!\perp Y \mid \varnothing \;||\; Y$

…

…

…

…

…

With conflicting constraints, we minimize the summed weight of unsatisfied constraints.

$$G^* \in \operatorname*{argmin}_{G \in \mathcal{G}} \sum_{k \in \mathbf{K}: G \not\models k} w(k)$$

Cell, Vol. 87, 1327–1338, December 27, 1996, Copyright ©1996 by Cell Press

The Essential Role of Hippocampal CA1 NMDA Receptor–Dependent Synaptic Plasticity in Spatial Memory

Joe Z. Tsien, Patricio T. Huerta, and Susumu Tonegawa
Howard Hughes Medical Institute
Center for Learning and Memory
Center for Cancer Research
Department of Biology
Massachusetts Institute of Technology
Cambridge, Massachusetts 02139

Summary

We have produced a mouse strain in which the deletion of the *NMDAR1* gene is restricted to the CA1 pyramidal cells of the hippocampus by using a new and general method that allows CA1-restricted gene knockout. The mutant mice grow into adulthood without obvious abnormalities. Adult mice lack NMDA receptor–mediated synaptic currents and long-term potentiation in the CA1 synapses and exhibit impaired spatial memory but unimpaired nonspatial learning. Our results strongly suggest that activity-dependent modifications of CA1 synapses, mediated by NMDA receptors, play an essential role in the acquisition of spatial memories.

Introduction

It has long been hypothesized that memory storage in the mammalian brain involves modifications of the synaptic connections between neurons. Hebb (1949) introduced an influential theory consisting of principles that neurons must exhibit for implementing associative memory. An important principle, known as the Hebb rule, is that of "correlated activity": when the presynaptic and the postsynaptic neurons are active simultaneously, their connections become strengthened. It is well established that *N*-methyl-D-aspartate receptors (NMDARs) can implement the Hebb rule at the synaptic level, and they are thus considered the crucial synaptic elements for the induction of activity-dependent synaptic plasticity. NMDARs act as coincidence detectors because they require both presynaptic activity (glutamate released by axonal terminals) and postsynaptic activity (depolarization that releases the Mg^{2+} block) as a condition for channel opening (Nowak et al., 1984; McBain and Mayer, 1994). Active NMDAR channels allow calcium influx into the postsynaptic cell, which triggers a cascade of biochemical events resulting in synaptic change. Long-term potentiation (LTP) is a widely used paradigm for increasing synaptic efficacy, and its induction requires, in at least one of its forms, the activation of NMDARs (Bliss and Lømo, 1973; Bliss and Collingridge, 1993). Conventionally, NMDAR-dependent LTP is elicited by giving a strong pattern of electrical stimulation (a 25–100 Hz train for ~1 s) to the inputs, which triggers a rapid and lasting increase in synaptic strength.

The hippocampus is the most intensely studied region for the importance of NMDARs in synaptic plasticity and memory. It is well known that lesions of the hippocampus in humans and other mammals produce severe amnesia for certain memories (Scoville and Milner, 1957; Morris et al., 1982; Zola-Morgan et al., 1986; reviewed by Squire, 1987). Importantly, it has been demonstrated that disruption of NMDARs in the hippocampus leads to blockade of synaptic plasticity and also to memory malfunction (reviewed by Morris et al., 1991; Rawlins, 1996). For instance, application of NMDAR antagonists (such as 2-amino-5-phosphonopropionic acid [AP5]) completely blocks the induction of LTP in most hippocampal synapses (Collingridge et al., 1983; Zalutsky and Nicoll, 1990; Hanse and Gustafsson, 1992). Morris et al. (1986) were the first to show that rats that received infusion of AP5 into the hippocampus were deficient in performing a spatial memory task in which the animals are required to form multiple spatial relations between a hidden platform in a circular pool (known as a water maze) and visible objects in the surrounding environment and swim to the platform to escape from the water. Subsequently, this issue was reinvestigated by using "gene knockout" mice. These genetically engineered mice lack a gene encoding a component that is thought to be at the downstream of activated NMDARs in the biochemical cascade for LTP induction (reviewed by Chen and Tonegawa, 1997). For example, mice with a deletion in the gene encoding the α subunit of calcium-calmodulin-dependent protein kinase II (αCaMKII) display impaired LTP in the CA1 region of the hippocampus and a deficit in spatial learning (Silva et al., 1992a, 1992b).

Even though the results of these genetic and pharmacological experiments are consistent with the notion that hippocampal LTP is the synaptic mechanism for spatial memory, other interpretations cannot be excluded. For instance, in the case of the gene knockout mice, every cell in the organism lacks the gene of interest. Consequently, all of the functions of the gene product, not only its role in LTP induction, are affected in the mutants. Hence, it is possible that spatial memory is independent of hippocampal LTP and that the memory deficit in mutants arises from lack of the gene product in other functions (such as developmental roles). Likewise, in pharmacological studies the target of the AP5 infusion is not restricted to the hippocampus (Butcher et al., 1991). Therefore, NMDARs expressed in neurons in the neighboring neocortex (and other brain areas) are also inhibited to a varying extent. Since NMDARs contribute substantially to the basal synaptic transmission of excitatory synapses in the neocortex (reviewed by Hestrin, 1996), it is likely that the infused AP5 may impair not only LTP induction in the hippocampus but also the computational ability of neocortical regions that play an important role in spatial memory.

A way to circumvent the aforementioned problems is to modify the gene knockout method such that the deletion is restricted to a certain region or a certain cell type within the brain. As described in the accompanying article (Tsien et al., 1996 [this issue of *Cell*]), we have exploited the *Cre/loxP* recombination system derived

Autophosphorylation at Thr^{286} of the α Calcium-Calmodulin Kinase II in LTP and Learning

Karl Peter Giese, Nikolai B. Fedorov, Robert K. Filipkowski, Alcino J. Silva*

The calcium-calmodulin–dependent kinase II (CaMKII) is required for hippocampal long-term potentiation (LTP) and spatial learning. In addition to its calcium-calmodulin (CaM)–dependent activity, CaMKII can undergo autophosphorylation, resulting in CaM-independent activity. A point mutation was introduced into the αCaMKII gene that blocked the autophosphorylation of threonine at position 286 (Thr^{286}) of this kinase without affecting its CaM-dependent activity. The mutant mice had no *N*-methyl-D-aspartate receptor–dependent LTP in the hippocampal CA1 area and showed no spatial learning in the Morris water maze. Thus, the autophosphorylation of αCaMKII at Thr^{286} appears to be required for LTP and learning.

Long-lasting changes in synaptic strength (such as LTP) are thought to underlie learning and memory (*1*). Pharmacological and genetic lesions of CaMKII impair LTP and learning (*2–4*). Additionally, increasing the concentrations of constitutively active CaMKII affects LTP and learning (*5, 6*). A model has been proposed that suggests that the autophosphorylated CaM-independent (constitutively active) state of CaMKII is crucial for LTP and learning (*7*). Autophosphorylation at Thr^{286} endows αCaMKII with the ability to switch from a CaM-dependent to a CaM-independent state (*8*). Consistent with the model, LTP induction triggers a long-lasting increase in the autophosphorylated form of CaMKII (*9, 10*) and in its CaM-independent activity (*11*). These studies, however, do not demonstrate that the autophosphorylation of CaMKII is required for either LTP or learning.

To determine whether the autophosphorylation of αCaMKII at Thr^{286} is required for LTP and learning, we substituted Thr^{286} (T) for alanine (A) (T286A). The T286A mutation results in a kinase that is unable to switch to its CaM-independent state (*8*). We used a gene-targeting strategy that utilizes a replacement vector containing the point mutation and a *neo* gene flanked by loxP sites (the Pointlox procedure) (Fig. 1, A and B) (*12*). All of the homozygous mutants analyzed were F2 mice from a cross between the chimeras (contributing 129 background) and C57BL/6 mice ($\alpha CaMKII^{T286A\text{-}129B6F2}$). Immunoblotting and immunocytochemical analyses (Fig. 1, C to E) determined that the point mutations and the loxP site did not alter the expression of the αCaMKII gene (*13*). We confirmed that the $\alpha CaMKII^{T286A\text{-}129B6F2}$ mutation decreased the total CaM-independent CaMKII activity in the mutants but did not affect their CaM-dependent activity (*14*). The residual CaM-independent activity in the mutants was presumably due to βCaMKII (*13, 15*).

Long-term potentiation was tested in the $\alpha CaMKII^{T286A\text{-}129B6F2}$ mutants with extracellular field recordings in the stratum radiatum of hippocampal slices (*16*). We focused our studies on the CA1 region because this region is important for learning (*17*). Long-term potentiation induced with a 100-Hz tetanus (1 s) was deficient in the $\alpha CaMKII^{T286A\text{-}129B6F2}$ mutants (Fig. 2A). Sixty minutes after the tetanus, the mutants (seven mice, seven slices) showed 110.8 ± 6.2% potentiation, whereas wild-type mice (10 mice, 10 slices) showed 153.5 ± 7.5% potentiation. There was no overlap in the extent of potentiations in wild-type and mutant slices (Fig. 2B). We also determined that other stimulation protocols revealed similar LTP impairments in the $\alpha CaMKII^{T286A\text{-}129B6F2}$ mutants (Fig. 2C). These LTP impairments were not caused by prepotentiation of synaptic transmission, because the relation between evoked fiber volleys and field excitatory postsynaptic potentials (fEPSPs) was indistinguishable between mutant (nine mice, nine slices) and wild-type mice (nine mice, nine slices) (Fig. 2D). This result also suggests that the $\alpha CaMKII^{T286A\text{-}129B6F2}$ mutation did not affect synaptic connectivity in the CA1 region. Synaptic responses collected during the 10-Hz tetanus were similar in mutant and wild-type mice (*18*), indicating that the LTP deficit of the mutants was not due to decreased synaptic transmission during tetanic stimulation.

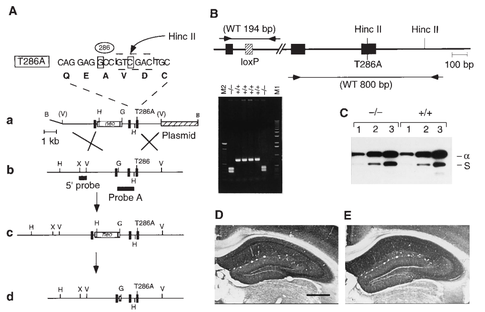

Fig. 1. Generation of the $\alpha CaMKII^{T286A\text{-}129B6F2}$ mutants with the Pointlox procedure. (**A**) The targeting construct (a), a partial map of the αCaMKII gene (b), the resulting targeted allele (c), and the targeted allele after Cre recombination (d) are illustrated (*11*). B, Bam HI; G, Bgl II; H, Hind III; V, Pvu II; X, Xba I. (**B**) A first PCR detected the loxP site (*12*) determining the genotype. A second PCR was used to identify the point mutations (*12*). The gel shows the Hinc II–digested PCR products from homozygotes (−/−) and wild-type (+/+) mice. M1 and M2 refer to molecular weight marker lanes. (**C**) Immunoblot analysis (*13*) indicated normal expression of αCaMKII (α) and synaptophysin (S) in the mutants. Lane 1, 2.5 μg of protein; lane 2, 5 μg of protein; and lane 3, 10 μg of protein. (**D** and **E**) Immunocytochemistry of adult coronal hippocampal sections (*13*) showed expression of αCaMKII in the somata and dendrites of mutants (E) and wild-type mice (D). Calibration bar, 0.5 mm.

K. P. Giese, N. B. Fedorov, A. J. Silva, Cold Spring Harbor Laboratory, Cold Spring Harbor, NY 11724, USA.
R. K. Filipkowski, Department of Neurophysiology, Nencki Institute, PL-02-093 Warsaw, Poland.
*To whom correspondence should be addressed.

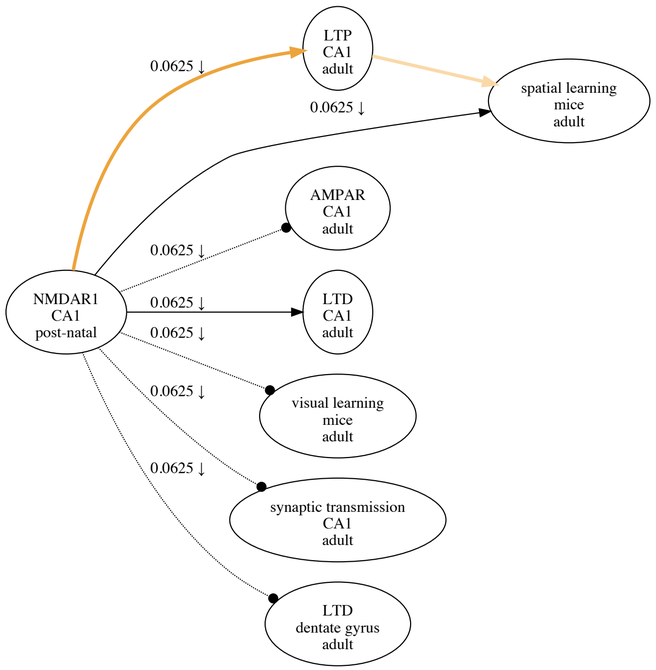
NMDAR1
CA1
post-natal
LTP
CA1
adult
spatial learning
mice
adult
AMPAR
CA1
adult
LTD
CA1
adult
visual learning
mice
adult
synaptic transmission
CA1
adult
LTD
dentate gyrus
adult
0.0625 ↓
0.0625 ↓
0.0625 ↓
0.0625 ↓
0.0625 ↓
0.0625 ↓
0.0625 ↓

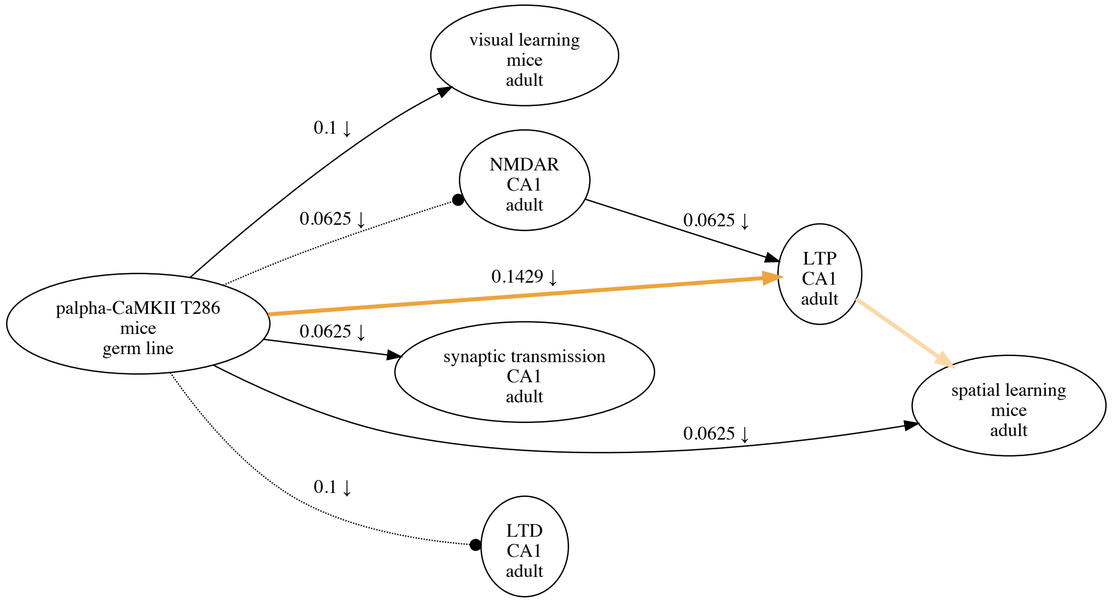
palpha-CaMKII T286
mice
germ line
visual learning
mice
adult
NMDAR
CA1
adult
LTP
CA1
adult
synaptic transmission
CA1
adult
spatial learning
mice
adult
LTD
CA1
adult
0.1 ↓
0.0625 ↓
0.0625 ↓
0.1429 ↓
0.0625 ↓
0.0625 ↓
0.1 ↓

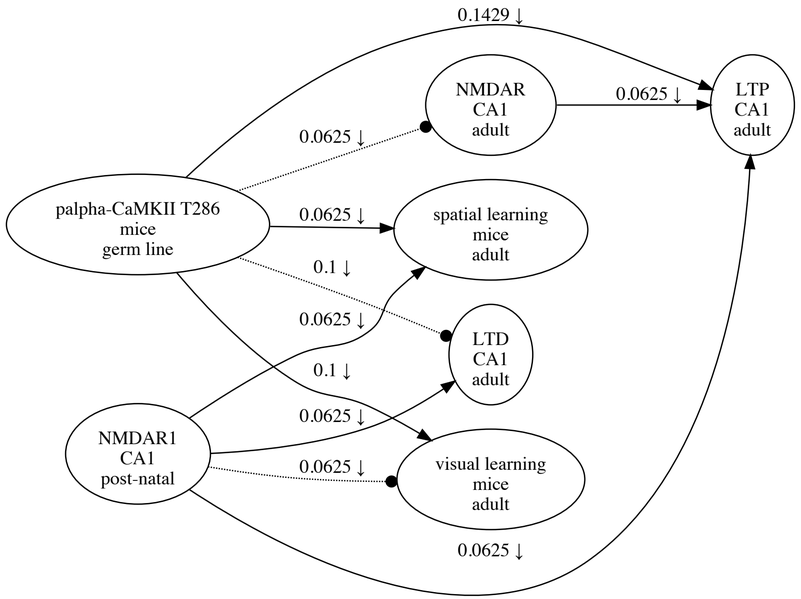
0.1429 ↓
NMDAR
CA1
adult
0.0625 ↓
LTP
CA1
adult
0.0625 ↓
palpha-CaMKII T286
mice
germ line
0.0625 ↓
spatial learning
mice
adult
0.1 ↓
0.0625 ↓
LTD
CA1
adult
0.1 ↓
0.0625 ↓
NMDAR1
CA1
post-natal
0.0625 ↓
visual learning
mice
adult
0.0625 ↓

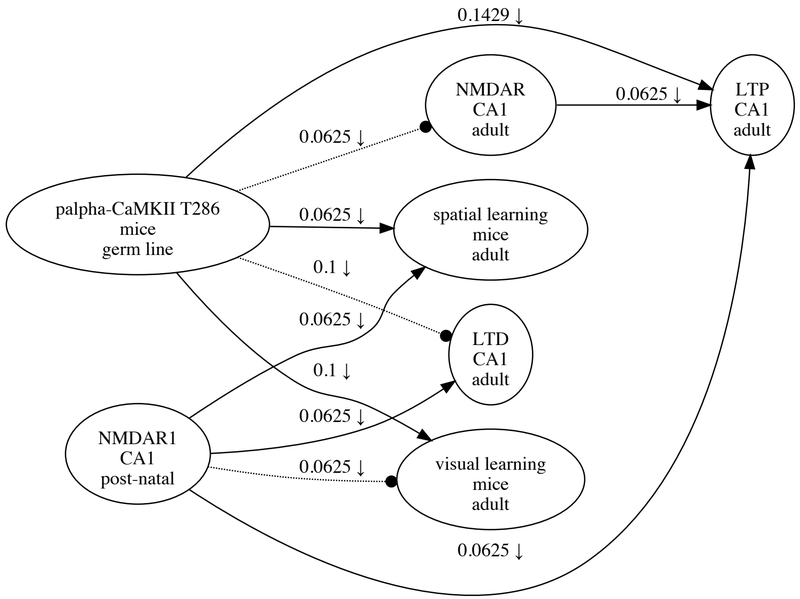

(in)dependence relation	ASP constraint
pα-CaMKII T286 $\perp\!\!\!\perp$ LTD | $\varnothing$ || pα-CaMKII T286	`indep(1,2,0,1,124,1).`
pα-CaMKII T286 $\not\perp\!\!\!\perp$ spatial learning | $\varnothing$ || pα-CaMKII T286	`dep(1,3,0,1,122,1).`
pα-CaMKII T286 $\not\perp\!\!\!\perp$ LTP | $\varnothing$ || pα-CaMKII T286	`dep(1,4,0,1,118,1).`
LTP $\not\perp\!\!\!\perp$ NMDAR | $\varnothing$ || NMDAR	`dep(4,5,0,16,103,1).`
pα-CaMKII T286 $\perp\!\!\!\perp$ NMDAR | $\varnothing$ || pα-CaMKII T286	`indep(1,5,0,1,110,1).`
pα-CaMKII T286 $\not\perp\!\!\!\perp$ visual learning | $\varnothing$ || pα-CaMKII T286	`dep(1,6,0,1,94,1).`
visual learning $\perp\!\!\!\perp$ NMDAR1 | $\varnothing$ || NMDAR1	`indep(6,7,0,64,31,1).`
LTD $\not\perp\!\!\!\perp$ NMDAR1 | $\varnothing$ || NMDAR1	`dep(2,7,0,64,61,1).`
spatial learning $\not\perp\!\!\!\perp$ NMDAR1 | $\varnothing$ || NMDAR1	`dep(3,7,0,64,59,1).`
LTP $\not\perp\!\!\!\perp$ NMDAR1 | $\varnothing$ || NMDAR1	`dep(4,7,0,64,55,1).`

Which edges have been ruled out by our evidence?

Which edges remain possible?

literature → research maps → (in)dependencies → causal graphs → degrees of freedom

$X \not\perp\!\!\!\perp Y \mid \varnothing \mid\mid \varnothing$

$Y \not\perp\!\!\!\perp Z \mid \varnothing \mid\mid \varnothing$

$X \not\perp\!\!\!\perp Z \mid \varnothing \mid\mid \varnothing$

$X \perp\!\!\!\perp Z \mid Y \mid\mid \varnothing$

$X \longrightarrow Y \longrightarrow Z$

$X \longleftarrow Y \longrightarrow Z$

$X \longleftarrow Y \longleftarrow Z$

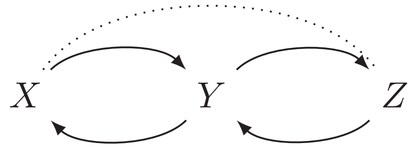

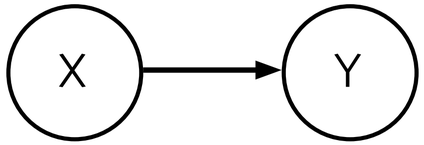

edge(X,Y).

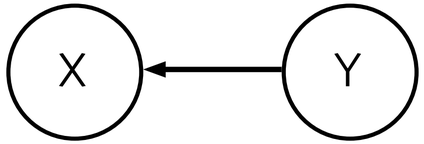

edge(Y,X).

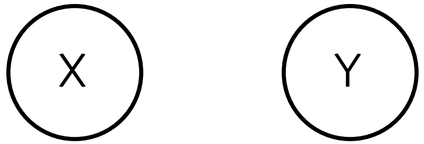

-edge(X,Y).
-edge(Y,X).

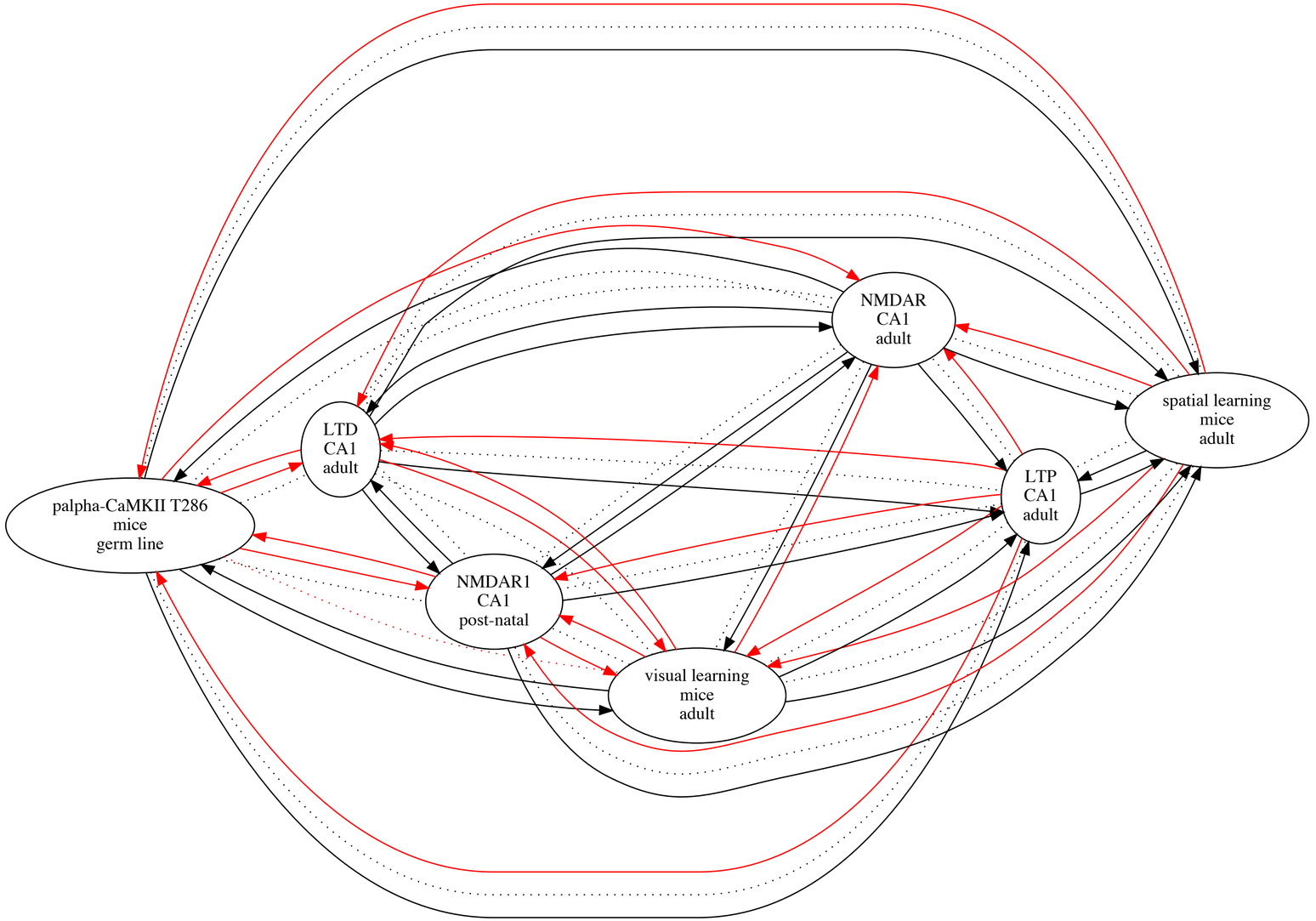

ruled out viable

Degree-of-freedom pattern	Interpretation
1. 	not connected
2. 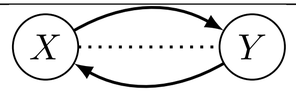	not connected, or connected in either direction
3. 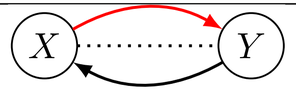	not connected, or connected in one direction
4. 	not connected, or connected in one direction
5. 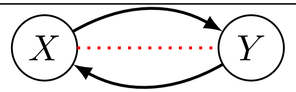	connected in either direction
6. 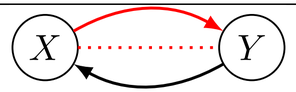	connected in one direction
7. 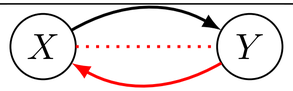	connected in one direction

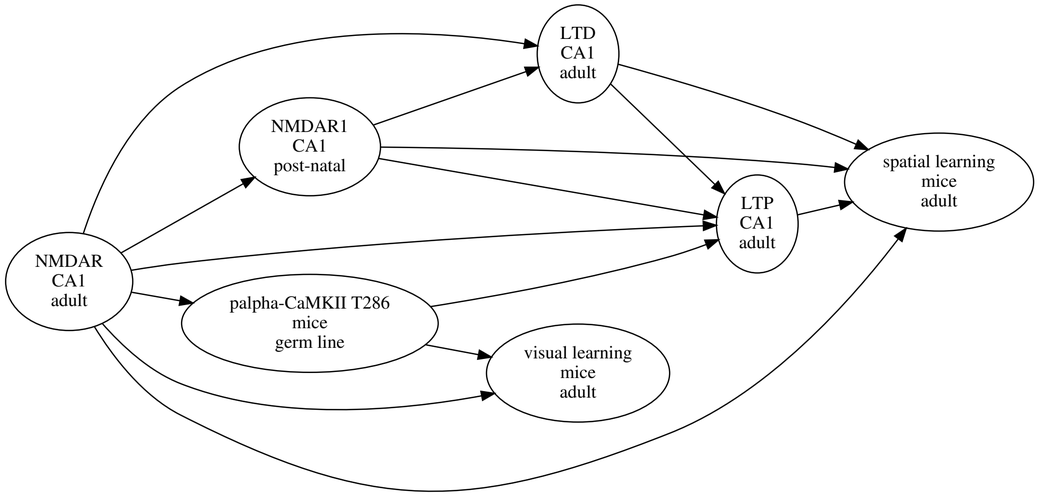
LTD
CA1
adult
NMDAR1
CA1
post-natal
spatial learning
mice
adult
LTP
CA1
adult
NMDAR
CA1
adult
palpha-CaMKII T286
mice
germ line
visual learning
mice
adult

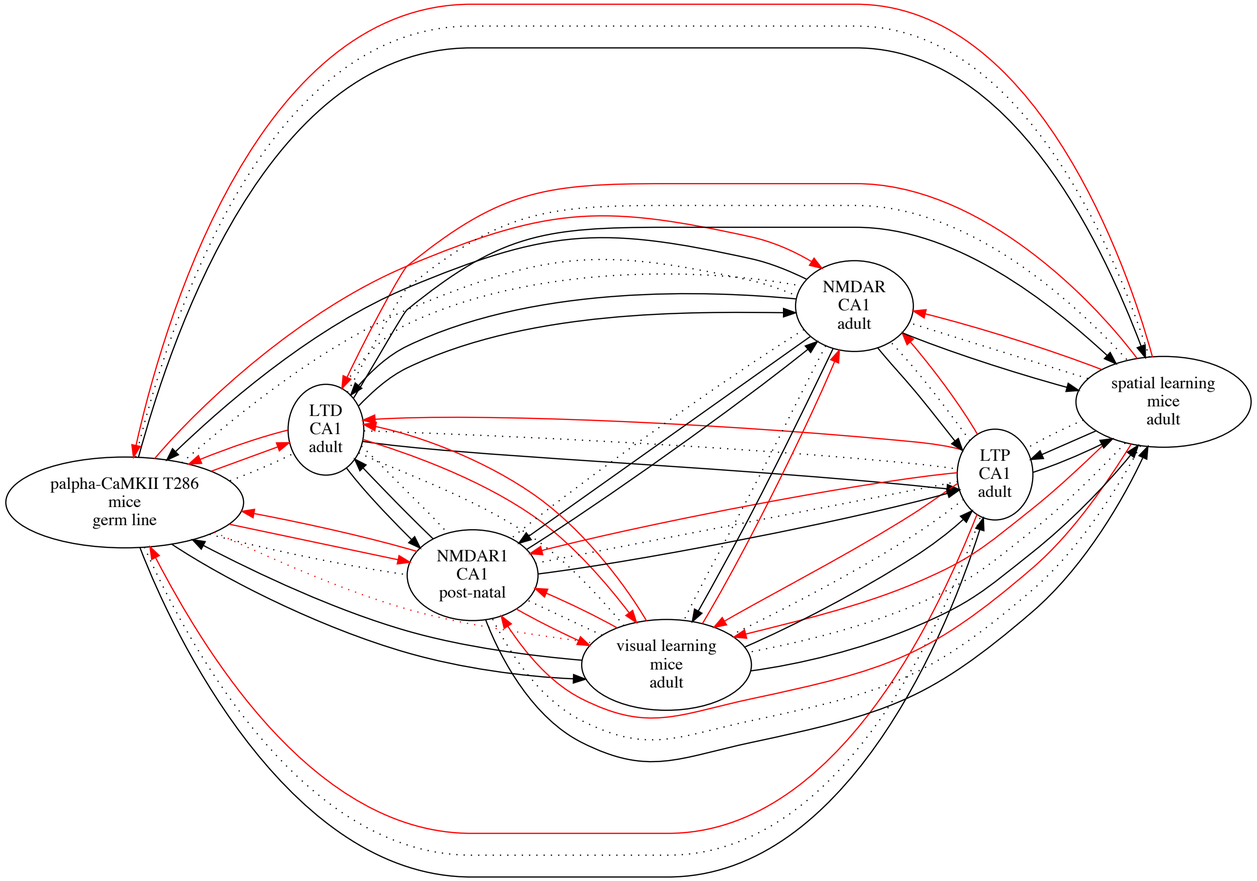
NMDAR
CA1
adult
spatial learning
mice
adult
LTD
CA1
adult
LTP
CA1
adult
palpha-CaMKII T286
mice
germ line
NMDAR1
CA1
post-natal
visual learning
mice
adult

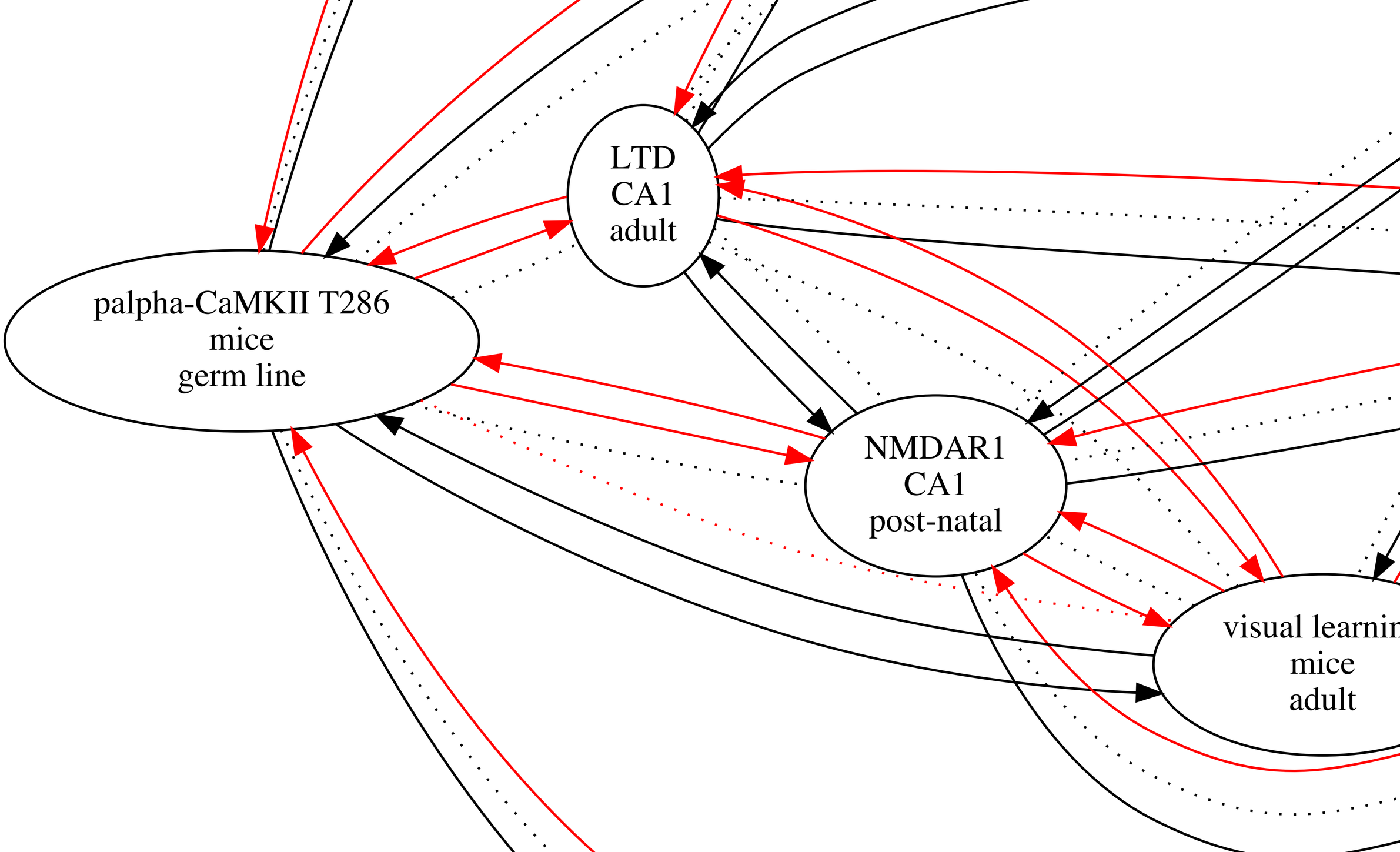
LTD
CA1
adult
palpha-CaMKII T286
mice
germ line
NMDAR1
CA1
post-natal
visual learnin
mice
adult

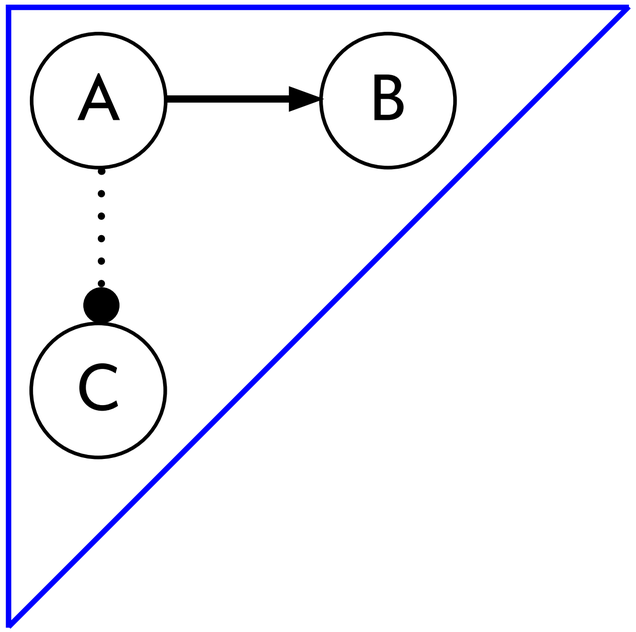
A
B
C

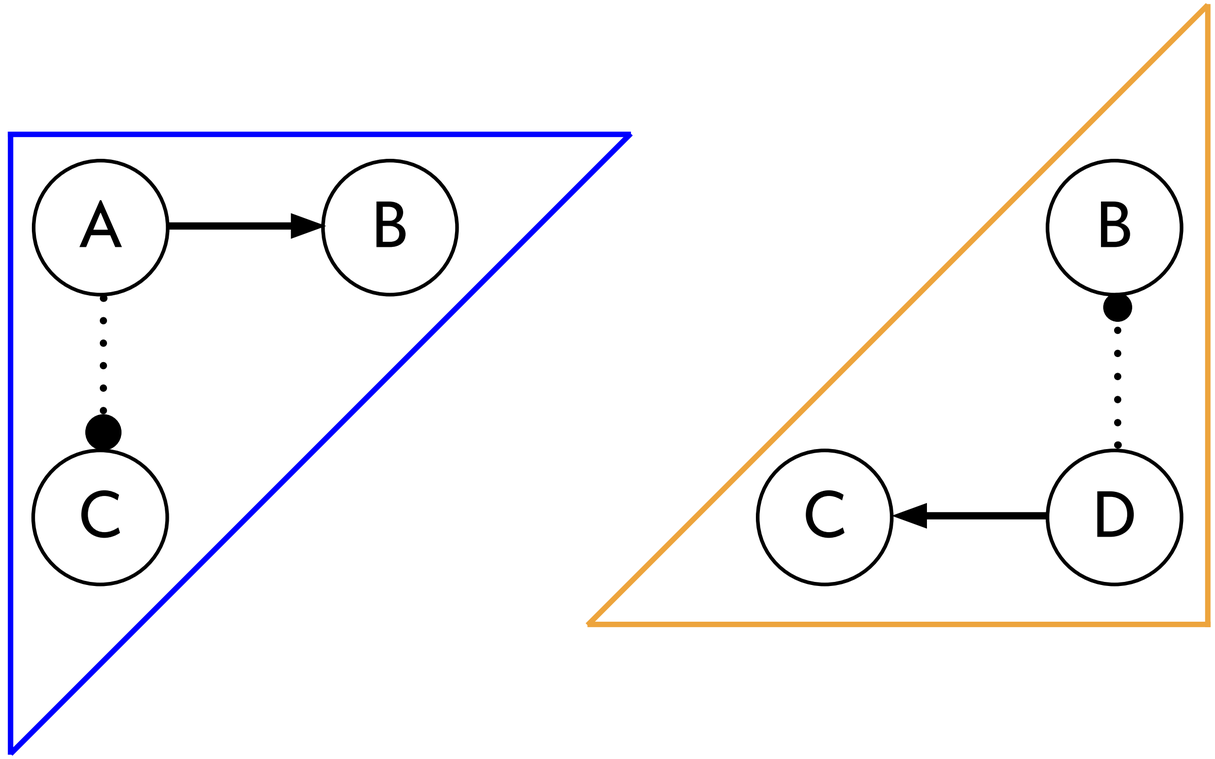
A
B
C
B
C
D

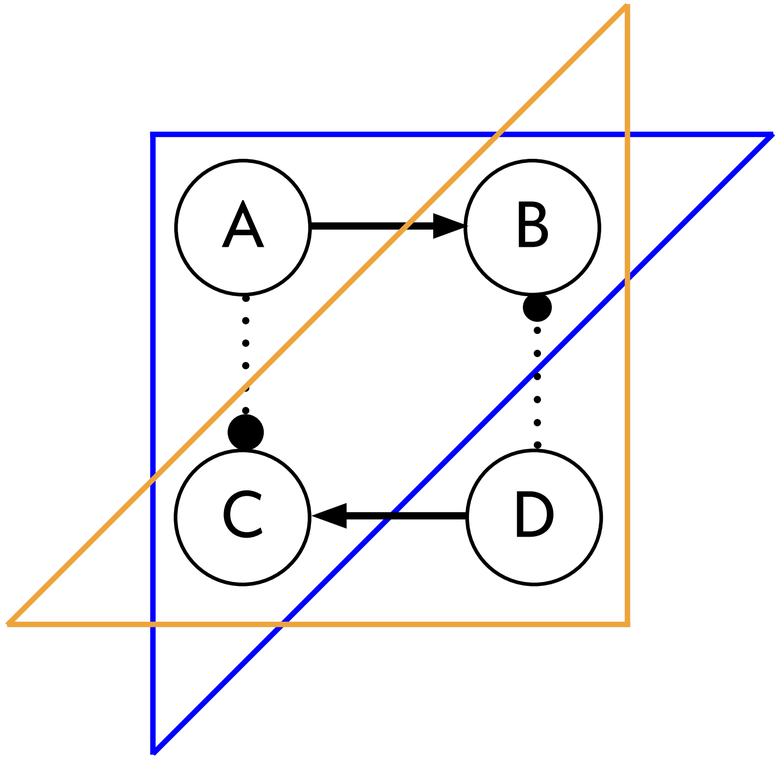
A
B
C
D

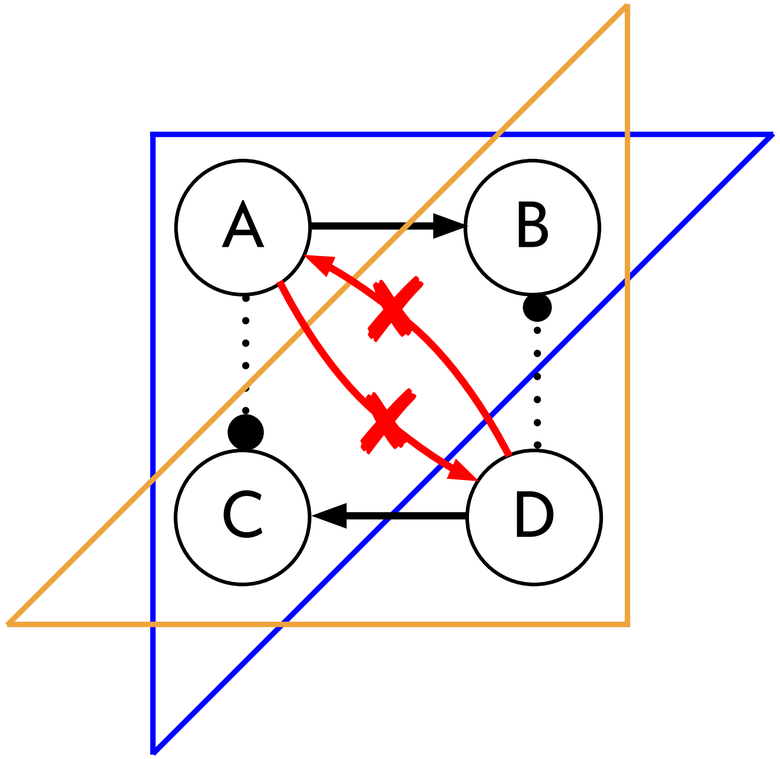
A
B
C
D

```
MATCH (w:Experiment)-[:agent]->(a:NeurolaxTerm)<-[:agent]-
(x:Experiment)-[:target]->(c:NeurolaxTerm)<-[:target]-(y:Experiment)-
[:agent]->(d:NeurolaxTerm)<-[:agent]-(z:Experiment)-[:target]->
(b:NeurolaxTerm)<-[:target]-(w:Experiment),
(a)<-[:agent]-(r:Experiment)-[:target]->(e:NeurolaxTerm),
(e)<-[:agent]-(q:Experiment)-[:target]->(d:NeurolaxTerm)
WHERE   (w.conclusion="No Relation")
AND NOT (x.conclusion="No Relation")
AND     (y.conclusion="No Relation")
AND NOT (z.conclusion="No Relation")
AND NOT (r.conclusion="No Relation")
AND NOT (q.conclusion="No Relation")
AND     ID(a)<ID(d)
RETURN a,b,c,d,e;
```

```
1 MATCH (w:Experiment)-[:agent]->(a:NeurolaxTerm)<-[:agent]-
  (x:Experiment)-[:target]->(c:NeurolaxTerm)<-[:target]-(y:Experiment)-
  [:agent]->(d:NeurolaxTerm)<-[:agent]-(z:Experiment)-[:target]->
  (b:NeurolaxTerm)<-[:target]-(w:Experiment),
```

$ MATCH (w:Experiment)-[:agent]->(a:NeurolaxTerm)<-[:agent]-(x:Experiment)-[:target]->(c:NeurolaxTerm)<-[:target]-(y:Experiment)-[:age...

Graph

Rows

*(5) NeurolaxTerm(5)

*(8) gives(8)

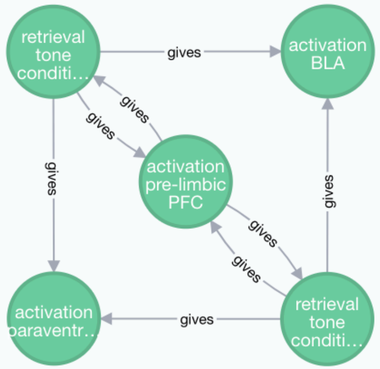

Displaying 5 nodes, 8 relationships (completed with 8 additional relationships).

AUTO-COMPLETE ON

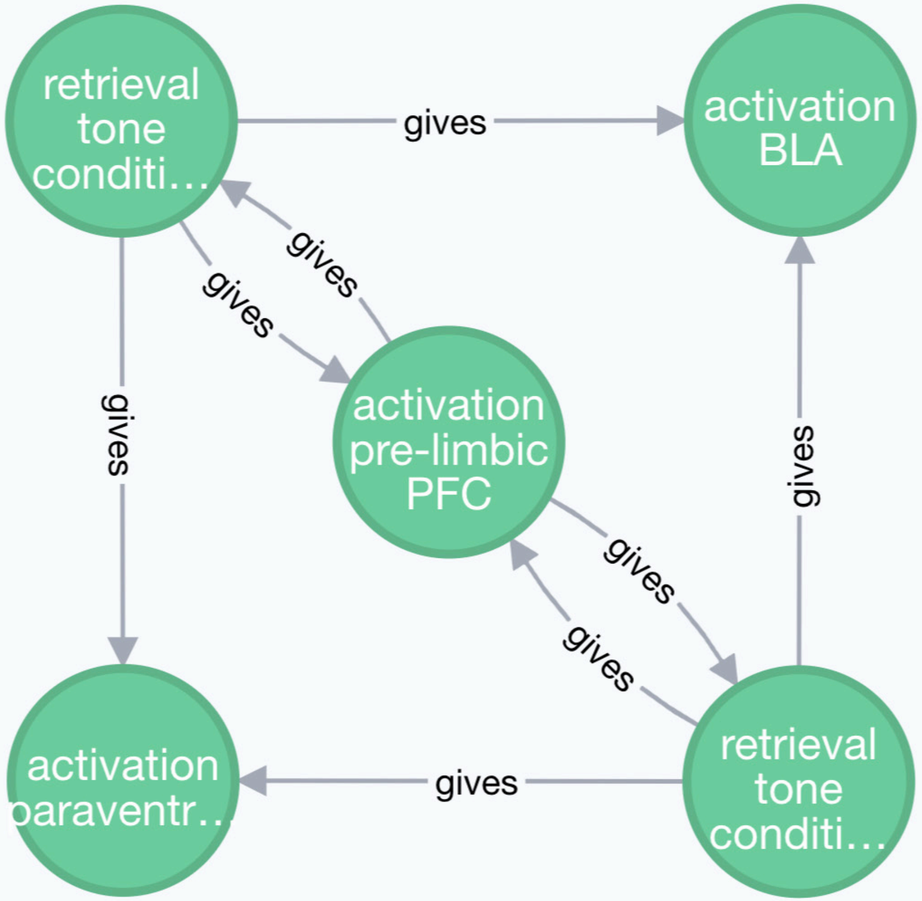
retrieval tone conditi…
gives
activation BLA
gives
gives
activation pre-limbic PFC
gives
gives
gives
gives
activation paraventr…
gives
retrieval tone conditi…

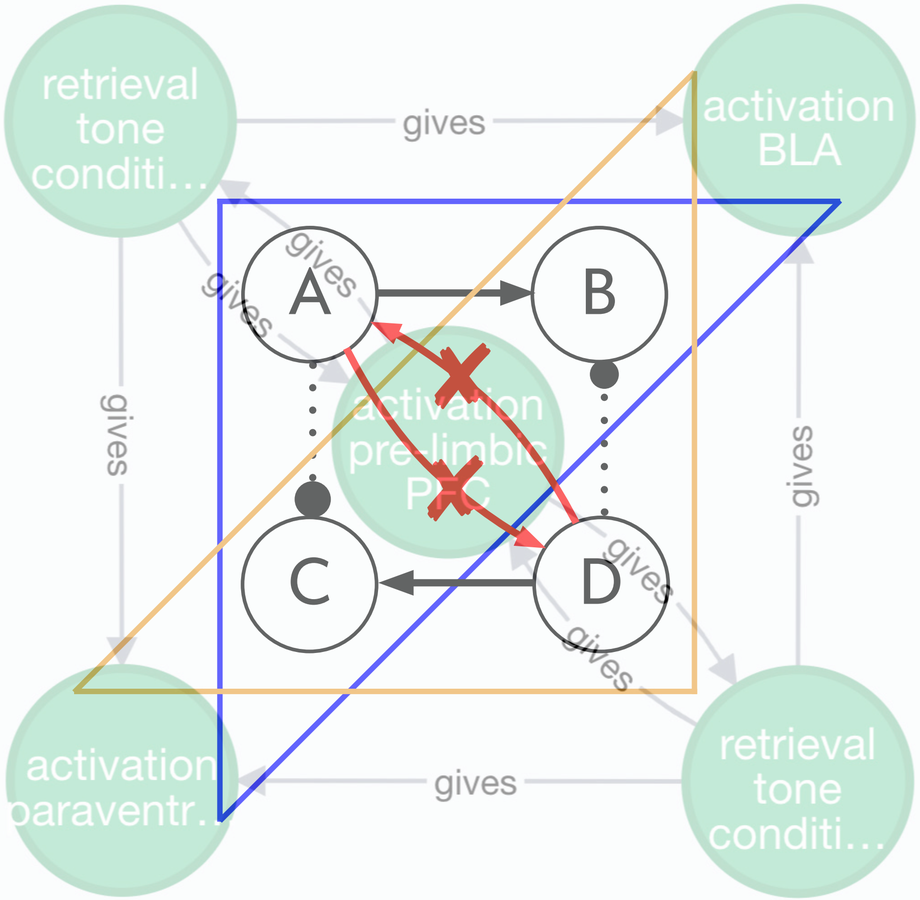
retrieval tone conditi…
gives
activation BLA
gives
gives
A
B
activation pre-limbic PFC
gives
gives
C
D
gives
gives
gives
activation paraventr…
gives
retrieval tone conditi…

A temporal shift in the circuits mediating retrieval of fear memory.

Do-Monte FH,Quiñones-Laracuente K,Quirk GJ

Nature 2015 Mar 26 7544519

Search PubMed for this article

Add Experiment

Empirical Hypothetical

Agent

What

Required

Where

Required

When

Required

Experiment

↑ ↓ ∅↑ ∅↓

Agent Approach

Required

Target

What

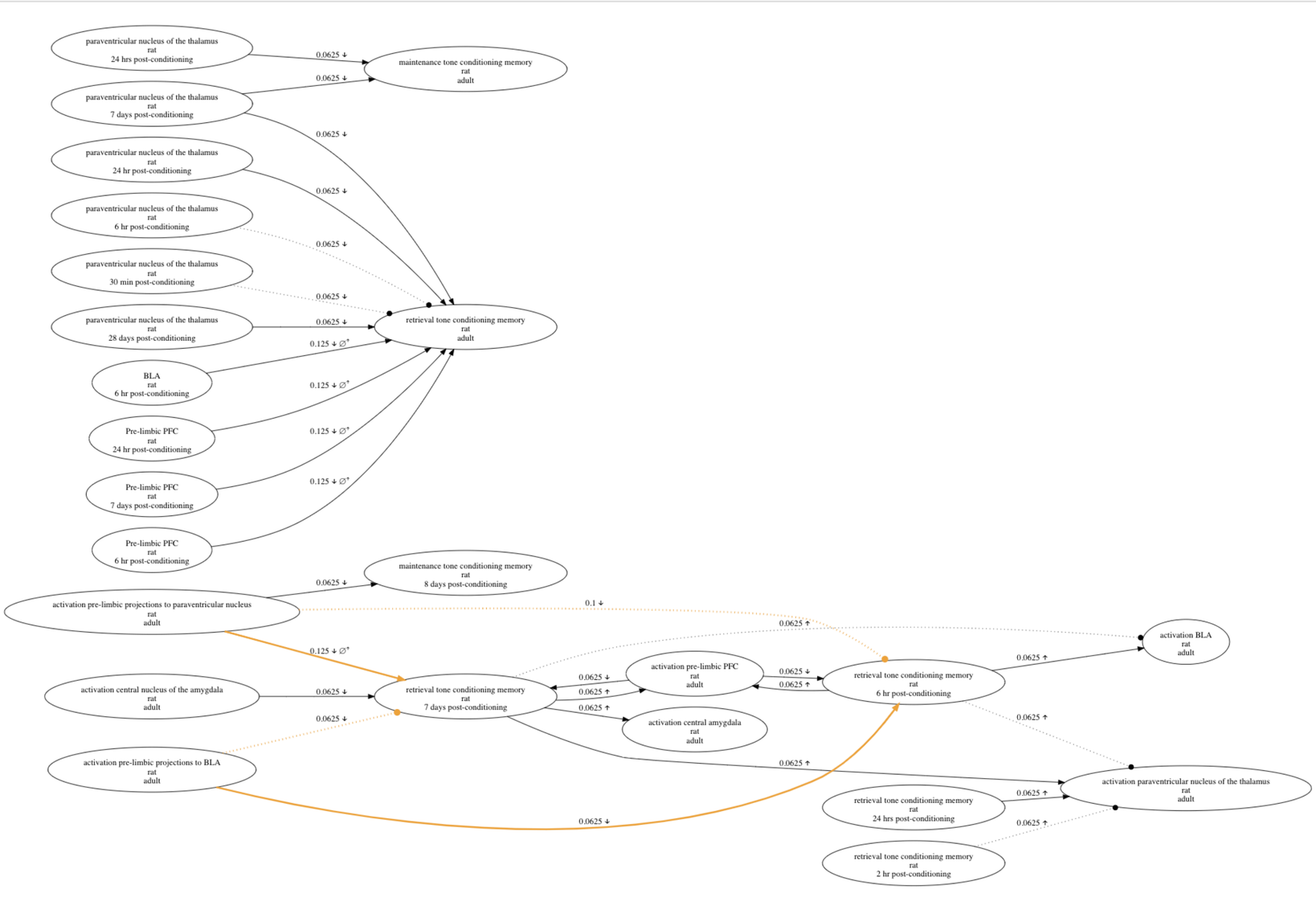

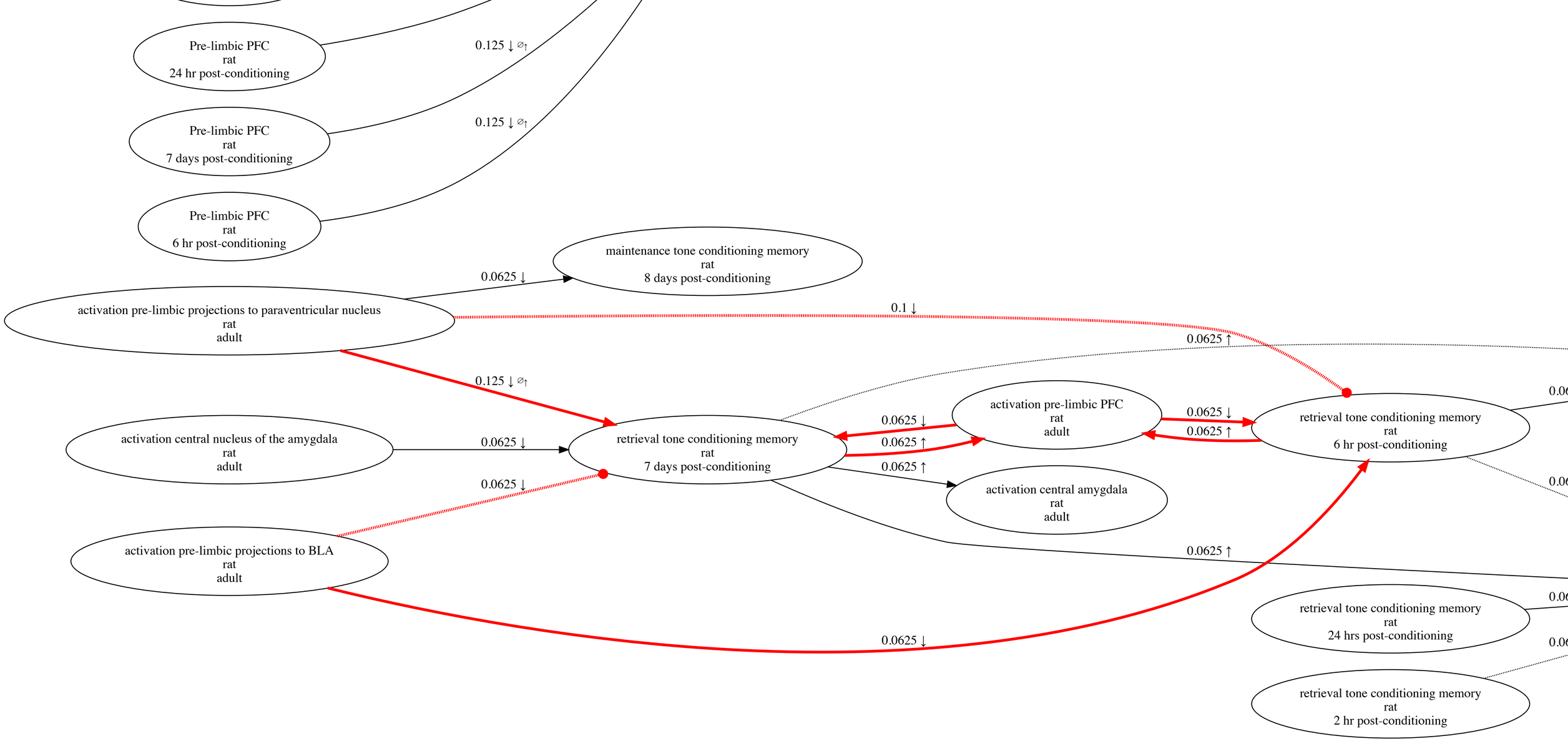
Pre-limbic PFC
rat
24 hr post-conditioning
0.125 ↓ ⌀↑
Pre-limbic PFC
rat
7 days post-conditioning
0.125 ↓ ⌀↑
Pre-limbic PFC
rat
6 hr post-conditioning
maintenance tone conditioning memory
rat
8 days post-conditioning
0.0625 ↓
activation pre-limbic projections to paraventricular nucleus
rat
adult
0.1 ↓
0.0625 ↑
0.125 ↓ ⌀↑
activation central nucleus of the amygdala
rat
adult
0.0625 ↓
retrieval tone conditioning memory
rat
7 days post-conditioning
0.0625 ↓
0.0625 ↑
activation pre-limbic PFC
rat
adult
0.0625 ↓
0.0625 ↑
retrieval tone conditioning memory
rat
6 hr post-conditioning
0.0625 ↑
activation central amygdala
rat
adult
0.0625 ↓
activation pre-limbic projections to BLA
rat
adult
0.0625 ↑
0.0625 ↓
retrieval tone conditioning memory
rat
24 hrs post-conditioning
retrieval tone conditioning memory
rat
2 hr post-conditioning

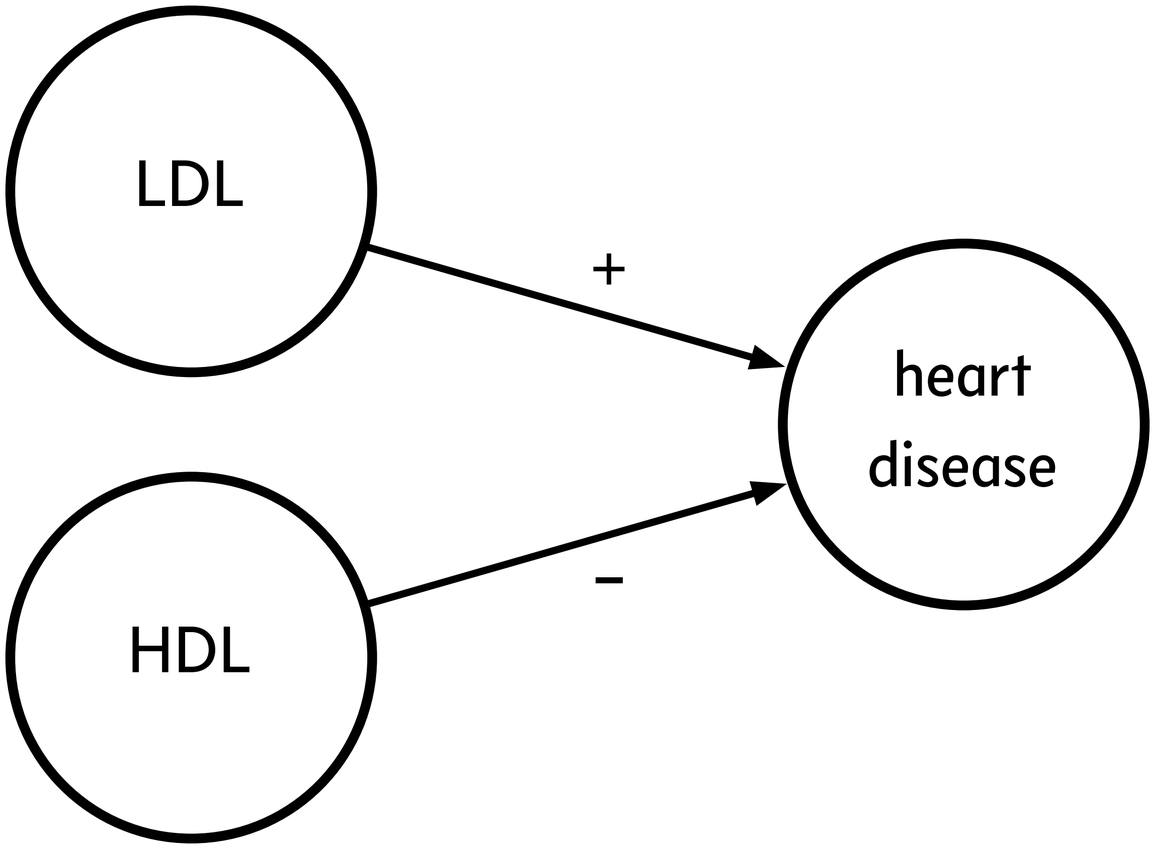
LDL
HDL
+
–
heart
disease

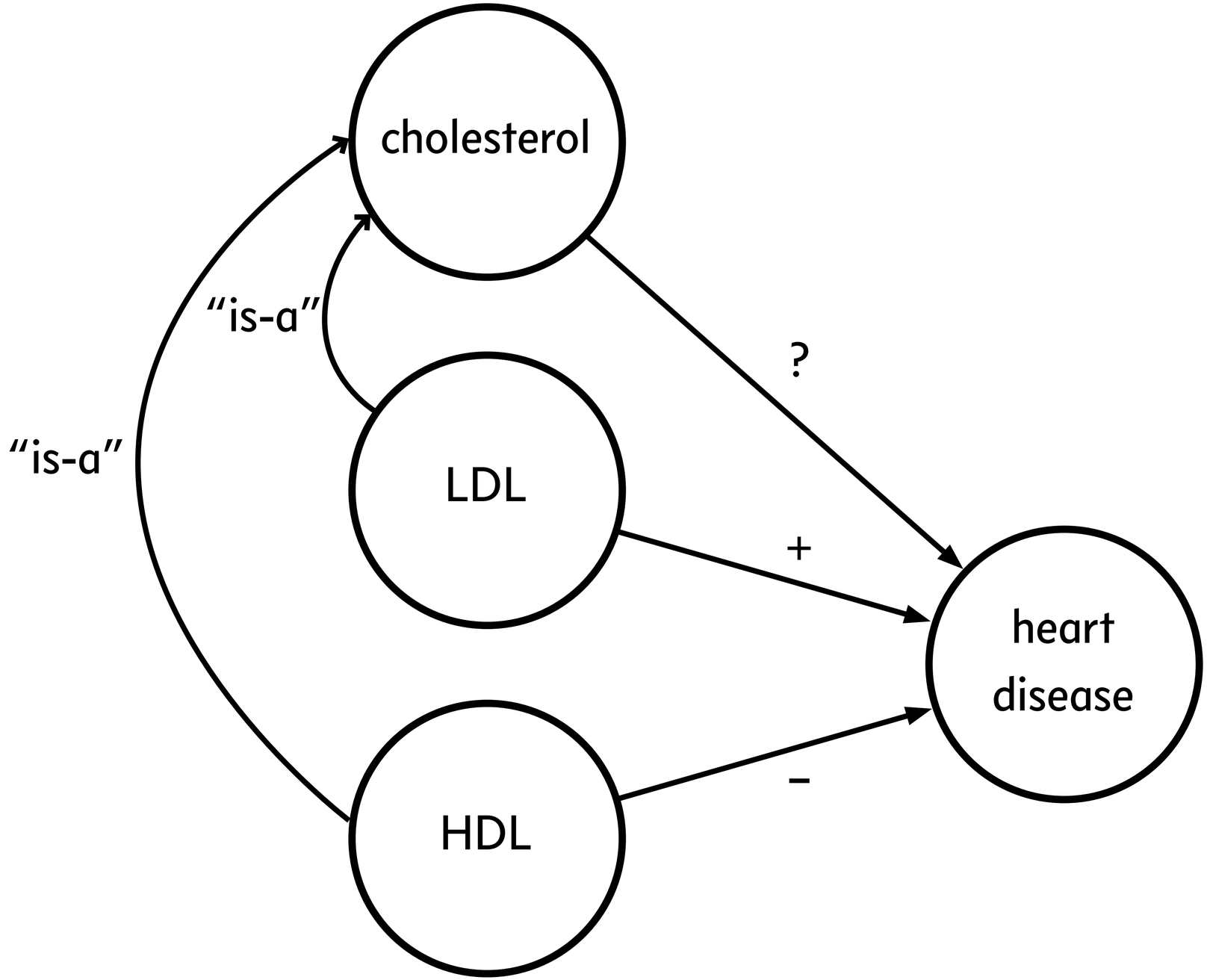
cholesterol
"is-a"
?
"is-a"
LDL
+
heart
disease
HDL
-

This approach allows us to classify hypotheses as *incorrect*, *trivial*, or *interesting*.

literature

research maps

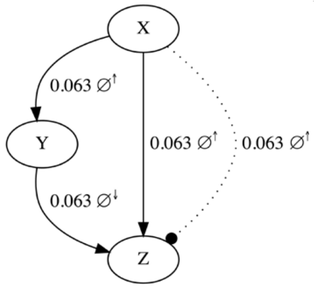

(in)dependencies

$$X \not\perp\!\!\!\perp Y \mid \varnothing \,||\, \varnothing$$

$$Y \not\perp\!\!\!\perp Z \mid \varnothing \,||\, \varnothing$$

$$X \not\perp\!\!\!\perp Z \mid \varnothing \,||\, \varnothing$$

$$X \perp\!\!\!\perp Z \mid Y \,||\, \varnothing$$

causal graphs

$$X \longrightarrow Y \longrightarrow Z$$

$$X \longleftarrow Y \longrightarrow Z$$

$$X \longleftarrow Y \longleftarrow Z$$

degrees of freedom

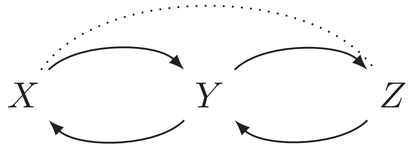

This approach allows us to classify hypotheses as *incorrect*, *trivial*, or *interesting*.

H_1: *X* and *Y* are independent.

```
indep(X,Y,C=0,J=0).
```

H_2: *X* and *Y* are directly connected.

```
edge(X,Y). OR edge(Y,X).
```

H_3: If we intervene on *Y*, *X* and *Z* will be dependent.

```
dep(X,Z,C=0,J=Y).
```

PUBLICATION

Frontiers in Neuroinformatics 2017

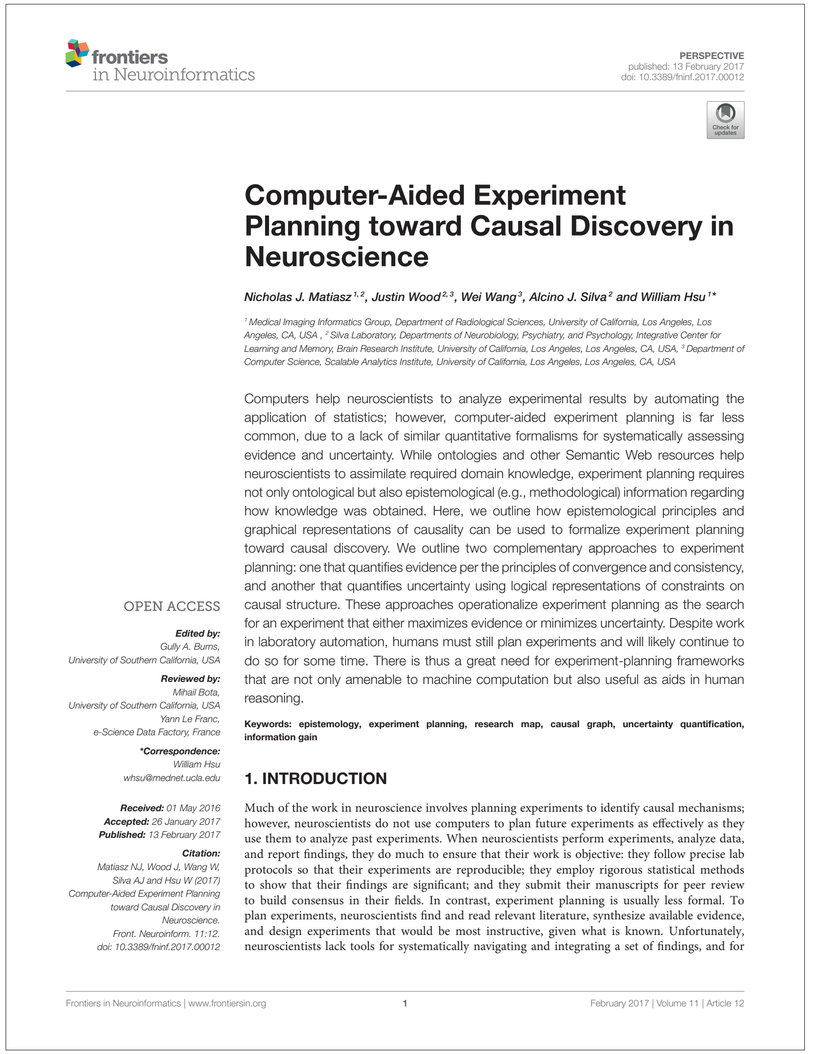

frontiers in Neuroinformatics

PERSPECTIVE
published: 13 February 2017
doi: 10.3389/fninf.2017.00012

Computer-Aided Experiment Planning toward Causal Discovery in Neuroscience

*Nicholas J. Matiasz[1,2], Justin Wood[2,3], Wei Wang[3], Alcino J. Silva[2] and William Hsu[1]**

[1] Medical Imaging Informatics Group, Department of Radiological Sciences, University of California, Los Angeles, Los Angeles, CA, USA , [2] Silva Laboratory, Departments of Neurobiology, Psychiatry, and Psychology, Integrative Center for Learning and Memory, Brain Research Institute, University of California, Los Angeles, Los Angeles, CA, USA, [3] Department of Computer Science, Scalable Analytics Institute, University of California, Los Angeles, Los Angeles, CA, USA

Computers help neuroscientists to analyze experimental results by automating the application of statistics; however, computer-aided experiment planning is far less common, due to a lack of similar quantitative formalisms for systematically assessing evidence and uncertainty. While ontologies and other Semantic Web resources help neuroscientists to assimilate required domain knowledge, experiment planning requires not only ontological but also epistemological (e.g., methodological) information regarding how knowledge was obtained. Here, we outline how epistemological principles and graphical representations of causality can be used to formalize experiment planning toward causal discovery. We outline two complementary approaches to experiment planning: one that quantifies evidence per the principles of convergence and consistency, and another that quantifies uncertainty using logical representations of constraints on causal structure. These approaches operationalize experiment planning as the search for an experiment that either maximizes evidence or minimizes uncertainty. Despite work in laboratory automation, humans must still plan experiments and will likely continue to do so for some time. There is thus a great need for experiment-planning frameworks that are not only amenable to machine computation but also useful as aids in human reasoning.

Keywords: epistemology, experiment planning, research map, causal graph, uncertainty quantification, information gain

OPEN ACCESS

Edited by:
Gully A. Burns,
University of Southern California, USA

Reviewed by:
Mihail Bota,
University of Southern California, USA
Yann Le Franc,
e-Science Data Factory, France

****Correspondence:***
William Hsu
whsu@mednet.ucla.edu

Received: *01 May 2016*
Accepted: *26 January 2017*
Published: *13 February 2017*

Citation:
Matiasz NJ, Wood J, Wang W, Silva AJ and Hsu W (2017) Computer-Aided Experiment Planning toward Causal Discovery in Neuroscience. Front. Neuroinform. 11:12. doi: 10.3389/fninf.2017.00012

1. INTRODUCTION

Much of the work in neuroscience involves planning experiments to identify causal mechanisms; however, neuroscientists do not use computers to plan future experiments as effectively as they use them to analyze past experiments. When neuroscientists perform experiments, analyze data, and report findings, they do much to ensure that their work is objective: they follow precise lab protocols so that their experiments are reproducible; they employ rigorous statistical methods to show that their findings are significant; and they submit their manuscripts for peer review to build consensus in their fields. In contrast, experiment planning is usually less formal. To plan experiments, neuroscientists find and read relevant literature, synthesize available evidence, and design experiments that would be most instructive, given what is known. Unfortunately, neuroscientists lack tools for systematically navigating and integrating a set of findings, and for

PUBLICATION

IEEE BIBM 2017

2017 IEEE International Conference on Bioinformatics and Biomedicine (BIBM)

Translating Literature into Causal Graphs: Toward Automated Experiment Selection

Nicholas J. Matiasz[*†§], Justin Wood[‡§], Wei Wang[‡], Alcino J. Silva[§], and William Hsu[*†]
[*]Medical Imaging Informatics, Department of Radiological Sciences
[†]Department of Bioengineering
[‡]Department of Computer Science
[§]Departments of Neurobiology, Psychiatry & Biobehavioral Sciences, and Psychology
University of California, Los Angeles 90095–8357
Email: whsu@mednet.ucla.edu

***Abstract*—Biologists synthesize research articles into coherent models—ideally, causal models, which predict how systems will respond to interventions. But it is challenging to derive causal models from articles alone, without primary data. To enable causal discovery using only literature, we built software for annotating empirical results in free text and computing valid explanations, expressed as causal graphs. This paper presents our meta-analytic pipeline: with the "research map" schema, we annotate results in literature, which we convert into logical constraints on causal structure; with these constraints, we find consistent causal graphs using a state-of-the-art, causal discovery algorithm based on answer set programming. Because these causal graphs show which relations are underdetermined, biologists can use this pipeline to select their next experiment. To demonstrate this approach, we annotated neuroscience articles and applied a "degrees-of-freedom" analysis for concisely visualizing features of the causal graphs that remain consistent with the evidence—a model space that is often too large for a machine to compute quickly, or for a researcher to examine exhaustively.**

I. INTRODUCTION

In biology, selecting the next experiment often requires causal reasoning: Biologists must examine the evidence and find logically consistent explanations. These consistent explanations may agree in some respects but disagree in others, depending on the amount of evidence available. It is on this basis that biologists hypothesize a causal mechanism and select an experiment to test it.

With primary data, biologists can identify causal mechanisms using causal discovery algorithms [1]. These methods have even motivated formal approaches to experiment selection [2]–[8]. But biologists often lack access to primary data; instead, they rely on literature, rendering many of these causal discovery methods unusable.

Here, we demonstrate a meta-analytic causal discovery method that can integrate multiple forms of causal information, including statistical findings from literature. We present a software pipeline for annotating empirical results in research articles and automatically deriving *every* consistent causal explanation, expressed as a set of causal graphs [9], [10]. This set of graphs is known as an *equivalence class* (see Figure 2 for an example). An equivalence class synthesizes the causal implications of results and provides a formal, hypothesis-generating device for selecting experiments: it encodes precisely which relations are determined, and which remain underdetermined. In principle, a researcher could derive an equivalence class by hand, but this manual computation is infeasible for all but the simplest of cases. To facilitate this sort of reasoning, we demonstrate a "degrees-of-freedom" analysis that concisely visualizes features of this model space.

Causal graphs are similar to biological pathway diagrams, but their mathematical properties make them more suitable for synthesizing literature. If pathway diagrams from different articles are simply "stitched" together—by overlapping common nodes and pooling all the diagrams' edges—the hybrid diagram may bias researchers, inviting them to reify specific pathways that the evidence does not support, or that the evidence even contradicts. Figures 1a and 1b are typical of biological pathway diagrams; they are not formal causal graphs but rather illustrations in which $X \rightarrow Y$ implies that a change in X preceded a change in Y, ostensibly implying a causal interaction. Note the consequence of stitching these two diagrams (Figure 1c): due to the $X \rightarrow Z$ edge, it appears that X can affect Z independently of Y. But that is not necessarily true. It's possible that in the experiment that led to Figure 1a, Y was unmeasured; in this case, Y still could have mediated X's effect on Z, but this mediation may have been unknown to the researchers, who instead focused on X and Z. This sort of bookkeeping can become very complicated, even for small systems. And pathway diagrams' imprecise semantics impede the development of an algorithmic solution to this problem.

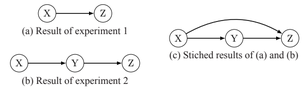

Fig. 1. Pathway diagrams from the literature cannot simply be "stitched" to derive causal inferences of empirical results. When the nodes and edges from (a) and (b) are simply pooled to produce (c), this new diagram's $X \rightarrow Z$ edge suggests that X can effect Z independently of Y—an interpretation that does not necessarily follow from the evidence that led to (a) and (b).

In contrast, causal graphs can be stitched with a principled procedure [8] based on the graphical concept *d-separation*

978-1-5090-3050-7/17/$31.00 ©2017 IEEE

CONTRIBUTIONS

1. Cumulative evidence index (CEI)
2. Meta-analytic causal discovery
3. Heuristics for experiment planning

Degree-of-freedom pattern, $\mathbf{D}_{X,Y}$	Suggested experiments, $\mathbf{S}_{\mathbf{D}_{X,Y}}$
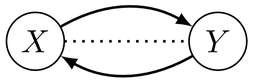	$\mathbf{J} = \varnothing$ $\mathbf{J} = \{X\}$ $\mathbf{J} = \{Y\}$
	$\mathbf{J} = \varnothing$ $\mathbf{J} = \{X\}$
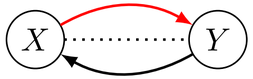	$\mathbf{J} = \varnothing$ $\mathbf{J} = \{Y\}$
	$\mathbf{J} = \{X\}$ $\mathbf{J} = \{Y\}$
	$\mathbf{J} = \{X\}$
	$\mathbf{J} = \{\varnothing\}$
	$\mathbf{J} = \{Y\}$

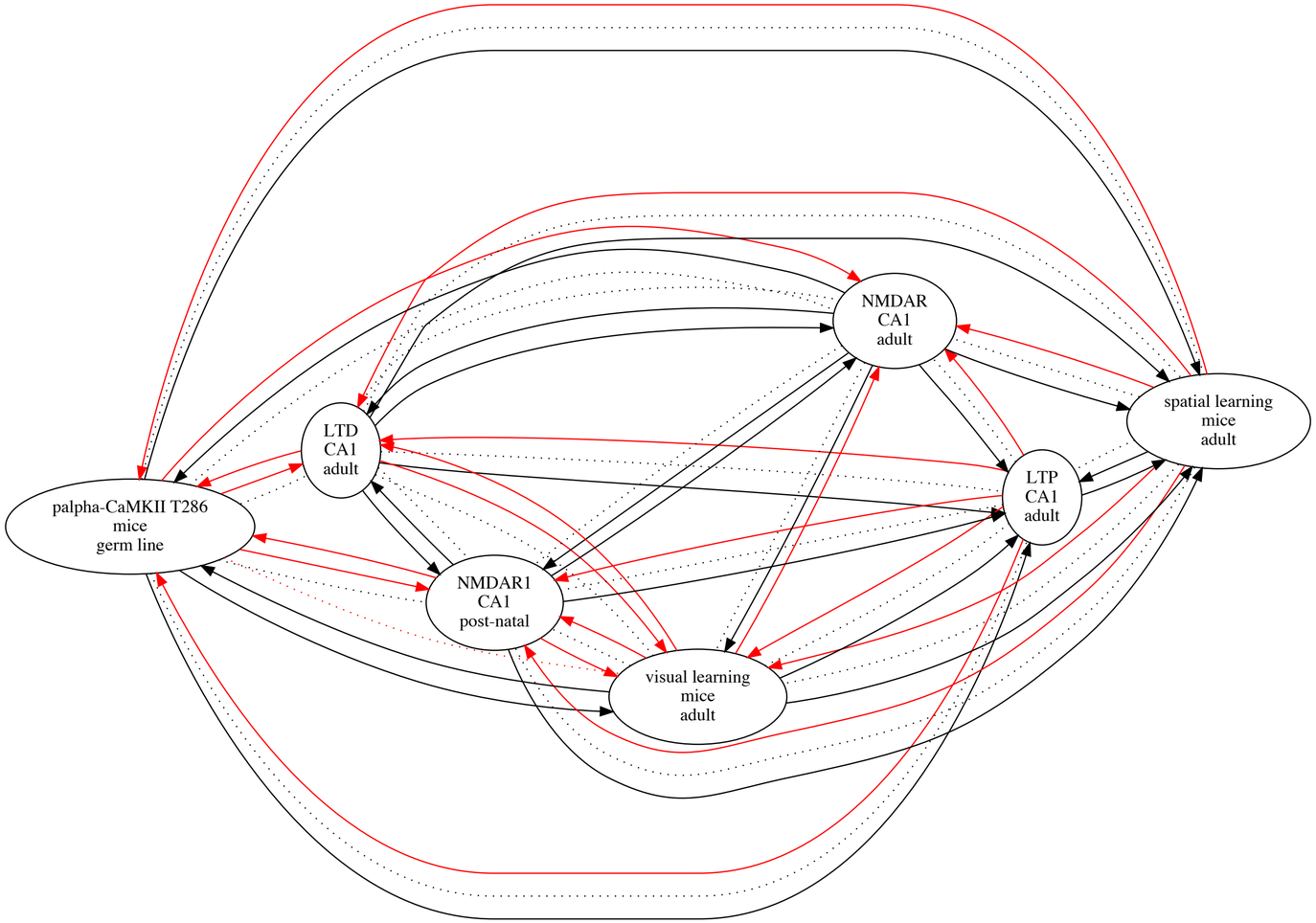

Experiment-selection algorithm: DOF only

Calculate DOFs for equivalence class

Find pair with maximum number of DOFs

Select experiment based on DOF pattern

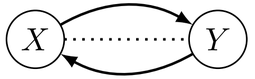	$\mathbf{J} = \varnothing$ $\mathbf{J} = \{X\}$ $\mathbf{J} = \{Y\}$
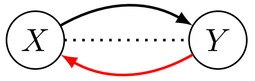	$\mathbf{J} = \varnothing$ $\mathbf{J} = \{X\}$
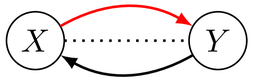	$\mathbf{J} = \varnothing$ $\mathbf{J} = \{Y\}$
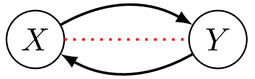	$\mathbf{J} = \{X\}$ $\mathbf{J} = \{Y\}$
	$\mathbf{J} = \{X\}$
	$\mathbf{J} = \{\varnothing\}$
	$\mathbf{J} = \{Y\}$

Experiment-selection algorithm: DOF & expectation metric

For each DOF, *d*, in equivalence class:

- Calculate *p*, empirical probability of *d*
- Calculate *r*, number of graphs removed if *d* is correct
- Calculate expectation for *d*: *e* = *p***r*

Select experiment based on *d* with largest expectation

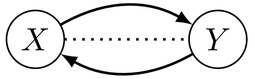	$\mathbf{J} = \varnothing$ $\mathbf{J} = \{X\}$ $\mathbf{J} = \{Y\}$
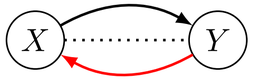	$\mathbf{J} = \varnothing$ $\mathbf{J} = \{X\}$
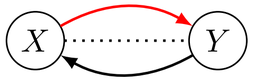	$\mathbf{J} = \varnothing$ $\mathbf{J} = \{Y\}$
	$\mathbf{J} = \{X\}$ $\mathbf{J} = \{Y\}$
	$\mathbf{J} = \{X\}$
	$\mathbf{J} = \{\varnothing\}$
	$\mathbf{J} = \{Y\}$

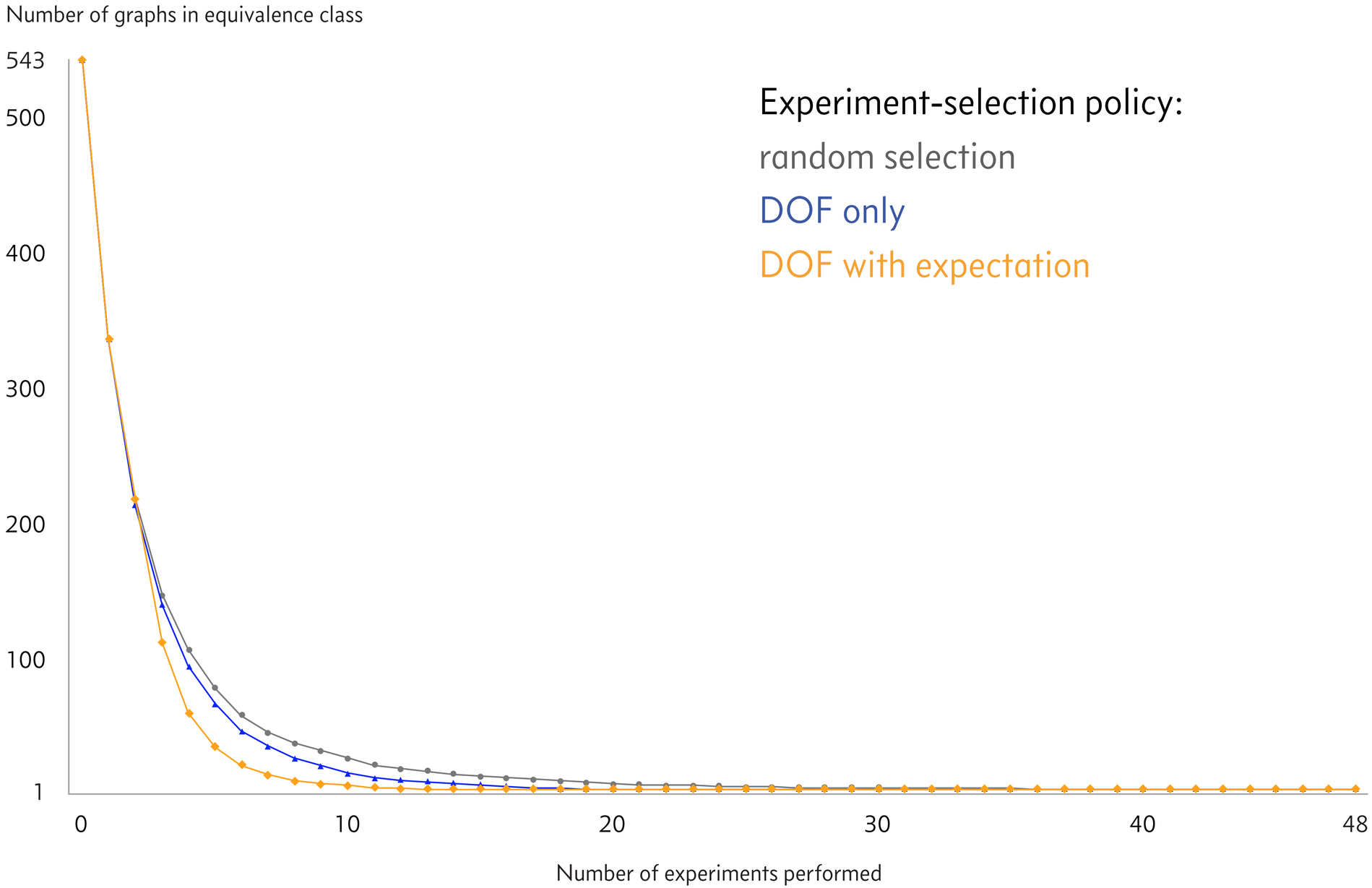
Number of graphs in equivalence class
543
500
400
300
200
100
1
0
10
20
30
40
48
Number of experiments performed
Experiment-selection policy:
random selection
DOF only
DOF with expectation

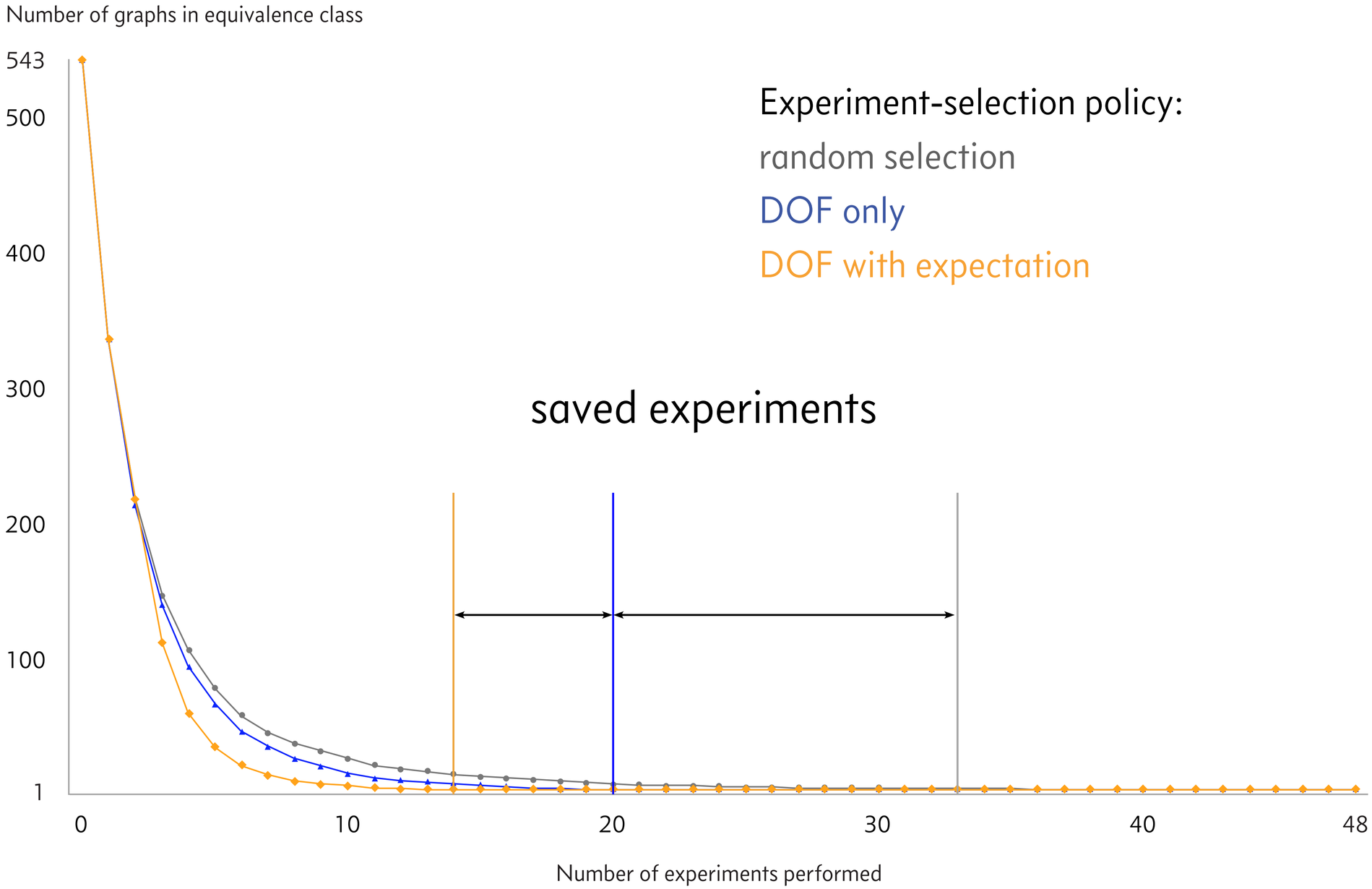
Number of graphs in equivalence class
543
500
400
300
200
100
1
0
10
20
30
40
48
Number of experiments performed
Experiment-selection policy:
random selection
DOF only
DOF with expectation
saved experiments

POLICY	NUMBER OF STUDIES NEEDED TO REACH: <50 GRAPHS	<10 GRAPHS	MINIMUM
DOF & expectation	5	9	15
DOF only	6	14	23
Random selection	7	19	47

POLICY	NUMBER OF SAT-SOLVER QUERIES NEEDED FOR: 4 VARIABLES	8 VARIABLES	14 VARIABLES
DOF & expectation	543	$\sim 10^{11}$	$\sim 10^{36}$
DOF only	18	84	273
Random selection	0	0	0

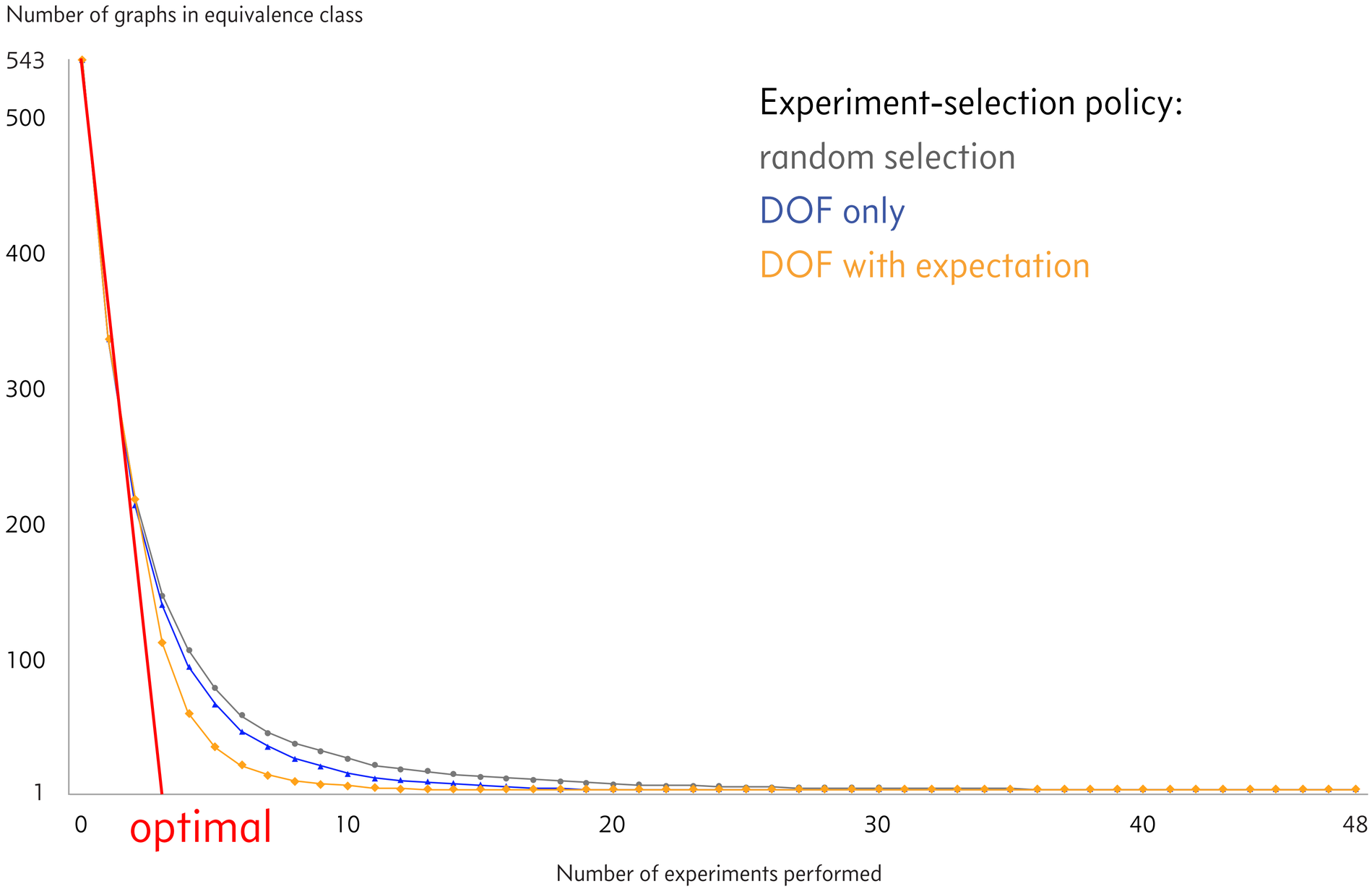
Number of graphs in equivalence class
543
500
400
300
200
100
1
0
optimal
10
20
30
40
48
Number of experiments performed
Experiment-selection policy:
random selection
DOF only
DOF with expectation

MANUSCRIPT IN PREPARATION

JASIST

Experiment selection in meta-analytic causal discovery

Nicholas J. Matiasz*
Departments of Bioengineering, Neurobiology, and Radiological Sciences, UCLA
924 Westwood Blvd., Ste. 420, Los Angeles, CA 90024; matiasz@ucla.edu

Justin Wood*
Departments of Computer Science and Neurobiology, UCLA
3551 Boelter Hall, 580 Portola Plaza, Los Angeles, CA 90095; juwood03@cs.ucla.edu

Wei Wang
Department of Computer Science, UCLA
3531-G Boelter Hall, 580 Portola Plaza, Los Angeles, CA 90095; weiwang@cs.ucla.edu

Alcino J. Silva
Departments of Neurobiology, Psychiatry & Biobehavioral Sciences, and Psychology, UCLA
695 Charles Young Dr. S., Rm. 2357, Los Angeles, CA 90095; silvaa@mednet.ucla.edu

William Hsu†
Departments of Radiological Sciences and Bioengineering, UCLA
924 Westwood Blvd., Ste. 420, Los Angeles, CA 90024; whsu@mednet.ucla.edu

Author Note

* These authors contributed equally to this work.
† Corresponding author

Meta-analytic causal discovery & experiment selection

literature

research maps

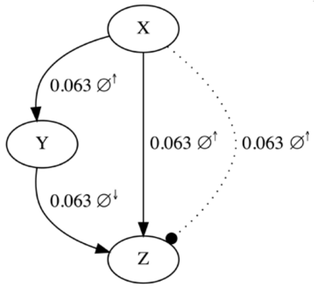

(in)dependencies

$$X \not\perp\!\!\!\perp Y \mid \varnothing \,||\, \varnothing$$

$$Y \not\perp\!\!\!\perp Z \mid \varnothing \,||\, \varnothing$$

$$X \not\perp\!\!\!\perp Z \mid \varnothing \,||\, \varnothing$$

$$X \perp\!\!\!\perp Z \mid Y \,||\, \varnothing$$

causal graphs

$$X \longrightarrow Y \longrightarrow Z$$

$$X \longleftarrow Y \longrightarrow Z$$

$$X \longleftarrow Y \longleftarrow Z$$

degrees of freedom

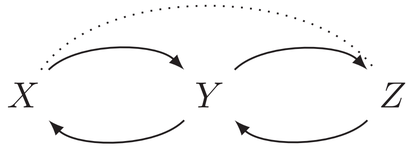

Future work

- Automate the annotation of literature
- Extend the research map schema
- Generalize the cumulative evidence index to entire maps
- Improve the scalability of SAT-based causal discovery methods
- Improve experiment-selection heuristics

Acknowledgements (alphabetical)

ADVISORS

William Hsu

Alcino J. Silva, CO-CHAIR

COMMITTEE MEMBERS

Denise Aberle

Alex Bui, CO-CHAIR

Ricky Taira

COLLABORATORS

Frederick Eberhardt

William Speier

Wei Wang

Justin Wood

WIFE

Gabrielle Green